UNIVERSITAT ROVIRA I VIRGILI

RUTHENIUM POLYPYRIDYL COMPLEXES AS PHOTOSENSITIZERS FOR MOLECULAR PHOTOVOLTAIC DEVICES: INFLUENCE OF THE DYE STRUCTURE AND THE PRESENCE OF ADDITIVES TO THE DEVICE PERFORMANCE

Anna Reynal Verdú

ISBN: 978-84-693-8863-1
Dipòsit Legal: T.1944-2010

ADVERTIMENT. La consulta d’aquesta tesi queda condicionada a l’acceptació de les següents condicions d'ús: La difusió d’aquesta tesi per mitjà del servei TDX (www.tesisenxarxa.net) ha estat autoritzada pels titulars dels drets de propietat intel·lectual únicament per a usos privats emmarcats en activitats d’investigació i docència. No s’autoritza la seva reproducció amb finalitats de lucre ni la seva difusió i posada a disposició des d’un lloc aliè al servei TDX. No s’autoritza la presentació del seu contingut en una finestra o marc aliè a TDX (framing). Aquesta reserva de drets afecta tant al resum de presentació de la tesi com als seus continguts. En la utilització o cita de parts de la tesi és obligat indicar el nom de la persona autora.

ADVERTENCIA. La consulta de esta tesis queda condicionada a la aceptación de las siguientes condiciones de uso: La difusión de esta tesis por medio del servicio TDR (www.tesisenred.net) ha sido autorizada por los titulares de los derechos de propiedad intelectual únicamente para usos privados enmarcados en actividades de investigación y docencia. No se autoriza su reproducción con finalidades de lucro ni su difusión y puesta a disposición desde un sitio ajeno al servicio TDR. No se autoriza la presentación de su contenido en una ventana o marco ajeno a TDR (framing). Esta reserva de derechos afecta tanto al resumen de presentación de la tesis como a sus contenidos. En la utilización o cita de partes de la tesis es obligado indicar el nombre de la persona autora.

WARNING. On having consulted this thesis you’re accepting the following use conditions: Spreading this thesis by the TDX (www.tesisenxarxa.net) service has been authorized by the titular of the intellectual property rights only for private uses placed in investigation and teaching activities. Reproduction with lucrative aims is not authorized neither its spreading and availability from a site foreign to the TDX service. Introducing its content in a window or frame foreign to the TDX service is not authorized (framing). This rights affect to the presentation summary of the thesis as well as to its contents. In the using or citation of parts of the thesis it’s obliged to indicate the name of the author.

Anna Reynal Verdú

Ruthenium polypyridyl complexes as photosensitizers for molecular photovoltaic devices:

Influence of the dye structure and the presence of additives to the device performance

Ph.D. Thesis

UNIVERSITAT ROVIRA I VIRGILI

Ph.D. Thesis

Ruthenium polypyridyl complexes as photosensitizers for molecular photovoltaic devices:

Influence of the dye structure and the presence of additives to the device performance

Anna Reynal Verdú

Supervised by Dr. Emilio Palomares Gil

(Institut Català d'Investigació Química - Universitat Rovira i Virgili)

Tarragona, July 2010

Emilio Palomares Gil, Group Leader at the Institute of Chemical Research of Catalonia (ICIQ) in Tarragona, and Research Professor of the Catalan Institution for Research and Advanced Studies (ICREA) in Barcelona

CERTIFY:

That the present research study, entitled "Ruthenium polypyridyl complexes as photosensitizers for molecular photovoltaic devices: influence of the dye structure and the presence of additives to the device performance" presented by **Anna Reynal Verdú** for the award of the degree of Doctor, has been carried out under my supervision in ICIQ and that she fulfills the requirements to obtain a "European Doctorate Mention".

Tarragona, July 2010

Prof. Dr. Emilio Palomares Gil

ICIQ
Institut
Català
d'Investigació
Química

UNIVERSITAT ROVIRA I VIRGILI

Acknowledgements

First of all I would like to thank my supervisor, Prof. Emilio Palomares, for trusting me when I joined the group and for his support, guidance and encouragement through my Ph.D. studies. These years have been very stimulating and instructive. I also would like to acknowledge all the people from Prof. Palomares group, in no particular order Toni, Miquel, Amparo, Josep, Eugenia, John, Javi, Margherita, James, Laia, Ivan, Aurelien, Lydia, Eva and Bea, for their encouragement, ideas, advices and friendship. I would like to emphasize my acknowledgements to Amparo, Toni, Josep and Eugenia, for the work done together, which has result in several publications.

I am grateful to Prof. Anton Vidal and his research group (in particular to Natalia, Juan and Sílvia) for giving some appraised samples which allowed me to get very nice results. All the people from the research support units at ICIQ who have helped me during my Ph.D. studies are also acknowledged. Special attention require Gabriel, Kerman, Enrique and Mariona.

I want to thank the opportunity of working and learning from other labs that Prof. Ramon Vilar (Imperial College London) and Prof. Randolph P. Thummel (University of Houston) offered to me. I have special appreciation to the people working on these groups (Inma, Fernando, Savvas, Beeta, Andy, Neil, Nurul, Verity, Chirag and Anna; Maya, Ruby, Dr. Zong, Chris, Nat and Theany). Thanks for all your help and support.

Prof. James Durrant and Dr. Brian O'Regan are also acknowledged for their nice discussions and for letting me to work and learn from their laboratories during my stay at Imperial College London. I also appreciate the efforts of Li and Tracy for helping me.

I would like to express my gratitude to my personal friends from all over the world. Thank you for all the good moments and for making my life pleasant everywhere I have been. Special attention require Nora, John, Aurelien Toni and Laia, whose advices have been very useful during the writing of this thesis.

I cannot finish this page without thanking my parents, Joan and Mª Àngels and my sister Sandra, for their encouragement and support during all my life. "Moltíssimes gràcies per haver-m'ho donat tot i més, pel vostre suport i per haver-me encoratjat a arribar tant lluny".

I also would like to thank to one of the most important persons of my life. Thank you very much Miquel, for being with me in the lab and at home.

Finally, I would like to acknowledge the ICIQ foundation and the Spanish MICINN (AP2008-02351) for the financial support of this research.

Abstract

The population and economical expansion of our planet is based on the consumption of energy. However, the utilisation of fossil fuels and the environmental contamination derived from their usage are arriving nowadays to an unsustainable level. For this reason, the research of new renewable energy sources has generated great interest in the scientific community.

A large amount of energy arrives to the surface of the Earth in the form of sunlight. Although solar cells which are able to convert sunlight into electricity have been commercialised, several research groups are still working on the development of more efficient and/or less expensive photovoltaic devices.

At present, one of the most studied alternative devices are dye sensitised solar cells (DSSCs). The operating principles of this class of electrochemical solar cell is discussed in further detail in Chapter 1. To date, DSSCs utilising ruthenium polypyridyl complexes have shown the highest efficiencies reported for this class of photovoltaic device. This is due to the photophysical, photochemical and electrochemical properties of ruthenium based dyes, which are explained in Chapter 2.

Besides the intrinsic photosensitiser properties, the efficiencies achieved by dye sensitised solar cells are strongly dependent on the charge transfer reactions that take place in the cells: the injection of electrons into the conduction band of the semiconductor by the dye, the transport of electrons through the semiconductor to the working electrode, the dye regeneration by the redox pair present in the electrolyte and the recombination reactions between the photoinjected electrons into the semiconductor and the oxidised species of the dye and the electrolyte.

The different sections comprising the experimental part of this thesis (Chapter 3) are: (1) the design, synthesis, purification and characterisation of a series of ruthenium complexes which contain polypyridyl ligands with different substituents (either electron-donating or electron-withdrawing groups); (2) the study of the photophysical and electrochemical properties of ruthenium complexes; (3) the introduction of the synthesised complexes, and other commercial dyes, in the preparation of photovoltaic molecular devices; and (4) the characterisation of the

different parameters which allow a quantitative analysis of a solar cell efficiency, as well as the determination of the reaction kinetics.

This thesis has been focused on determining the influence of the dye molecular structure (Chapter 4, articles A, B and C) and the presence of a coadsorbent (Chapter 5, article D) on solar cell efficiency. In particular, articles A and B discuss how the electron-donating or electron-withdrawing properties of different substituents in one of the polypyridyl ligands coordinated to the ruthenium metal center can affect the reactions that take place in a DSSC. Furthermore, the charge transfer processes of a solar cell sensitised with the most efficient dyes reported to date have been compared in article C. Finally, article D consists of a study of the effects of sensitising different dyes in the presence of a coadsorbent on the different parameters that quantify the efficiency of a solar cell.

Resum

L'increment de població i l'expansió econòmica al nostre planeta depenen estrictament de la consumició d'energia. Actualment, per això, el consum de combustibles fòssils i la contaminació derivada del seu ús comencen a arribar a un nivell insostenible. Per aquest motiu, la recerca de noves fonts d'energia renovables s'ha estès amb gran interès dins de la comunitat científica.

Una gran quantitat d'energia arriba diàriament a la superfície del nostre planeta en forma de llum solar. Tot i que ja s'han comercialitzat alguns dispositius per a la conversió de llum en energia elèctrica, nombrosos grups de recerca treballen actualment en el desenvolupament d'uns dispositius més eficaços i/o menys costosos econòmicament.

Una de les alternatives més estudiades actualment són les cel·les solars sensitivitzades amb un colorant (en anglès: DSSCs). El funcionament d'aquest tipus de cel·les electroquímiques es discuteix amb més detall al Capítol 1. Avui en dia, les cel·les solar sensitivitzades amb complexes polipiridílics de ruteni han demostrat les eficiències més elevades per a aquests tipus de dispositius. Aquest fet és degut a les propietats fotofísiques, fotoquímiques i electroquímiques dels colorants basats en ruteni, detallades al Capítol 2.

A més de les propietats intrínseques dels colorants utilitzats, l'eficiència assolida per les cel·les solars sensitivitzades amb un colorant està intensament determinada per les reaccions de transferència de càrrega que hi tenen lloc: la injecció d'electrons a la banda de conducció del semiconductor per part del colorant, el transport d'electrons a través del semiconductor fins a l'elèctrode de treball, la regeneració del colorant per part de l'electròlit i les reaccions de recombinació que tenen lloc entre els electrons injectats al semiconductor i les espècies oxidades dels colorants i l'electròlit.

Les etapes principals de la part experimental d'aquesta tesi (Capítol 3) han sigut: (1) el disseny, la síntesi, la purificació i la caracterització d'una sèrie de complexes de ruteni que contenen lligands polipiridílics amb diferents substituents (grups electro-donadors i electro-acceptors); (2) l'estudi de les propietats fotofísiques i electroquímiques dels complexes de ruteni; (3) la introducció dels colorants sintetitzats, així com altres complexes comercials, a la preparació de dispositius fotovoltaics; i (4) la caracterització dels diferents paràmetres que permeten avaluar l'eficiència d'una cel·la solar, així com la determinació de les cinètiques de les reaccions que tenen lloc en aquests tipus de dispositius fotovoltaics.

Aquesta tesi s'ha focalitzat en la determinació de la influència de l'estructura molecular dels colorants (Capítol 4, articles A, B i C) i la presència d'un coadsorbent (Capítol 5, article D) en l'eficiència de les cel·les solars. Més concretament, als articles A i B s'han estudiat com les propietats electro-donadores o electro-acceptores de diferents substituents en un dels lligands polipiridílics coordinats al ruteni poden afectar les reaccions ocorren en una cel·la solar. A més a més, els processos de transferència de càrrega que tenen lloc en una cel·la solar sensitivitzada amb els colorants més eficients publicats actualment s'han comparat a l'article C. Finalment, l'article D comprèn un estudi de l'efecte en els diferents paràmetres que quantifiquen l'eficiència de les cel·les solars degut a la cosensitivització d'un coadsorbent juntament amb dos colorants que tenen estructures moleculars diferents.

Resumen

El incremento de la población y la expansión económica en nuestro planeta dependen estrictamente del consumo de energía. Actualmente, el consumo de combustibles fósiles y la contaminación derivada de su uso están llegando a una nivel insostenible. Por este motivo, la investigación de nuevas fuentes de energía renovables se ha extendido con gran interés dentro de la comunidad científica.

Una gran cantidad de energía llega diariamente a la superficie de nuestro planeta en forma de luz solar. Aunque ya se han comercializado algunos dispositivos para la conversión de luz en energía eléctrica, numerosos grupos de investigación trabajan en el desarrollo de unos dispositivos más eficaces y/o menos costosos económicamente.

Una de las alternativas más estudiadas actualmente son las celdas solares sensitivizadas con un colorante (en inglés: DSSCs). El funcionamiento de este tipo de celdas electroquímicas se discute con más detalle en el Capítulo 1. Actualmente, las celdas solares sensitivizadas con complejos polipiridílicos de rutenio han demostrado las eficiencias más elevadas para este tipo de dispositivos. Este hecho es debido a las propiedades fotofísicas, fotoquímicas y electroquímicas de los colorantes basados en rutenio, detalladas en el Capítulo 2.

Además de las propiedades intrínsecas de los colorantes usados, la eficiencia lograda por las celdas solares sensitivizadas con un colorante está intensamente determinada por las reacciones de transferencia de carga que tienen lugar entre sus componentes: la inyección de electrones a la banda de conducción del semiconductor por parte del colorante, el transporte de electrones a través del semiconductor hasta el electrodo de trabajo, la regeneración del colorante por parte del electrolito y las reacciones de recombinación que tienen lugar entre los electrones inyectados en el semiconductor y las especies oxidadas presentes en el colorante y el electrolito.

Las etapas principales de la parte experimental de esta tesis (Capítulo 3) han sido: (1) el diseño, la síntesis, la purificación y la caracterización de una serie de complejos de rutenio que contienen ligandos polipiridílicos con distintos substituyentes (grupos electro-dadores y electro-aceptores); (2) el estudio de las propiedades fotofísicas y electroquímicas de los complejos de rutenio; (3) la introducción de los colorantes sintetizados, así como otros complejos comerciales, en la preparación de dispositivos fotovoltaicos; y (4) la caracterización de los distintos parámetros que permiten evaluar la eficiencia de una celda solar, así como la determinación de las cinéticas de las reacciones que tienen lugar en este tipo de dispositivos fotovoltaicos.

Esta tesis se ha focalizado en la determinación de la influencia de la estructura molecular de los colorantes (Capítulo 4, artículos A, B y C) y en la presencia de un coadsorbente (Capítulo 5, artículo D) en la eficiencia de las celdas solares. Más concretamente, en los artículos A y B se ha estudiado como las propiedades electro-dadoras o electro-aceptoras de distintos substituyentes en uno de los ligandos polipiridílicos coordinados al rutenio pueden afectar las reacciones que tienen lugar en una celda solar. Además, en el artículo C, los procesos de transferencia de carga que ocurren en una celda sensitivizada con los colorantes más eficientes publicados actualmente se han comparado. Finalmente, el artículo D comprende un estudio del efecto de los distintos parámetros que cuantifican la eficiencia de las celdas solares debido a la cosensitivización de un adsorbente juntamente con dos colorantes que tienen estructuras moleculares diferentes.

Table of contents

Chapter 1. Dye sensitised solar cells

A brief introduction to photovoltaic devices based on molecular photosensitisers is presented in Chapter 1. The constituent materials are described and the principles of operation of complete functional devices are explained.

TABLE OF CONTENTS

1.1. Introduction

In 2006, world primary energy consumption was $4.98 \cdot 10^{20}$ J, and this is expected to increase in the future as a result of population and economic growth.[1] The principal energy supply to meet the energy needs of our planet comes from liquid fuels, coal and natural gas. However, the non-renewable nature of fossil fuels, in addition to the high emissions of CO_2 into the atmosphere when they are used has made them an important issue in the last two decades. For this reason, the search for a sustainable, clean and secure energy source has been extended to a wide range of possible alternatives including solar, wind and biomass. Since the Earth receives a huge amount of energy from sunlight ($4.3 \cdot 10^{20}$ J in 1 h), it seems perfectly logical to consider solar energy as the most likely possible renewable energy resource that could be exploited in the future.[2]

Nowadays, the majority of photovoltaic devices are based on semiconductor p-n junction solar cells, however many other systems and materials have been developed in order to improve the efficiency or reduce the total cost of photovoltaic converters.[3] One of the most studied alternative systems is the dye sensitised solar cell (DSSC). Since the first publication regarding the principles of operation of this molecular photovoltaic device,[4] the study and improvement of this kind of energy converter has attracted the attention of numerous scientific groups. DSSCs are based on the absorption of light by photosensitisers, and the most used and efficient dyes are based on ruthenium polypyridyl complexes. The well known and easily tuneable photophysical, photochemical and electrochemical properties of these dyes make them excellent candidates for light harvesting systems and energy conversion devices.[5]

1.2. Operating principles of dye sensitised solar cells

DSSCs are regenerative photoelectrochemical cells based on the sensitisation of a nanocrystalline semiconductor with a dye able to absorb a wide range of the solar spectrum.[6] The most widely used semiconductor in the working electrode of a DSSC is TiO_2, which is supported onto a transparent fluorine-doped tin oxide (FTO) conducting glass. The counter electrode consists of a layer of platinum coated on FTO conducting glass. The two electrodes are sealed together with a polymer and the cell is completed with a redox electrolyte (Figure 1.1).

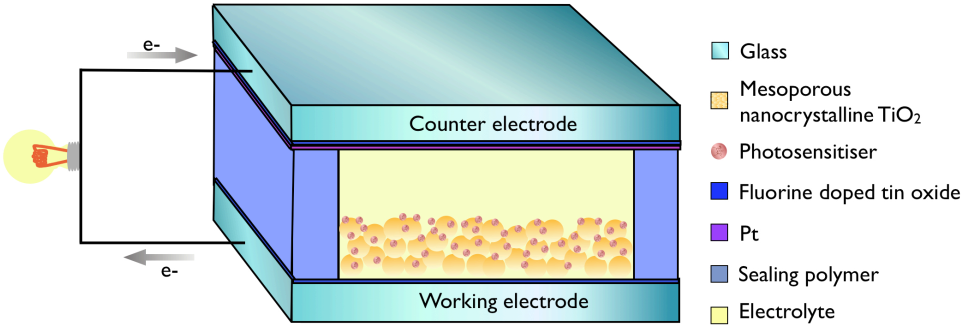

Figure 1.1. Schematic representation of the cross-section of a DSSC

Figure 1.2 shows a schematic representation of a DSSC. Upon absorption of sunlight, the photosensitiser promotes an electron from its ground state to the excited state, corresponding to the metal to ligand charge transfer transition (MLCT) of the dye when $Ru^{(II)}$ polypyridyl dyes are used (Equation 1.1). This electron is subsequently injected into the conduction band of the semiconductor (Equation 1.2), which arrives at the back contact and flows through an external circuit to the counter electrode. At the counter electrode, electrons are transferred to the redox pair present in the electrolyte. The most commonly used electrolyte contains the I^-/I_3^- redox couple, and at the counter electrode triiodide is regenerated to iodide (Equation 1.3). Finally, the cycle is completed with the regeneration of the oxidised dye by electron donation from the electrolyte (Equation 1.4).

Photoexcitation: $S + h\nu \rightarrow S^*$ (Equation 1.1)

Electron injection: $S^* + TiO_2 \rightarrow S^+ + e^- \text{-} TiO_2$ (Equation 1.2)

Electrolyte regeneration: $I_3^- + 2\,e^-\text{-Pt} \rightarrow 3I^-$ (Equation 1.3)

Oxidised dye regeneration: $2\,S^+ + 3\,I^- \rightarrow 2\,S + I_3^-$ (Equation 1.4)

The regenerative cycle of dye sensitised solar cells is based on reversible reactions, and the devices can convert sunlight into electricity without suffering permanent chemical transformations.

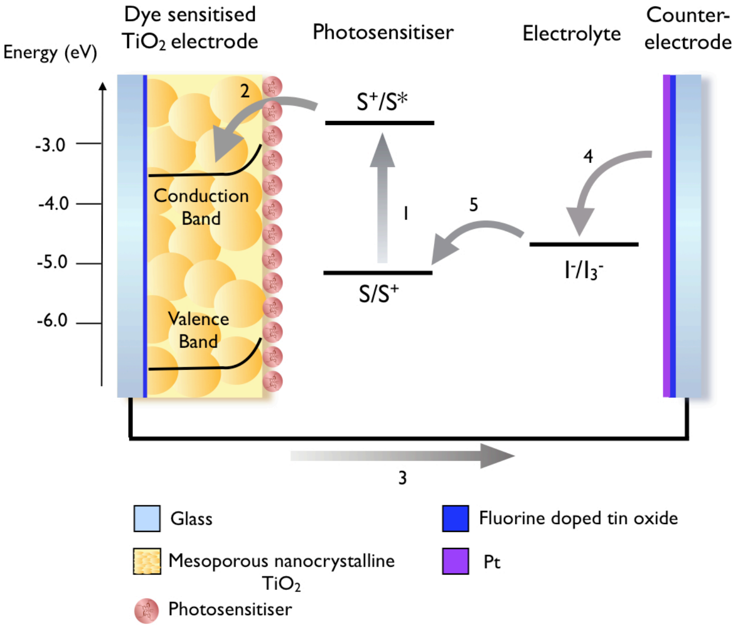

Figure 1.2. Scheme showing the operating principle and energy level diagram of a dye sensitised solar cell. S, S^+, S^* represent the photosensitiser in the ground, oxidised and excited state, respectively. (1) Photoexcitation of the dye, (2) electron injection from the excited dye to the semiconductor, (3) external circuit, (4) regeneration of the electrolyte, and (5) regeneration of the oxidised dye

However, this system has undesirable loss reactions, which decrease the total efficiency of the device (Figure 1.3). The three main loss reactions observed are (1) deactivation of the dye excited state (Equation 1.5), (2) recombination of photoinjected electrons in the semiconductor with the oxidised photosensitiser (Equation 1.6), and (3) recombination of photoinjected electrons in the semiconductor with the oxidised form of the redox mediator (Equation 1.7). The latter recombination reaction is also called the "dark current".

Dye excited state deactivation: $S^* \rightarrow S + \text{heat}/h\nu$ (Equation 1.5)

Back electron transfer: $e^-\text{-TiO}_2 + S^+ \rightarrow \text{TiO}_2 + S$ (Equation 1.6)

Electron recombination with the redox couple: $I_3^- + 2\ e^-\text{-}TiO_2 \rightarrow 3\ I^- + 2\ TiO_2$ (Equation 1.7)

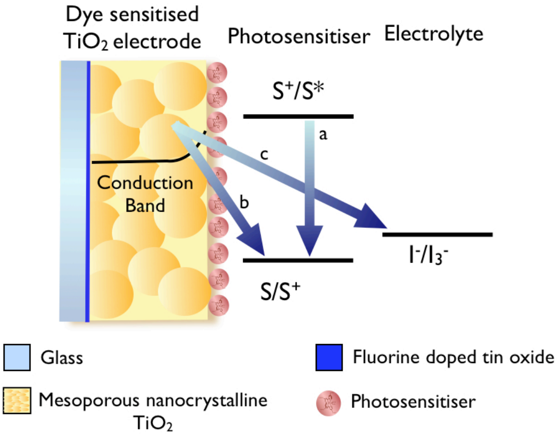

Figure 1.3. Scheme of the loss reactions occurring in a DSSC. (a) Dye excited state deactivation, (b) e^--TiO_2/S^+ back electron transfer, and (c) e^--TiO_2/I_3^- recombination reaction

Despite the loss processes which occur in DSSC, the reason for the relatively high efficiencies observed in optimised devices is due to the rather favourably balanced kinetic competition which ensures forward electron transfer reactions dominate over the loss processes mentioned. For most of the dyes, loss reactions are several orders of magnitude slower than the forward processes when the devices are working under normal operating conditions, allowing efficient charge separation to occur (Table 1.1).[7]

Forward processes	Loss processes
Electron injection from the excited dye into the semiconductor conduction band (10^{-12} - 10^{-9} s)	Excited state deactivation (> 10^{-9} s)
Dye regeneration by the redox electrolyte (10^{-9} - 10^{-6} s)	Back electron transfer from the TiO_2 to the oxidised dye (10^{-6} - 10^{-3} s)
	Electron recombination between the TiO_2 and the electrolyte (10^{-3} - 10^{1} s)

Table 1.1. Timescales of forward and loss processes occurring in DSSC

1.3. Quantitative parameters of solar cell performance

The performance of a dye sensitised solar cell can be quantified by several parameters: the photovoltage and photocurrent generated by the solar cell, the incident photon to current conversion efficiency and the overall light to energy conversion efficiency.

1.3.1. Photocurrent and photovoltage

The photocurrent is the electrical flux through a device under light irradiation. When the cell is operated at short circuit, this is when the external circuit is closed and the voltage is zero, the maximum current flow is obtained. The short circuit current (I_{sc}, A) increases with light intensity and is proportional to the area of the solar cell. The solar circuit current density (J_{sc}, mA·cm^{-2}) is defined as in Equation 1.8, where I_{sc} is the short circuit photocurrent in A and the area of the cell is given in cm^2.

$$J_{sc} = \frac{I_{sc}}{\text{Cell area}} \qquad \text{(Equation 1.8)}$$

The photovoltage is the electrical force generated upon radiation of light that can drive electrical current from one point to another one. Cell efficiency is measured under open circuit conditions, *i.e.* where the working and counter electrodes are not connected through an external circuit. Under such conditions the maximum voltage of a given cell is obtained when the I_{sc} equals zero. In dye sensitised solar cells, the open circuit voltage (V_{oc}) corresponds to the difference in energy between the quasi-Fermi level of the semiconductor under illumination and the redox potential of the mediator present in the electrolyte (Figure 1.4).[8]

However, the experimentally measured voltage in solar cells with most sensitisers is often different from the difference between the Fermi level and the redox potential, due to recombination processes.[9] For this reason, the study of electron transfer reactions in DSSC, particularly the recombination processes and the mechanisms which underpin these reactions is very important in the development of efficient devices. Furthermore, the modifications of the semiconductor surface or changes of the electrolyte redox couple have strong effects on the V_{oc}.

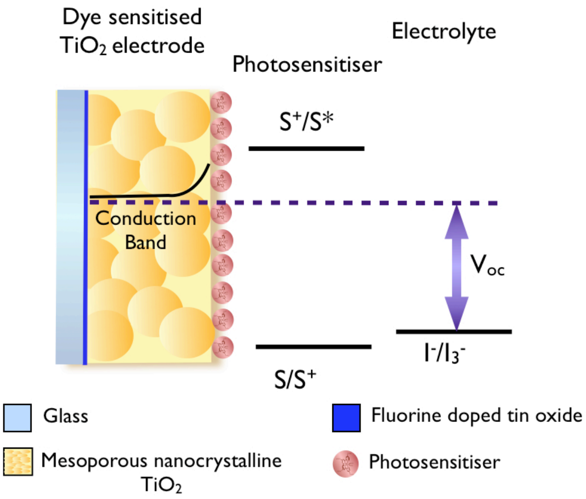

Figure 1.4. Energy level diagram of the working electrode and electrolyte of a DSSC

1.3.2. Incident Photon to Current Conversion Efficiency

The incident photon to current conversion efficiency (IPCE, %) is used to describe the number of electrons generated by the solar cell and detected in the external circuit, as a ratio of the number of incident photons which illuminate it for a given wavelength. It can be calculated from Equation 1.9, where J_{sc} is the short circuit photocurrent ($mA\cdot cm^{-2}$), λ is the incident light wavelength (nm), P_{lamp} is the power of the incident light ($W\cdot m^{-2}$) and 1240 is the conversion factor of the energy of photons. The IPCE is strongly affected by (1) the light harvesting efficiency of the dye, which depends on the photophysical properties of the dye; (2) the yield of electron injection into the conduction band of the semiconductor, which depends on both the redox potential and the injection kinetics of the excited photosensitiser, and (3) the charge collection efficiency at the working electrode, which depends on the structure and morphology of the semiconductor film.

$$\mathrm{IPCE}\ \frac{1240\cdot J_{sc}}{\lambda\cdot P_{lamp}}\cdot 100 \qquad \text{(Equation 1.9)}$$

1.3.3. Overall efficiency

The overall conversion efficiency (η_{eff}, %) of DSSCs depends on the photocurrent measured at short circuit (J_{sc}, mA·cm^{-2}), the open circuit photovoltage (V_{oc}, V), the fill factor of the cell (ff, %) and the power of the incident light (P_{lamp}, W·m^{-2}) (Equation 1.10).

$$\eta_{eff} = \frac{J_{sc} \cdot V_{Voc} \cdot ff}{P_{lamp}} \cdot 100 \qquad \text{(Equation 1.10)}$$

The fill factor (%) is essentially an indicative measurement of the quality of a solar cell. It is obtained by dividing the maximum power density obtained by a solar cell (P_{ff}, W·m^{-2}) by the maximum theoretical power density (P_{max}, W·m^{-2}) (Equation 1.11). The power can be obtained as the product between the current and the voltage (Equation 1.12). The maximum theoretical power density of a solar cell is therefore the product of V_{oc} (V) and I_{sc} (A) (Figure 1.5).

$$ff = \frac{P_{ff}}{P_{\max}} = \frac{V_{ff} \cdot I_{ff}}{V_{oc} \cdot I_{sc}} \cdot 100 \qquad \text{(Equation 1.11)}$$

$$P = V \cdot I \qquad \text{(Equation 1.12)}$$

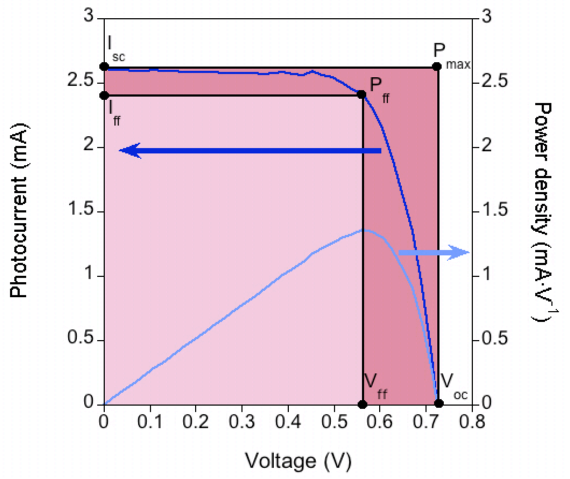

Figure 1.5. Current-voltage (I-V) and power-voltage (P-V) curves from a ruthenium polypyridyl dye (N719)

1.4. Fundamental constituents of dye sensitised solar cells

DSSCs are devices composed of multiple components, and their overall efficiency depends strongly on the individual properties of each constituent. Strong efforts have been spent on the optimisation of the materials used in the fabrication of solar cells, such as the semiconductor metal oxide, the photosensitiser, the electrolyte and the counter electrode.

1.4.1. Working electrode

In DSSCs, the semiconductor acts as a supporting material for dye adsorption and as an electron transport pathway. The TiO_2 nanoparticles are deposited onto glass coated with a thin layer of a transparent conductive material. The most commonly used conductive material is fluorine doped tin oxide. Although other metal oxides such as tin-doped indium oxide (ITO) present higher conductivities, its thermal instability strongly increases the resistance of the material when the glass is exposed to high temperatures during a long period of time.

Three important processes take place in the working electrode: light harvesting, charge separation and electron transport. Light harvesting is performed by the chromophoric agent, which consists of a photosensitiser. Charge separation occurs at the interface between the dye and the semiconductor, with electron travelling through the TiO_2 and holes through the electrolyte. Electron recombination also take place at the interface between the surface of the semiconductor and the dye or the electrolyte.

1.4.1.1. Band theory of solids

The electronic properties of solid materials are controlled by the nature and position of the valence and conduction bands. The band gap can be defined as the difference in energy between the valence band (VB) and the conduction band (CB). For conducting materials, the two bands are overlapping and allow the free movement of electrons, while for semiconductors and insulators the two bands have different energy levels. Insulators have a large band gap where electrons cannot be promoted to the conduction band without applying extreme conditions. In semiconductors, electrons can be both thermally or optically excited to the conduction band, generating a hole in the valence band. Electron-hole pairs, also called excitons, can be generated either by increasing the temperature or by the absorption of light.

1.4.1.2. Characteristics of titanium dioxide

Although several semiconductors such as TiO_2, ZnO, SnO_2 or Nb_2O_5 have been explored for DSSCs, titanium dioxide is the most common metal oxide semiconductor, since it is an abundant, inert, non-toxic, stable and cheap material.[10] The three most common crystalline structures are rutile, anatase and brookite. Pure brookite nanoparticles are extremely difficult to prepare in the laboratory under mild conditions, therefore rutile and anatase are the most used crystalline forms.[10] Although rutile is the most thermodynamically stable crystalline form, anatase shows higher photocurrents in DSSCs due to its morphology, packing structure and electron transport. Anatase TiO_2 has a larger surface area due to smaller particle size, which allows the anchoring of larger amounts of dye and the higher conductivity between the different nanoparticles is associated with the better packing of the film.[11] The larger band gap of anatase compared to rutile prevents light absorption in the near UV-region (350 - 400 nm), which can cause long term degradation of the cell due to the strong oxidation effect of the formation of holes in the valence band.[12]

1.4.1.3. Titanium dioxide as a semiconductor in dye sensitised solar cells

Semiconductors absorb light with an energy equal to the difference in energy between the valence and the conduction bands (E_{bg}, J) (Equation 1.13), where h is Planck's constant ($6.626 \cdot 10^{-34}$ $m^2 \cdot Kg \cdot s^{-1}$) and c is the light speed ($3 \cdot 10^8$ $m \cdot s^{-1}$). For large band gap semiconductors such as anatase TiO_2, the difference between the ground and excited state energy levels is of the order of 3 eV. Such an amount of energy to promote an electron from the valence band to the conduction band is provided by UV light ($\lambda < 400$ nm). Therefore, in order to use sunlight as a source of energy, whose spectrum also includes visible and near IR, a dye able to "sensitise" TiO_2 to these wavelengths, and to inject electrons into the conduction band of the semiconductor is necessary (Figure 1.6).

$$\lambda = \frac{h \cdot c}{E_{bg}} \qquad \text{(Equation 1.13)}$$

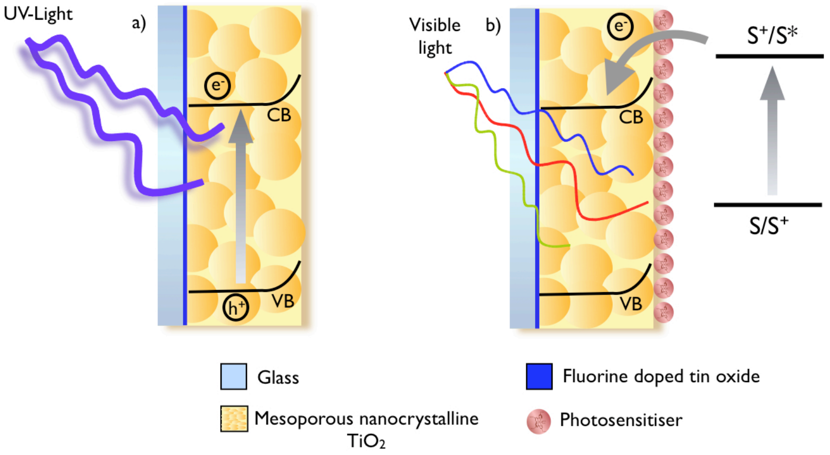

Figure 1.6. Schematic representation of (a) the formation of an exciton in a semiconductor by the absorption of UV-light, and (b) electron injection into the conduction band of a semiconductor by the absorption of visible light by a photosensitiser

The semiconductor in DSSCs is deposited in the form of mesoporous crystalline nanoparticles. The most important characteristics for a TiO_2 film that have to be optimised are the surface area, the porosity, the light scattering and the electron diffusion.[13] The semiconductor must have a large surface area in order to anchor as much dye as possible, which is obtained with the preparation of small TiO_2 nanoparticles. The size of the nanoparticles also affects the size of the pores and the light scattering properties of the nanoparticles. The porosity of the film has to be optimised in order to allow the electrolyte penetration through the thickness of the film and ensure fast dye regeneration. Furthermore, the level of porosity has to be controlled in order to have enough interparticle connectivity so that electrons can diffuse through the film and reach the working electrode. The thickness of the film (d, cm) is also a key parameter to reach high conversion efficiencies, since charges at the back contact can only be collected if the thickness of the film is lower than the electron diffusion length (L_n, cm) (Equation 1.14). L_n is defined as the distance that electron can travel before recombining with an electron acceptor,[14] and it is dependant on the electron diffusion coefficient (D_e, $cm^2 \cdot s^{-1}$) and the lifetime of the electron (τ_e, s) (Equation 1.15).

$$L_n > d \qquad \text{(Equation 1.14)}$$

$$L_n = \sqrt{D_e \cdot \tau_e} \qquad \text{(Equation 1.15)}$$

The diameter of the nanoparticles is in the range of 10 - 25 nm, large enough in order to not exhibit quantum size effects. For this reason, the semiconductor film can be considered as a network composed of bulk nanocrystals.

At first glance, the properties of mesoporous nanocrystalline films would seem disadvantageous compared to their compact single crystal analogues because (1) the electrolyte penetrates into the pores of the semiconductor producing a huge junction contact area, increasing the probability of electron recombination, (2) the inherent conductivity of the film is very low, (3) the multiple traps present in the film decrease the electron diffusion coefficient,[15] and (4) the small size of the nanoparticles in contact with the electrolyte restricts the amount of electrical field a particle can support. However, such disadvantages are offset by the optical transparency of the nanoparticles and the enormous surface area of the films, which allows an extremely large number of photosensitiser molecules to be adsorbed onto the surface of the semiconductor.

1.4.2. Molecular sensitiser

1.4.2.1. Characteristics of molecular sensitisers

The function of the photosensitiser in DSSC is to absorb a wide range of the solar spectrum and to inject electrons into the conduction band of the semiconductor. For this reason, the design of the dye has been tuned to fulfil several structural, photophysical and electrochemical requirements.[16]

The absorption spectra of the sensitisers should cover as wide as possible a range of the visible and near infrared regions and possess a high molar extinction coefficient, in order to maximise the absorption of the solar spectrum light (Figure 1.7). The solar radiation conditions are defined by the air mass (AM) value. Air mass zero (AM-0) corresponds to the radiation that a device receives in the absence of an atmosphere between the light source and the solar cell. However, the extraterrestrial solar spectrum is different from the sunlight spectrum that arrives at the surface of the Earth due to light scattering and absorption by H_2O, H_2, O_2, CO_2, O_3 and other species present in the atmosphere. Furthermore, the incident light falling on solar devices can be irradiated in the form of direct light, which comes straight from the sun, or in a diffuse form, which is light reflected off clouds, the ground or other objects. For this reason, AM-1.5G is defined as the corrected solar spectrum, including both direct and diffuse radiation, considering the sun at an angle of 48.19°. Although the solar flux is 982 $W \cdot m^{-2}$, it has been standardised to 1000 $W \cdot m^{-2}$.

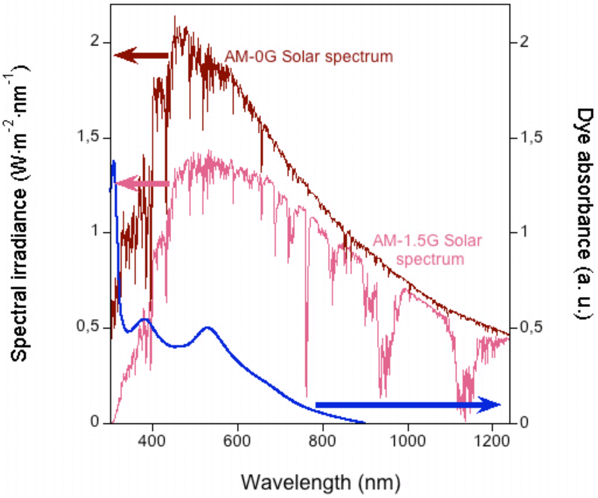

Figure 1.7. AM-0G solar spectra (—), AM1.5G solar spectra[17] (—) and absorption spectra of cis-dithiocyanato-bis-(4,4′-dicarboxy-2,2′-bipyridine)ruthenium(II) dye (—)

The structure of the dye has to include one or more anchoring groups in order to bind strongly to the surface of the semiconductor and ensure a quantitatively efficient electron injection. Photosensitisers can interact with the surface of metal oxides through covalent bonds, hydrogen bonding, electrostatic interactions, hydrophobic interaction, Van der Waals forces or entrapment inside the pores.[18] However, the formation of covalent bonds between the hydroxyl groups present at the surface of the semiconductor nanoparticles and the different anchoring groups of the dyes increases the amount of absorbed dye as well as the stability of the cell and the strength of the electronic coupling between the π^* molecular orbital of the dye and the orbitals of the TiO_2 semiconductor, and decreases the rate of dye desorption.[19] Although most of the sensitisers are linked to the semiconductor surface through carboxylic acid groups, a variety of different groups such as phosphonic acid,[20] boronic acid,[21] sylanes[22], other derivatives or moieties have been used. The attachment of dyes through carboxylic acid groups is reversible, and the sensitisers can be desorbed from the films under basic conditions. Furthermore, several binding modes of a carboxylic acid group to the surface of a metal oxide are possible depending on the dye structure, the binding groups, the crystalline form of the metal oxide and the surface environment (Figure 1.8).[23, 24]

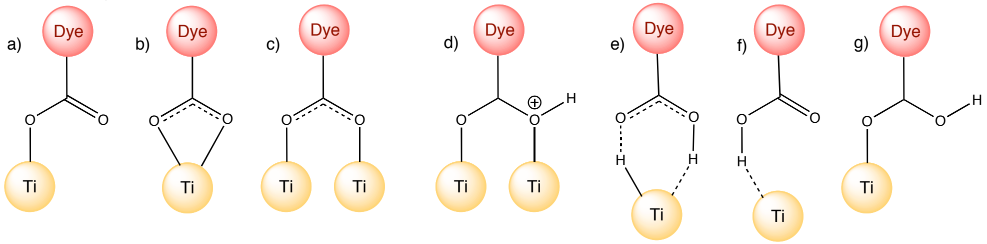

Figure 1.8. Possible binding modes of a carboxylic acid group to TiO_2. (a) Ester linkage, (b) chelate binding, (c, d) bidentate bridges, (e, f) hydrogen bonding interactions, and (g) monodentate binding through the CO

The redox properties of the dye are also important for efficient charge separation: the LUMO energy level must be higher than the conduction band energy level of the semiconductor in order to be able to inject electrons into the TiO_2, and the HOMO must be sufficiently low to permit fast electron regeneration by the electrolyte redox couple. The HOMO-LUMO band gap should be about 1.5 eV for optimum absorption of sunlight. Furthermore, the spatial orientation of the HOMO and LUMO influences not only the electron injection of the dye into the semiconductor conduction band and the photosensitiser regeneration but also the electron recombination between the photoinjected electrons in the TiO_2 and the oxidised dye.[25, 26] The LUMO should be in close contact with the semiconductor surface, while the dye cation should be separated from the electrode surface.

Another chemical aspect of photosensitisers regards their solubility in organic solvents. The dye should be soluble in a volatile solvent to permit their adsorption onto the surface of the semiconductor, but should not be desorbed by the electrolyte solution. Finally, the redox reactions involving the dyes must be reversible and the photosensitisers should be stable enough to permit many oxidation/reduction cycles without decomposition of the molecules.

1.4.2.2. Classes of molecular sensitisers

Many different compounds have been investigated for solar cell applications. They can be divided in three major groups: metal containing complexes,[27] organic dyes[28, 29] and natural compounds[30].

Mononuclear and polynuclear transition metal complexes have been widely studied as photosensitisers.[31] Systematic optimisation of the dye components such as the introduction of different anchoring ligands or the insertion of different chromophoric groups has been tested in dyes based on different metal ions, such as Ru$^{(II)}$,[32, 33] Os$^{(II)}$,[34-36] Pt$^{(II)}$,[37, 38] Re$^{(I)}$,[39] Cu$^{(I)}$[40, 41] or Fe$^{(II)}$[42,]

[43] (Figure 1.9). However, the most used compounds by far in DSSCs are ruthenium complexes. The easily tuneable redox and photophysical properties and the synthetic approach of these complexes, which allows the sequential introduction of different ligands, make these compounds excellent potential candidates for semiconductor sensitisation.

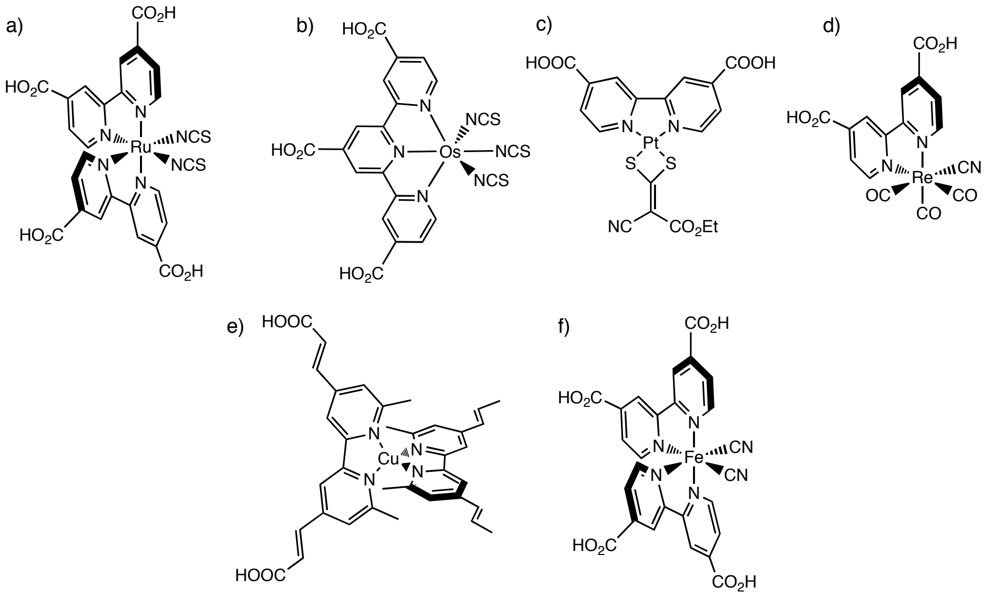

Figure 1.9. Molecular structures of metal based sensitisers. (a) Octahedral $Ru^{(II)}$ complex,[44] (b) octahedral $Os^{(II)}$ complex,[45] (c) square planar $Pt^{(I)}$ complex,[37] (d) octahedral $Re^{(I)}$ complex,[39] (e) tetrahedral $Cu^{(II)}$ complex,[41] and (f) octahedral $Fe^{(II)}$ complex[42]

In addition to metal complex sensitisers, a wide range of organic dyes have been explored. This kind of dye offers several advantages compared to their metal containing analogues, such as higher molar extinction coefficients, cheap and relatively easy preparation and purification techniques, a large variety of different structures and chromophoric groups available, the accessibility of the reagents and the obvious fact that they do not contain precious metals such as Ru or Pt. Organic dyes such as porphyrins, phthalocyanines, perylenes, squaraines, conjugated donor-acceptor moieties, etc. have been explored (Figure 1.10).[28, 29, 46] However, the efficiencies obtained with devices prepared from organic dyes are still lower than ruthenium based DSSCs. The main unfavourable characteristics of metal free dyes are the narrow absorption bands, causing poorer sunlight harvesting, the tendency to form aggregates, which prevents electron injection into the TiO_2 conduction band, and a lower stability compared to metal complexes.

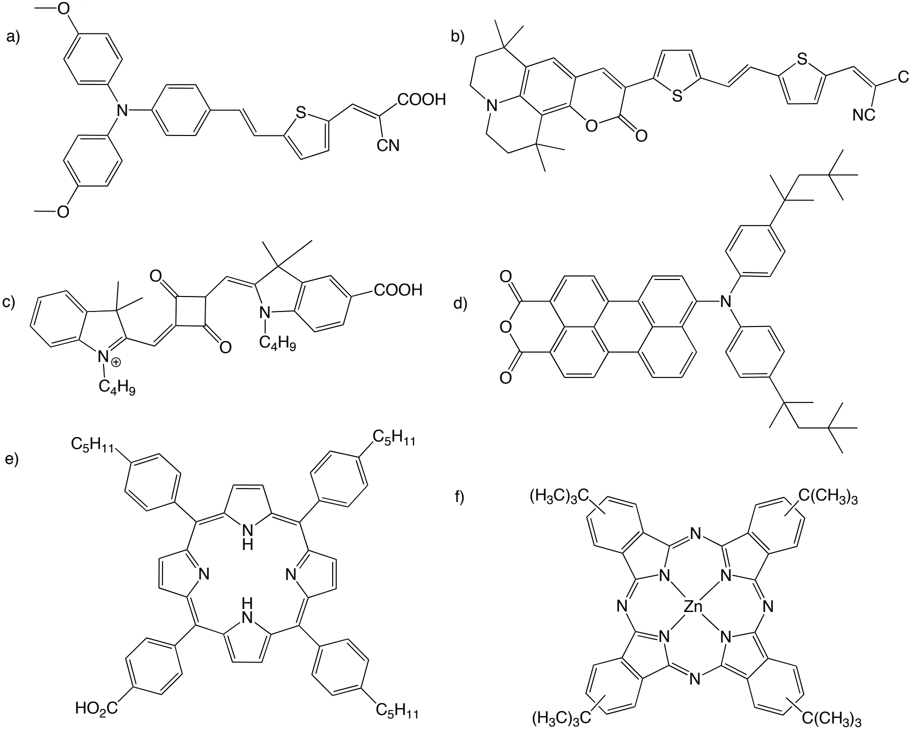

Figure 1.10. Molecular structures of a series of organic dyes. (a) Donor-π-acceptor dye with a triphenyl amine donor moiety,[47] (b) donor-π-acceptor dye with a coumarin donor moiety,[48] (c) squaraine dye,[49] (d) perylene dye,[50] (e) porphyrin dye,[51] and (f) phthalocyanine dye[52]

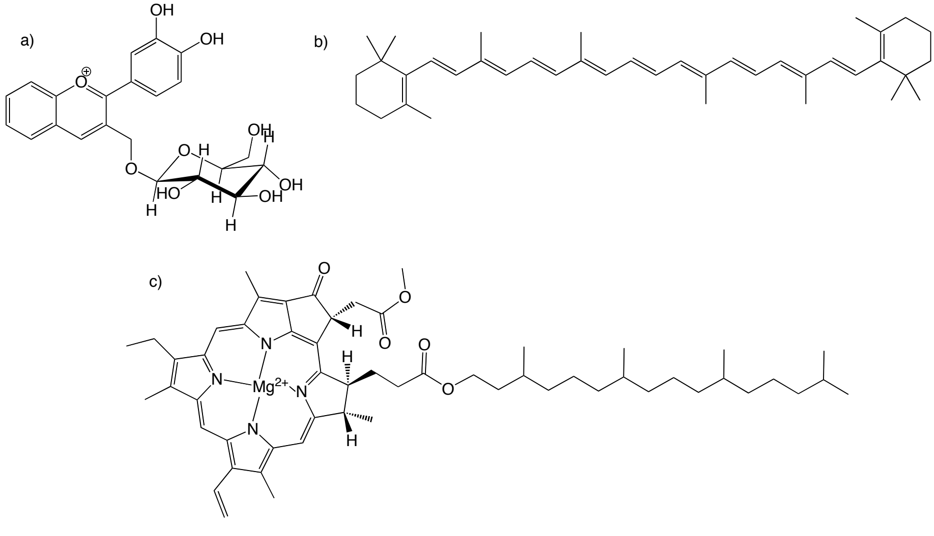

Figure 1.11. Molecular structures of natural dyes used in DSSCs. (a) Cyanin dye,[30] (b) β-carotene dye,[53] and (c) chlorophyll a dye[54]

Natural photosensitisers can also be used as dyes in photovoltaic molecular devices. Natural dyes are pigments extracted from plants, flowers and fruits that have been used mainly for educational purposes, as a fast, low cost and environmentally friendly source for the preparation of DSSCs. The most studied dyes are anthocyanins, but the overall efficiencies of this kind of dye are generally much lower compared to organic or metal complex sensitisers (Figure 1.11).[30, 54, 55]

1.4.3. Electrolyte

The electrolyte is the hole transporting material located between the surface of the semiconductor and the counter electrode of a DSSC. There are three different kinds of electrolytes employed in DSSC: liquid electrolytes (including electrolytes where the redox mediators are dissolved into organic solvents or electrolytes composed of ionic liquids), quasi-solid state electrolytes and solid electrolytes.

However, in all these cases, the electrolyte must have a good contact between the counter and working electrodes as well as high conductivity to permit fast charge transport between the platinum counter electrode and the oxidised dye. The electrolyte should also be thermally, optically, chemically, and electrochemically stable and neither degrade nor desorb the dye from the metal oxide surface. Furthermore, the redox mediator should have adequate redox potentials to allow efficient dye regeneration. Finally the electrolyte should not absorb in the visible region of the spectra, since it would reduce light absorption by the dye.

1.4.3.1. Organic solvent based electrolytes

Up to now, the most efficient DSSCs are based on organic solvent electrolytes because of their low viscosity, fast ion diffusion and high percolation into the pores of the semiconductor.[56] This kind of electrolyte contains a redox couple, ionic liquid components and additives dissolved into an organic solvent.

The most efficient redox couple for the regeneration of the oxidised dye is the iodide/triiodide couple. However, the two major problems regarding the use of I^-/I_3^- are the severe corrosion problems for the device sealing materials, causing difficulties in device sealing and stability. In addition, the triiodide shows partial absorption of visible light. Alternative redox mediators such as Br^-/Br_3^-,[57] $SCN^-/(SCN)_2$,[58, 59] $SeCN/(SeCN)_2$, ferrocene$^+$/ferrocene,[60] $Co^{(II)}/Co^{(III)}$ complexes,[61, 62] or $Cu^{(I)}/Cu^{(II)}$ complexes[63] have been tested in DSSC, however inferior device efficiencies have been obtained. The most common counterions of the iodide/triiodide couple are imidazolium and lithium, which can also affect the performance of the solar cell. Small cations such as Mg^{2+}, Li^+, Na^+ or H^+ can penetrate into the pores of the nanoparticles forming an ambipolar ion$^+$/e$^-$ with the photoinjected electrons of the conduction band, which increases the transport velocity of electrons in the TiO_2 network.[64] On the other hand, relatively large molecules such as imidazolium cations can be adsorbed onto the surface of the semiconductor nanoparticles, forming a Helmholz layer, which restricts the contact of triiodide with the electrons from the TiO_2 conduction band.[65]

Ionic liquids can also be used as a source of iodide in organic solvent based electrolytes for DSSC. The addition of ionic liquids in organic solvent based electrolytes usually increases the ionic conductivity.[66] Furthermore, the use of different additives has been extensively used in order to optimise the DSSC performance. Further discussion of the effects of additives in solar cells is explained in Chapter 5.

1.4.3.2. Ionic liquid electrolytes

Room temperature ionic liquids are attractive candidates as non-volatile solvents for electrolytes.[67] They are formed from an aromatic or non-aromatic cation such as imidazolium, pyridinium or quaternary ammonium ions and different anions from the family of halides, pseudohalides, BF_4^- or PF_6^- (Figure 1.12).[68] Ionic liquids posses good chemical and thermal stability, very low vapour pressure, non-flammability, high ionic conductivity and wide electrochemical window, which are very useful properties for long-lived electrochemical devices.[69] However, their high viscosity usually limits the transport of the redox shuttle components, which occurs by diffusion, and the dye regeneration is therefore not as good as for organic solvent based electrolytes.

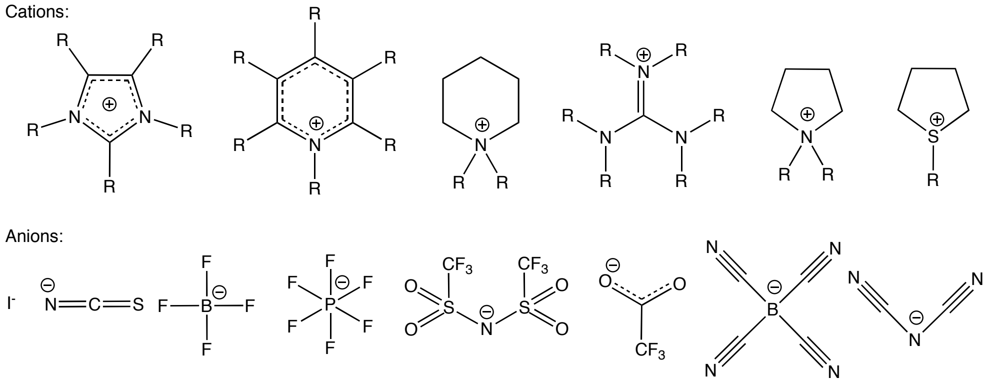

Figure 1.12. Molecular structure of the most commonly used cations and anions in ionic liquids. R corresponds to H, alkyl chains or other substituents

As well as in solvent based electrolytes, different additives are added to ionic liquid electrolytes in order to increase the photocurrent or the photovoltage of the devices.

1.4.3.3. Quasi-solid state electrolytes

Quasi-solid state electrolytes are gel based materials with dispersed amounts of liquid electrolyte.[70] This kind of electrolyte has the cohesive property of a solid electrolyte and the high ion diffusion characteristics of a liquid electrolyte. Quasi-solid state electrolytes are prepared by physical or chemical polymerisation of a gel, inorganic material or monomer which incorporates large amounts of liquid electrolyte.

1.4.3.4. Solid-state electrolytes

Solid state electrolytes can be divided into either hole transport materials (HTM) or redox couple containing solid electrolytes. The first group require a layer of an organic or inorganic large bandgap HTM to be deposited from solution or by vacuum deposition. Inorganic HTMs such as CuI, CuBr or CuSCN have shown low stability. One of the most used organic HTM is spiro-OMeTAD (2,2'-7,7'-tetrakis(*N,N*-di-*p*-methoxyphenylamine)9,9'-spirobifluorene). The solar cell mechanism using HTM is equivalent to liquid or solid electrolytes: the oxidised dye is regenerated by the electrons from the HOMO energy level of the HTM instead of by the redox mediator from liquid electrolytes. At the same time, the HTM is reduced by the electrons that arrive at the counter electrode. However, the performance of DSSCs using solid electrolytes is reduced due to the low conductivity of HTMs, the increased charge recombination between the semiconductor and the HTM and the low interfacial contact surface between the dye molecules and the solid electrolyte due to incomplete percolation of electrolyte into the porous of the nanoparticles. Solid electrolytes can also incorporate in their polymeric structure a redox couple such as I^-/I_3^-. Although the efficiencies obtained with this kind of electrolyte are higher than with HTM based electrolytes, because of higher interfacial contact between the electrolyte and the oxidised dye and lower charge recombination reactions, they are not as high as the efficiencies obtained with liquid solvent-based DSSCs.

1.4.5. Counter electrode

The counter electrode reduces the oxidised species present in the electrolyte redox couple, or, from a different point of view, it collects the holes from the hole conducting material in a solid state dye solar cell. For efficient DSSCs, the counter electrode should posses low resistance and a high rate of reduction of the redox mediator present in the electrolyte.[71]

The material most widely used as the counter electrode is the highly transparent FTO conductive glass with a thin layer of platinum (< 10 μm). Although different deposition techniques have been tested to create the molecular catalyst thin layer, thermal deposition of a Pt thin film shows more stability and a higher triiodide reduction rate.[72]

Different materials have been used as low cost alternative materials to the platinum coated counter electrode. Metal substrates such as steel or Ni have been tested as molecular catalysts. However, the I^-/I_3^- redox species present in the electrolyte is highly corrosive towards these metals. Carbon materials such as graphite or black carbon have also been tested. High efficiencies have been obtained with thick layers of carbon, due to the high surface contact area with the redox mediator.[73] Conducting polymers have also been used as counter electrodes, allowing the preparation of flexible devices.

1.4.6. The effect of additives

The maximum open circuit voltage of a DSSC is the difference in energy between the quasi-Fermi level of the semiconductor when illuminated and the redox potential of the electrolyte.[8] The V_{oc} is mainly affected by changes in the position of the conduction band edge of the semiconductor and by variations in the e^--TiO_2/electrolyte$^+$ recombination rate.

The conduction band of the TiO_2 can be shifted by the presence of additives either in the electrolyte[74, 75] or as coadsorbents,[76, 77] or by exposing the cell to sufficiently high light intensities.

The composition of the electrolyte strongly affects the performance of DSSCs. Two main kinds of additives, adsorptive cations and nitrogen containing molecules, can be intercalated between the TiO_2 nanoparticles or adsorbed onto their surface. The presence of these additives can affect electron injection, the open circuit voltage, the electron diffusion kinetics and the dye regeneration rate. Cations such as Li^+, Na^+, Cs^+, K^+ or tetrabutylammonium$^+$ (TBA^+) charge the surface positively causing a downward shift of the conduction band position.[78] This effect increases the driving force for electron injection (and therefore increases injection rate) and improves the photocurrent, although the open circuit voltage is reduced.[65, 75] On the other hand, ammonia and other nitrogen containing heterocyclic molecules, such as 4-*tert*butylpyridine (TBP),[79] can be adsorbed onto the surface of the semiconductor increasing cell voltage by shifting the conduction band of the TiO_2 upwards due to deprotonation of the TiO_2 surface, leading to a negatively charged surface.[80] Nitrogen containing molecules can also decrease the electron recombination between the photoinjected electrons and the redox mediator by preventing the electrolyte from reaching the TiO_2 surface.

Coadsorbents, such as chenodeoxycholic acid (Cheno),[81, 82] are small molecules anchored onto the surface of the semiconductor together with the dye. They mostly consist of a hydrophobic chain and an anchoring group such as carboxylic acid or phosphonic acid, that can block exposed areas of TiO_2 which are not covered by photosensitisers. In addition to the barrier effect for e^--TiO_2/electrolyte$^+$, coadsorbents can shift down the conduction band of the semiconductor by protonating the TiO_2 surface.

The intercalation of coadsorbents between photosensitiser molecules can also prevent dye aggregation, an effect especially important in organic photosensitisers, which strongly reduces electron injection into the conduction band of the semiconductor.

1.5. Ph.D. Aims

To date, the highest efficiencies in dye sensitised solar cells have been reported using ruthenium polypyridyl complexes. Although this kind of device was reported by Grätzel and O'Regan in 1991,[4] many of the processes occurring between the different components of these devices are still not well defined and even the best efficiencies reached by some photosensitisers remain exceptional and are not always easy to reproduce.

For this reason, the objective of this thesis is the study of the influence of one of the fundamental constituents of DSSCs, namely the dye sensitiser, on the overall efficiency of these devices. In particular, the relationship between the performance of DSSCs and molecular structure of the ruthenium dyes is investigated. Furthermore, the effect of the addition of coadsorbents on the function of ruthenium polypyridyl photosensitisers in DSSC is discussed.

A series of novel ruthenium(II) polypyridyl complexes is designed, synthesised and characterised. The molecular structure of these ruthenium complexes is composed of a 4,4'-dicarboxy-2,2'-bipyridine, whose function is to attach the dye to the semiconductor surface, two thiocyanate groups, which shift the absorption spectra to the red and four different phenanthroline ligands with different substituent groups, both electron donating and electron accepting. These ruthenium complexes, as well as other commercially available dyes, were used in the preparation of DSSC solar cell devices. The performance of these solar cells was measured, as well as the kinetics of the forward electron transfer processes and the recombination reactions occurring at the TiO_2/dye/electrolyte interface. This allows differences in solar cell performance to be directly correlated with the structure of each of the dyes under investigation.

The effect of the addition of different coadsorbents, such as chenodeoxycholic acid or citric acid, on the electron transfer kinetics in DSSCs was also measured. The aim of these additives is to decrease recombination between the photoinjected electrons in the conduction band of the semiconductor and the redox species present in the electrolyte.

1.6. References

1. Energy Information Administration, *International Energy Outlook*, **2009**, (US Dept of Energy, Washington DC).
2. Lewis, N. S.; Nocera, D. G., *Proc. Natl. Acad. Sci. U. S. A.* **2006,** *103* (43), 15729-15735.
3. Green, M. A., *Physica E* **2002,** *14* (1-2), 11-17.
4. O'Regan, B.; Grätzel, M., *Nature* **1991,** *353* (6346), 737-740.
5. Campagna, S.; Puntoriero, F.; Nastasi, F.; Bergamini, G.; Balzani, V., *Top. Curr. Chem.* **2007,** *280* (Photochemistry and Photophysics of Coordination Compounds I), 117-214.
6. Nazeeruddin, M. K.; Grätzel, M., *Compr. Coord. Chem. II* **2004,** *9*, 719-758.
7. Martinson, A. B. F.; Hamann, T. W.; Pellin, M. J.; Hupp, J. T., *Chem. Eur. J.* **2008,** *14* (15), 4458-4467.
8. Frank, A. J.; Kopidakis, N.; van de Lagemaat, J., *Coord. Chem. Rev.* **2004,** *248* (13-14), 1165-1179.
9. Nissfolk, J.; Fredin, K.; Hagfeldt, A.; Boschloo, G., *J. Phys. Chem. B* **2006,** *110* (36), 17715-17718.
10. Jose, R.; Thavasi, V.; Ramakrishna, S., *J. Am. Ceram. Soc.* **2009,** *92* (2), 289-301.
11. Park, N. G.; van de Lagemaat, J.; Frank, A. J., *J. Phys. Chem. B* **2000,** *104* (38), 8989-8994.
12. Li, G.; Richter, C. P.; Milot, R. L.; Cai, L.; Schmuttenmaer, C. A.; Crabtree, R. H.; Brudvig, G. W.; Batista, V. S., *Dalton Trans.* **2009,** (45), 10078-10085.
13. Barbé, C. J.; Arendse, F.; Comte, P.; Jirousek, M.; Lenzmann, F.; Shklover, V.; Grätzel, M., *J. Am. Ceram. Soc.* **1997,** *80* (12), 3157-3171.
14. Grätzel, M., *Inorg. Chem.* **2005,** *44* (20), 6841-6851.
15. Benkstein, K. D.; Kopidakis, N.; van de Lagemaat, J.; Frank, A. J., *J. Phys. Chem. B* **2003,** *107* (31), 7759-7767.
16. Robertson, N., *Angew. Chem., Int. Ed.* **2006,** *45* (15), 2338-2345.
17. AM1.5G Global Solar Spectrum (ASTM G173-03) source of data ASTM/NREL, http://rredc.nrel.gov/solar/spectra/am1.5/,
18. Kalyanasundaram, K.; Gratzel, M., *Coord. Chem. Rev.* **1998,** *177*, 347-414.
19. Galoppini, E., *Coord. Chem. Rev.* **2004,** *248* (13-14), 1283-1297.
20. Gillaizeau-Gauthier, I.; Odobel, F.; Alebbi, M.; Argazzi, R.; Costa, E.; Bignozzi, C. A.; Qu, P.; Meyer, G. J., *Inorg. Chem.* **2001,** *40* (23), 6073-6079.
21. Altobello, S.; Bignozzi, C. A.; Caramori, S.; Larramona, G.; Quici, S.; Marzanni, G.; Lakhmiri, R., *J. Photochem. Photobiol., A* **2004,** *166* (1-3), 91-98.
22. Ghosh, P.; Spiro, T. G., *J. Am. Chem. Soc.* **1980,** *102* (17), 5543-5549.
23. Vittadini, A.; Selloni, A.; Rotzinger, F. P.; Gratzel, M., *J. Phys. Chem. B* **2000,** *104* (6), 1300-1306.
24. Meyer, T. J.; Meyer, G. J.; Pfennig, B. W.; Schoonover, J. R.; Timpson, C. J.; Wall, J. F.; Kobusch, C.; Chen, X.; Peek, B. M., *Inorg. Chem.* **1994,** *33* (18), 3952-3964.
25. Clifford, J. N.; Palomares, E.; Nazeeruddin, M. K.; Grätzel, M.; Nelson, J.; Li, X.; Long, N. J.; Durrant, J. R., *J. Am. Chem. Soc.* **2004,** *126* (16), 5225-5233.
26. Haque, S. A.; Handa, S.; Peter, K.; Palomares, E.; Thelakkat, M.; Durrant, J. R., *Angew. Chem., Int. Ed.* **2005,** *44* (35), 5740-5744.

27. Polo, A. S.; Itokazu, M. K.; Murakami Iha, N. Y., *Coord. Chem. Rev.* **2004,** *248* (13-14), 1343-1361.

28. Mishra, A.; Fischer, M. K. R.; Bäuerle, P., *Angew. Chem., Int. Ed.* **2009,** *48* (14), 2474-2499.

29. Ooyama, Y.; Harima, Y., *Eur. J. Org. Chem.* **2009,** *2009* (18), 2903-2934.

30. Smestad, G. P.; Gratzel, M., *J. Chem. Educ.* **1998,** *75* (6), 752.

31. Bignozzi, C. A.; Argazzi, R.; Kleverlaan, C. J., *Chem. Soc. Rev.* **2000,** *29* (2), 87-96.

32. Nazeeruddin, M. K.; Zakeeruddin, S. M.; Lagref, J. J.; Liska, P.; Comte, P.; Barolo, C.; Viscardi, G.; Schenk, K.; Grätzel, M., *Coord. Chem. Rev.* **2004,** *248* (13-14), 1317-1328.

33. Islam, A.; Sugihara, H.; Arakawa, H., *J. Photochem. Photobiol., A Chem.* **2003,** *158* (2-3), 131-138.

34. Heimer, T. A.; Bignozzi, C. A.; Meyer, G. J., *J. Phys. Chem.* **1993,** *97* (46), 11987-11994.

35. Kuciauskas, D.; Freund, M. S.; Gray, H. B.; Winkler, J. R.; Lewis, N. S., *J. Phys. Chem. B* **2001,** *105* (2), 392-403.

36. Altobello, S.; Argazzi, R.; Caramori, S.; Contado, C.; Da Fre, S.; Rubino, P.; Chone, C.; Larramona, G.; Bignozzi, C. A., *J. Am. Chem. Soc.* **2005,** *127* (44), 15342-15343.

37. Islam, A.; Sugihara, H.; Hara, K.; Singh, L. P.; Katoh, R.; Yanagida, M.; Takahashi, Y.; Murata, S.; Arakawa, H.; Fujihashi, G., *Inorg. Chem.* **2001,** *40* (21), 5371-5380.

38. Geary, E. A. M.; Yellowlees, L. J.; Jack, L. A.; Oswald, I. D. H.; Parsons, S.; Hirata, N.; Durrant, J. R.; Robertson, N., *Inorg. Chem.* **2005,** *44* (2), 242-250.

39. Hasselmann, G. M.; Meyer, G. J., *J. Phys. Chem. B* **1999,** *103* (36), 7671-7675.

40. Alonso-Vante, N.; Nierengarten, J.-F.; Sauvage, J.-P., *J. Chem. Soc., Dalton Trans.* **1994,** (11), 1649-1654.

41. Bessho, T.; Constable, E. C.; Grätzel, M.; Redondo, A. H.; Housecroft, C. E.; Kylberg, W.; Nazeeruddin, M. K.; Neuburger, M.; Schaffner, S., *Chem. Commun.* **2008,** (32), 3717-3719.

42. Ferrere, S., *Chem. Mater.* **2000,** *12* (4), 1083-1089.

43. Ferrere, S.; Gregg, B. A., *J. Am. Chem. Soc.* **1998,** *120* (4), 843-844.

44. Nazeeruddin, M. K.; De Angelis, F.; Fantacci, S.; Selloni, A.; Viscardi, G.; Liska, P.; Ito, S.; Takeru, B.; Grätzel, M., *J. Am. Chem. Soc.* **2005,** *127* (48), 16835-16847.

45. Argazzi, R.; Larramona, G.; Contado, C.; Bignozzi, C. A., *J. Photochem. Photobiol., A* **2004,** *164* (1-3), 15-21.

46. Imahori, H.; Umeyama, T.; Ito, S., *Acc. Chem. Res.* **2009,** *42* (11), 1809-1818.

47. Hagberg, D. P.; Yum, J.-H.; Lee, H.; De Angelis, F.; Marinado, T.; Karlsson, K. M.; Humphry-Baker, R.; Sun, L.; Hagfeldt, A.; Grätzel, M.; Nazeeruddin, M. K., *J. Am. Chem. Soc.* **2008,** *130* (19), 6259-6266.

48. Wang, Z.-S.; Cui, Y.; Dan-oh, Y.; Kasada, C.; Shinpo, A.; Hara, K., *J. Phys. Chem. C* **2007,** *111* (19), 7224-7230.

49. Yum, J.-H.; Walter, P.; Huber, S.; Rentsch, D.; Geiger, T.; Nüesch, F.; De Angelis, F.; Grätzel, M.; Nazeeruddin, M. K., *J. Am. Chem. Soc.* **2007,** *129* (34), 10320-10321.

50. Edvinsson, T.; Li, C.; Pschirer, N.; Schöneboom, J.; Eickemeyer, F.; Sens, R.; Boschloo, G.; Herrmann, A.; Müllen, K.; Hagfeldt, A., *J. Phys. Chem. C* **2007,** *111* (42), 15137-15140.

51. Forneli, A.; Planells, M.; Sarmentero, M. A.; Martinez-Ferrero, E.; O'Regan, B. C.; Ballester, P.; Palomares, E., *J. Mater. Chem.* **2008,** *18* (14), 1652-1658.

52. Cid, J. J.; Yum, J. H.; Jang, S. R.; Nazeeruddin, M. K.; Martinez-Ferrero, E.; Palomares, E.; Ko, J.; Grätzel, M.; Torres, T., *Angew. Chem., Int. Ed.* **2007,** *46* (44), 8358-8362.

54. Kay, A.; Graetzel, M., *J. Phys. Chem.* **1993,** *97* (23), 6272-6277.
55. Calogero, G.; Marco, G. D., *Sol. Energy Mater. Sol. Cells* **2008,** *92* (11), 1341-1346.
56. Kong, F. T.; Dai, S. Y.; Wang, K. J., *Adv. OptoElec.* **2007,** *2007*.
57. Wang, Z.-S.; Sayama, K.; Sugihara, H., *J. Phys. Chem. B* **2005,** *109* (47), 22449-22455.
58. Oskam, G.; Bergeron, B. V.; Meyer, G. J.; Searson, P. C., *J. Phys. Chem. B* **2001,** *105* (29), 6867-6873.
59. Bergeron, B. V.; Marton, A.; Oskam, G.; Meyer, G. J., *J. Phys. Chem. B* **2004,** *109* (2), 937-943.
60. Gregg, B. A.; Pichot, F.; Ferrere, S.; Fields, C. L., *J. Phys. Chem. B* **2001,** *105* (7), 1422-1429.
61. Sapp, S. A.; Elliott, C. M.; Contado, C.; Caramori, S.; Bignozzi, C. A., *J. Am. Chem. Soc.* **2002,** *124* (37), 11215-11222.
62. Nusbaumer, H.; Moser, J.-E.; Zakeeruddin, S. M.; Nazeeruddin, M. K.; Gratzel, M., *J. Phys. Chem. B* **2001,** *105* (43), 10461-10464.
63. Hattori, S.; Wada, Y.; Yanagida, S.; Fukuzumi, S., *J. Am. Chem. Soc.* **2005,** *127* (26), 9648-9654.
64. Kopidakis, N.; Schiff, E. A.; Park, N. G.; van de Lagemaat, J.; Frank, A. J., *J. Phys. Chem. B* **2000,** *104* (16), 3930-3936.
65. Watson, D. F.; Meyer, G. J., *Coord. Chem. Rev.* **2004,** *248* (13-14), 1391-1406.
66. Papageorgiou, N.; Athanassov, Y.; Armand, M.; Bonhote, P.; Pettersson, H.; Azam, A.; Gratzel, M., *J. Electrochem. Soc.* **1996,** *143* (10), 3099-3108.
67. Gorlov, M.; Kloo, L., *Dalton Trans.* **2008,** (20), 2655-2666.
68. Zakeeruddin, S. M.; Grätzel, M., *Adv. Funct. Mater.* **2009,** *19* (14), 2187-2202.
69. Welton, T., *Chem. Rev.* **1999,** *99* (8), 2071-2084.
70. Nogueira, A. F.; Longo, C.; De Paoli, M. A., *Coord. Chem. Rev.* **2004,** *248* (13-14), 1455-1468.
71. Murakami, T. N.; Grätzel, M., *Inorg. Chim. Acta* **2008,** *361* (3), 572-580.
72. Papageorgiou, N.; Maier, W. F.; Gratzel, M., *J. Electrochem. Soc.* **1997,** *144* (3), 876-884.
73. Murakami, T. N.; Ito, S.; Wang, Q.; Nazeeruddin, M. K.; Bessho, T.; Cesar, I.; Liska, P.; Humphry-Baker, R.; Comte, P.; Pechy, P.; Gratzel, M., *J. Electrochem. Soc.* **2006,** *153* (12), A2255-A2261.
74. Schlichthorl, G.; Huang, S. Y.; Sprague, J.; Frank, A. J., *J. Phys. Chem. B* **1997,** *101* (41), 8141-8155.
75. Pelet, S.; Moser, J.-E.; Gratzel, M., *J. Phys. Chem. B* **2000,** *104* (8), 1791-1795.
76. Neale, N. R.; Kopidakis, N.; van de Lagemaat, J.; Grätzel, M.; Frank, A. J., *J. Phys. Chem. B* **2005,** *109* (49), 23183-23189.
77. Zhang, Z.; Evans, N.; Zakeeruddin, S. M.; Humphry-Baker, R.; Grätzel, M., *J. Phys. Chem. C* **2007,** *111* (1), 398-403.
78. Fredin, K.; Nissfolk, J.; Boschloo, G.; Hagfeldt, A., *J. Electroanal. Chem.* **2007,** *609* (2), 55-60.
79. Kusama, H.; Kurashige, M.; Arakawa, H., *J. Photochem. Photobiol., A* **2005,** *169* (2), 169-176.
80. Boschloo, G.; Haeggman, L.; Hagfeldt, A., *J. Phys. Chem. B* **2006,** *110* (26), 13144-13150.
81. Neale, N. R.; Kopidakis, N.; van de Lagemaat, J.; Gratzel, M.; Frank, A. J., *J. Phys. Chem. B* **2005,** *109* (49), 23183-23189.

82. Lee, K.-M.; Suryanarayanan, V.; Ho, K.-C.; Justin Thomas, K. R.; Lin, J. T., *Sol. Energy Mater. Sol. Cells* **2007,** *91* (15+16), 1426-1431.

Chapter 2. Coordination chemistry of 2,2'-bipyridines, 2,2':6',2''-terpyridines and 1,10-phenanthrolines with ruthenium

Despite the many different kinds of photosensitisers, ruthenium polypyridyl complexes are the most commonly used and well studied. Chapter 2 consists of an introduction to the synthetic methods, properties and main applications of polypyridyl ligands coordinated to ruthenium.

TABLE OF CONTENTS

2.1. Introduction to bipyridines, terpyridines and phenanthrolines

Pyridine is an important aromatic heterocyclic organic compound, and its structure is present in many natural products and synthetic molecules.[1] Pyridyl moieties are versatile building blocks for the preparation of polypyridyl ligands.[2]

Oligopyridines are molecules of great importance due to their ability to form stable complexes with numerous metal centers. The structure of these ligands strongly affects their optical and electrochemical properties. The functionalisation of polypyridyl ligands with different groups allows their use in a wide range of applications, which exploit their photophysical, photochemical and redox properties.

Bipyridines and terpyridines are heterocyclic aromatic molecules based on 6-membered nitrogen containing rings, linked through a single bond between the different carbon positions of the pyridyl moieties.

The most used and best studied bipyridine is the bidentate chelate 2,2’-bipyridine (bpy), due to its ability to form stable complexes with metals.[3] However, six possible bipyridine regioisomers can be distinguished (Figure 2.1), from which three are symmetrical isomers (2,2’-, 3,3’- and 4,4’-), while the other three are asymmetrical isomers (2,3’-, 2,’4’- and 3,4’-).[4]

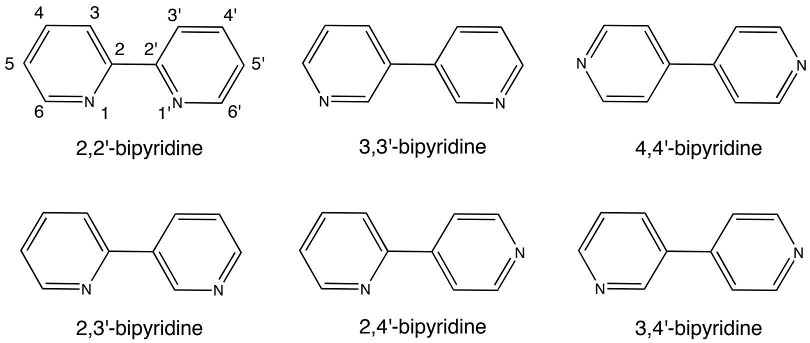

Figure 2.1. Molecular structure of the 6 possible isomers of bipyridine

Similarly to bipyridines, there is a wide range of terpyridine isomers with variations on the interconnection between the pyridyl rings (Figure 2.2). Depending on the relative position of the nitrogen atoms, these terpyridine ligands can bind metals as tridentate, bidentate, monodentate or bridging ligands. Specifically, 2,2':6',2"-terpyridine (tpy) is an important isomer due to its ability to act as a tridentate ligand in the formation of coordination compounds with a wide range of metal centers.[5] This molecule contains three nitrogen atoms with the pyridyl rings attached through their *ortho*-positions.

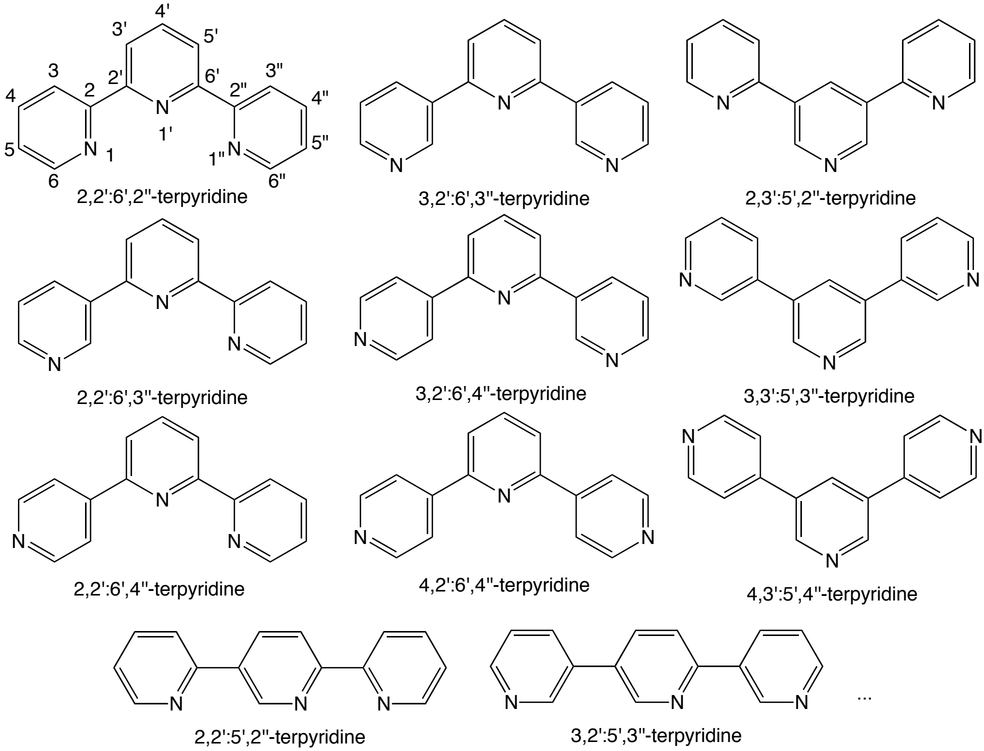

Figure 2.2. Molecular structures of some of the possible terpyridine isomers

Numerous derivatives have been prepared from the basic bipyridine and terpyridine structures upon functionalisation with different groups (Figure 2.3). Synthetic approaches to polypyridyl derivatives include both the functionalisation with substituent groups at the different positions of the aromatic rings and the incorporation of fused aromatic or aliphatic rings.

Selective functionalisation of polypyridyl ligands with electron-donating or electron-withdrawing groups is often used to modify the redox and photophysical properties of their coordination complexes, as well as to anchor the ligands or the metal complexes to solid surfaces.[6] However, the introduction of substituents at certain positions can break the symmetry of the ligand, leading to the formation of various isomers when coordinated to metals. The different isomers of polypyridyl metal complexes can show divergent photophysical, photochemical and electrochemical properties, as well as having an isomer mixture can be a disadvantage for some applications such as biological labelling or some catalytic processes. It is worth pointing out that the introduction of different substituents at the 4' position of the 2,2':6',2"-terpyridine ligand does not increase the number of isomers when coordinated to a metal center.[7]

One of the most important bipyridine derivatives are phenanthrolines, whose structure contains a fused aromatic ring between the two pyridyl groups.[8, 9]

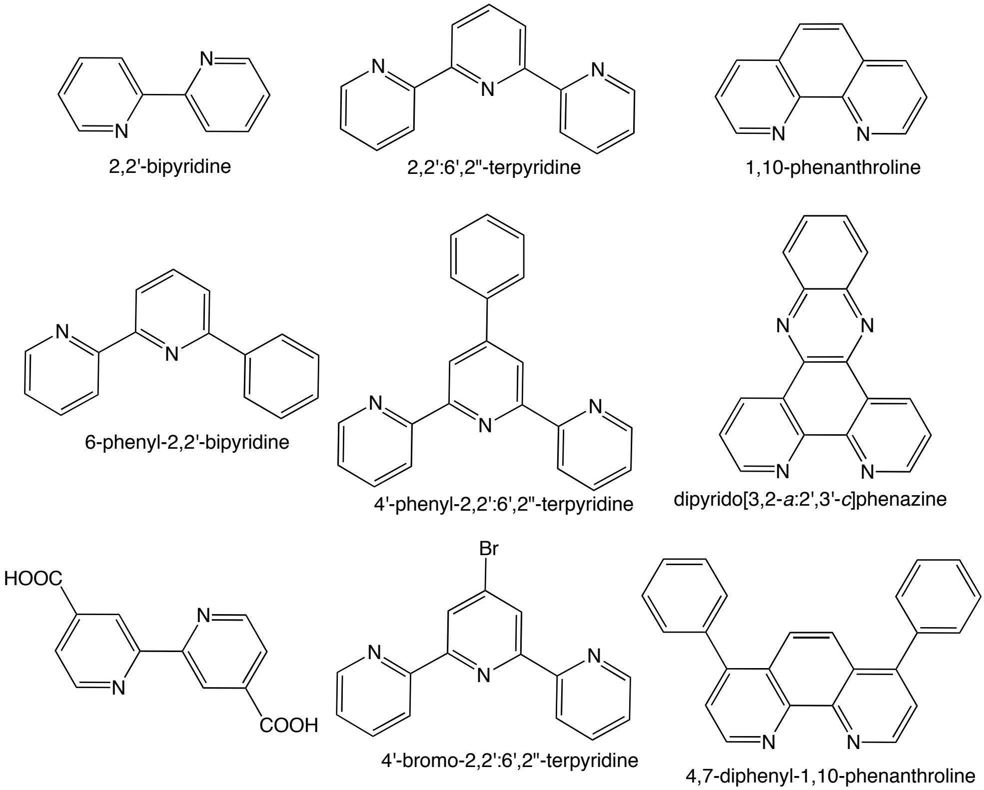

Figure 2.3. Polypyridyl bidentate and tridentate ligands derived from bipyridine and terpyridine units

Phenanthrolines are aromatic molecules composed of three fused benzene rings with two carbons replaced by two nitrogen atoms in a peripheral position in each of the two outer rings. Consequently, ten phenanthroline isomers can be found depending on the position of the nitrogen atoms (Figure 2.4): 1,10-, 1,9-, 1,8-, 1,7-, 2,7-, 2,8-, 2,9-, 3,7-, 3,8-, 4,7-. However, the most common phenanthroline is the 1,10- isomer (phen), also called *o*-phenanthroline.

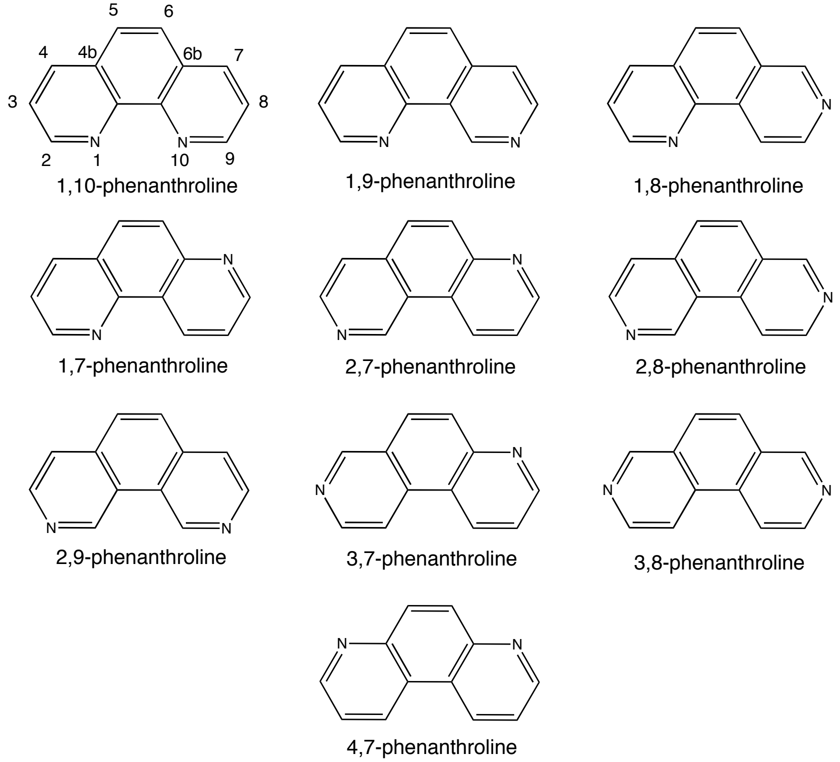

1,10-phenanthroline
1,9-phenanthroline
1,8-phenanthroline
1,7-phenanthroline
2,7-phenanthroline
2,8-phenanthroline
2,9-phenanthroline
3,7-phenanthroline
3,8-phenanthroline
4,7-phenanthroline

Figure 2.4. Molecular structure of the different regioisomers of phenanthroline

As shown before, there exists a wide range of derivatives and isomers for bipyridines, terpyridines and phenanthrolines depending on the nature and number of substituents, as well as on the relative position of their nitrogen atoms. From this enormous group of molecules, this thesis is focused on the study of 2,2'-bipyridine (bpy), 1,10-phenanthroline (phen) and 2,2':6',2"-terpyridine (tpy).

2.1.1. Coordination chemistry

The major application of nitrogen containing aromatic heterocycles involves the formation of complexes with numerous metal centers.[3, 5, 10] Polypyridyl ligands interact with the d orbitals of transition metals through both σ-donor and π-acceptor molecular orbitals located on the nitrogen atoms and the conjugated aromatic system, respectively. Furthermore, the geometry and the angle between the different nitrogen donor atoms (bite angle) strongly affects the nature of the bond between the pyridine-based chelating ligands and the metal center.[2]

The pyridyl moieties of non-coordinated 2,2'-bipyridine can rotate around the inter-ring C-C bond, and its torsional angle reaches a minimum in energy when the two pyridyl moieties are coplanar and with the nitrogens in a *trans* conformation.[11] This planar spatial disposition is favourable due to the π-conjugation of the rings, while the repulsive interaction between the nitrogen lone electron pairs induces a twist of 180 ° to the angle between the pyridyl rings. On the other hand, this molecule adopts a *cis* planar conformation when linked in a bidentate mode to a metal center, forming a stable five-membered ring (Figure 2.5).

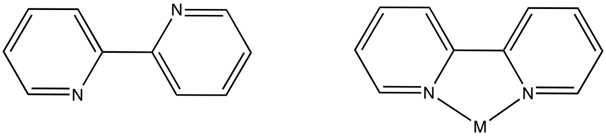

Figure 2.5. Molecular conformation of 2,2′-bipyridine as free ligand (left) and coordinated to a metal ion (right)

The 2,2':6',2"-terpyridine molecule commonly acts as tridentate meridional ligand in the formation of coordination compounds with a wide range of metal centers.[5] Moreover, the mono- and bidentate species are thought to be intermediates in the formation of the complexes.

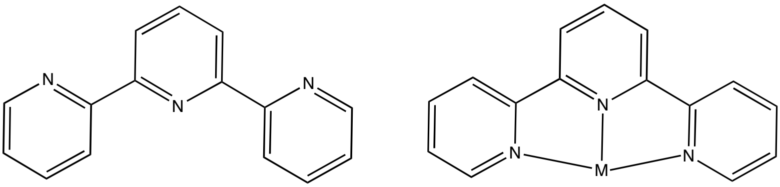

Figure 2.6. Molecular conformation of 2,2′:6′,2″-terpyridine as free ligand (left) or coordinated to a metal center (right)

Terpyridines, in the solid state, adopt a planar conformation with the nitrogen atoms in a *trans*, *trans* relative spatial disposition to one other, in order to minimise the repulsion of the nitrogen lone electron pairs. However, when a terpyridine is coordinated to a metal center in a tridentate mode, the ligand adopts a planar *cis*,*cis* conformation, resulting in a change in the angle between the central and the terminal rings and in the bond lengths (Figure 2.6).[12]

Most of the phenanthrolines are solids, with a rigid structure due to the presence of the central ring. Therefore, the two nitrogen atoms are forced into a *cis* conformation allowing a faster complexation with metals.[10, 13]

The chemistry of 2,2'-bipyridines, 2,2':6',2''-terpyridines, 1,10-phenanthrolines and their derivatives has been extensively studied.[2] Numerous synthetic procedures involving coupling reactions, cycloadditions, condensations and other methods have been developed for the preparation of polypyridyl ligands and their deivatives.[6, 14-16]

2.1.2. Main characteristics and applications

Polypyridyl ligands, when non-coordinated to metals, exhibit intense absorption bands in the ultraviolet (UV) region. The absorption spectra is red shifted under acidic conditions, indicative of the protonation of the nitrogen atoms.[17]

The presence of low lying π^* molecular orbitals in most of the bipyridines, terpyridines and phenanthrolines allows for a non-radiative relaxation of the excited state through an intersystem crossing and/or internal conversion and, thus, the molecules are not fluorescent in organic solvents.[18-20] However, the introduction of substituents, such as highly extended conjugated moieties or electron donor groups can increase the luminescence quantum yield.[21]

These optical properties of polypyridyl ligands, together with their ability to form coordination complexes with a variety of metal ions, allows their application in analytical chemistry. The UV-visible or the luminescence spectra of these ligands can change upon the recognition of a specific analyte, allowing the use of these molecules as fluorescent or colorimetric chemosensors (Figure 2.7).[22, 23]

Figure 2.7. Observed luminescence quenching of 3,3'-dihydroxybipyridine upon the addition of 10^{-3} M Cu^{2+}. Source: [24]

As previously mentioned, 2,2'-bipyridines, 2,2':6',2''-terpyridines and 1,10-phenanthrolines can interact through the nitrogen atoms as bi- or tridentate chelate ligands with a large number of metals of different sizes and charges, with the formation of five membered rings.[10] However, it must be mentioned that other isomers of this group of molecules can act as a bridge between two metal centers or as monodentate ligands.[25] This group of nitrogen containing heterocyclic molecules are neutral ligands that form charged complexes when coordinated to metal cations. Although this kind of ligand can stabilise a wide range of different oxidation states, the greater part of transition metal ions coordinated to nitrogen-containing heterocyclic ligands are found in the +2 or +3 oxidation states, acquiring an octahedral, tetrahedral or square planar geometry.[5]

The major application of polypyridyl ligands is due to the photophysical, photochemical and electrochemical properties which are derived from their complexation with almost all the transition, alkaline, alkaline earth and lanthanide metals. Polypyridyl complexes have been extensively studied and used in a wide range of applications, such as supramolecular chemistry,[26] solar light harvesting,[27] luminescence labelling of biological molecules,[28] catalysis[29] and light emitting devices[30].

Special attention has been paid during the last 30 years to the spectroscopic and redox properties of ruthenium polypyridyl complexes, which have been widely studied and used in many fields.[31, 32] The characteristics and main applications of ruthenium complexes is further discussed in the following section.

2.2. Introduction to ruthenium polypyridyl complexes

Ruthenium was discovered in 1844 in Tartu, Estonia, by Karl Karlovitch Klaus, who named this new metal *Ruthenia*, the latin name for Russia.[33]

Ruthenium, just like osmium, is a unique metal due to its ability to form complexes covering the widest range of oxidation states theoretically allowed for a transition metal: from 8 in [RuO_4] to -2 in [$Ru(CO)_4$], the most common being $Ru^{(II)}$ and $Ru^{(III)}$ oxidation states.[34] The kinetic stability of the ruthenium complexes formed in a broad range of oxidation states, the reversible nature of most of their redox pairs and the wide range of well-known synthetic reactions for their preparation make these complexes very attractive for use in a wide range of studies. In this work, attention has been particularly focused on the study of $Ru^{(II)}$ complexes.

The bonding properties of ruthenium complexes can be explained by crystal field theory and molecular orbital theory. From the point of view of crystal field theory, the properties of ruthenium complexes arise from electrostatic interactions between the metal ion and chelating ligands, which result in the splitting of d-orbital energies. From the molecular orbital theory point of view, the ruthenium properties can be explained from the charge transfer between the metal and chelating ligands due to the interaction between the s, p and d atomic orbitals of the metal center, which have appropriate geometry with the orbitals of the chelating ligands.

The coordination chemistry of ruthenium with oligopyridine ligands has been extensively studied. Due to the very many polypyridyl ligands available, ruthenium polypyridyl complexes are extremely versatile with wide ranging photophysical, photochemical and redox properties which can be optimised for a particular purpose.[31] In addition to the many well known synthetic reactions for the preparation of ruthenium complexes, the possibility of the functionalisation of these ligands with appropriate anchoring groups allows the attachment of these complexes onto a variety of surfaces.

2.3. Properties of ruthenium complexes with polypyridyl ligands

2.3.1. Photophysical and photochemical properties

A photochemical or photophysical process takes place when a molecule absorbs a photon and promotes an electron from the ground state to the excited state. This high energy state is unstable and thus, the molecule tends to undergo some type of deactivation process. Excited state deactivation can occur *via* (a) the emission of light (luminescence), (b) the liberation of the excess energy in form of heat (thermal deactivation), (c) the interaction with other molecules present in the local environment (quenching process) and (d) the formation of a new species (photochemical reaction).[35]

The photochemistry of ruthenium complexes coordinated to different polypyridyl ligands has been extensively investigated in the last few decades.[36] Specifically, the prototype molecule $[Ru(bpy)_3]^{2+}$ has been one of the most studied molecules due to its high stability, strong and long-lived luminescence and ability to undergo redox reactions.

2.3.1.1. Absorption spectroscopy

Polypyridyl complexes of $Ru^{(II)}$ have a d^6 electronic configuration and a preferred octahedral geometry. Surrounding the metal ion, polypyridine ligands interact with ruthenium through σ-donor orbitals located on the nitrogen atoms and π-donor and π*-acceptor molecular orbitals delocalised on the aromatic rings.[37] The spectroscopical and electrochemical properties of ruthenium complexes are usually described through a simplified linear combination of atomic orbitals (Figure 2.8).[38] Each molecular orbital is denominated as metal (M) or ligand (L) in agreement with its prevalent localisation.

The molecular orbital diagram for an octahedral complex of a transition metal such as $Ru^{(II)}$ indicates that different transitions between the different chelating ligands and metal orbitals can take place upon the absorption of light. These transitions can be classified as (a) metal-centered transitions (MC), also called d-d transitions, when the electrons are promoted from a π_M metal orbital to a σ^*_M orbital; (b) ligand-centered (LC) or π-π* ligand to ligand transitions, for transitions mainly localised on the chelating ligands, and (c) transitions between molecular orbitals with different localisation: metal-to-ligand charge transfer (MLCT), or ligand-to-metal charge transfer transitions (LMCT). Electronic transitions that occur to a lesser extent are those from a metal-centered orbital to solvent (charge transfer to solvent, CTTS).[38]

The light absorption processes are only allowed for transitions in which the ground and the excited state have the same spin value. These transitions can be observed as intense bands in the absorption spectra of the molecules. On the other hand, transitions from the ground state to excited states with different spin values are considered forbidden and can rarely be observed in absorption spectra.

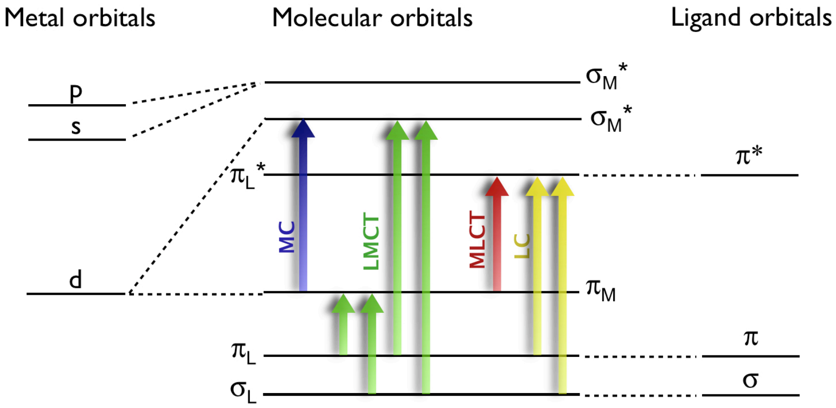

Figure 2.8. Simplified molecular orbital diagram for a transition metal complex in an octahedral geometry showing different electronic transitions

The MC, MLCT and LC transitions of an octahedral transition metal complex are related to the ligand field strength, the redox potential of the metal complex and the intrinsic properties of the ligands, respectively.[39] For this reason, changes in the molecular structure of the ligands attached to the ruthenium metal ion can vary dramatically the relative energy positions of the excited states, with the consequent change in their photophysical properties.[40]

2.3.1.2. Emission spectroscopy

The behaviour of excited species is usually represented in a Jablonski diagram (Figure 2.9). In most of the ruthenium polypyridyl complexes, three states are involved in the photochemical activation process: a singlet ground state and a singlet and triplet excited state.

The multiplicity of the ground state for most ruthenium (II) polypyridyl complexes is a singlet (S_0) and the absorption of a photon leads to the promotion of an electron from an occupied orbital to a higher energy unoccupied orbital with the same spin multiplicity (S_1). However, the lowest excited state is often a triplet (T_1) and, although it cannot be populated with excited electrons directly by light absorption, it can be so through the deactivation of higher excited states. The S_1 state rapidly decays *via* intersystem crossing to the T_1 due to the strong spin-orbital coupling in metal complexes.[31] The quantum yield for the formation of the lowest triplet excited state is often equal to 100 %, yielding a short-lived fluorescence. The photo-excited state deactivation occurs though both a radiative (phosphorescence) and a non-radiative way.

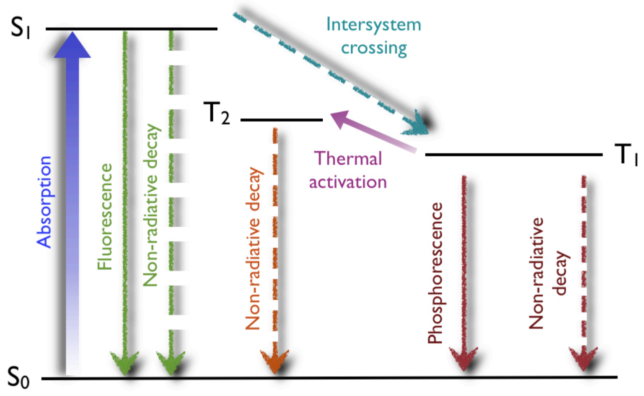

Figure 2.9. Jablonski diagram for ruthenium polypyridyl complexes

Most ruthenium bipyridyl complexes show a lowest excited state as a triplet T_1, whose deactivation results in an intense long-lived luminescence. However, at high temperatures, radiationless deactivation can take place *via* thermally activated T_2 metal centered excited state.

The behaviour of ruthenium terpyridyl complexes is completely different from their bipyridyl analogues.[41] No emission is detected at room temperature in ruthenium terpyridyl complexes due to a non-radiative relaxation of the excited state (T_1) *via* a transition by a T_2 metal centered excited state to the ground state. However, when the temperature decreases, the transition is less efficient and some luminescence can be observed. Furthermore, the optical properties of these complexes can be modified by the introduction of substituents on the ligands, allowing improvements in the luminescence quantum efficiency and/or lifetime.[42]

The observed excited state lifetime (τ) of the ruthenium polypyridyl complexes depends on the rate constants for radiative (k_r) and non-radiative (k_{nr}) decays to the ground state. The emission lifetime which can be described by the Arrhenius equation (where k_t is the pre-factor for the thermally activated process and E_a is the activation energy barrier to the T_2 state) (Equation 2.1).[43] The relationship between the emission quantum yield (Φ) and k_r is given by Equation 2.2 (η_{isc} is the efficiency of intersystem crossing, normally considered unity).

$$1/\tau = k_r + k_{nr} + k_t^{\left(E_a/R\cdot T\right)} \qquad \text{(Equation 2.1)}$$

$$\Phi = \eta_{isc} \cdot k_r \cdot \tau \qquad \text{(Equation 2.2)}$$

The thermal population of the short-lived metal centered states has an important effect on the excited state lifetime of the molecules. Some ruthenium bis(tridentate) complexes show fast emission decays due to the non-radiative deactivation of the lowest excited state T_1 *via* thermal population of the metal centered orbital T_2. For this reason, an increase of the energy gap between the T_1 and the T_2 excited states it is a good approach for increasing the excited state lifetime.[44]

2.3.2. Redox properties

Ru^{2+} polypyridyl complexes are octahedral and diamagnetic, with a t_{2g}^6 configuration. However, due to their high number of stable oxidation states, ruthenium polypyridyl complexes serve as both electron acceptor and electron donors.[45]

The oxidation of a d^6 Ru^{2+} polypyridine complex involves removal of an electron from the highest energy occupied molecular orbital (HOMO), usually a π_M (t_{2g}) metal centered orbital, with the formation of paramagnetic low spin d^5 Ru^{3+} complexes, which are inert to ligand substitution (Equation 2.3).

$$[Ru^{II}(NN)_3]^{2+} \rightarrow [Ru^{II}(NN)_3]^{3+} + e^- \qquad \text{(Equation 2.3)}$$

On the other hand, the reduction of a $Ru^{(II)}$ polypyridyl complex may involve the introduction of one electron into the lowest unoccupied molecular orbital (LUMO), located either into a metal-centered (σ^*_M) or into a ligand-centered orbital (π^*_L), depending on their relative energy level arrangement. Generally, polypyridine ligands coordinated to ruthenium metal ions are easily reduced, and the reduction takes place on the ligand (Equation 2.4). In this case, ruthenium metal ions maintain their d^6 low spin configuration. These species are usually inert and the reduction reaction is reversible. However, when the lowest energy empty orbital is a metal centered orbital, the electron is added to the metal centered orbital. The reduction of these complexes produce an unstable low spin d^7 electronic configuration which leads to a rapid ligand dissociation, which makes the reaction irreversible (Equation 2.5).

$[Ru^{II}(NN)_3]^{2+} + e- \rightarrow [Ru^{II}(NN)_2(NN^-)]^{2+}$ (Equation 2.4)

$[Ru^{II}(NN)_3]^{2+} + e- \rightarrow [Ru^{I}(NN)_3]^{+} \rightarrow [Ru^{I}(NN)_2]^{+} + NN$ (Equation 2.5)

The electrochemical behaviour of polypyridyl ruthenium complexes depends on the nature of the ligands surrounding the metal ion. The redox potentials of a metal couple can be predicted by using the ligand electrochemical parameters (E_L) described by Lever in 1990.[46] E_L is a function of the σ and π donor and acceptor properties of the ligand and is independent to the metal in which the ligand is bound.[47]

2.3.3. Tuning of spectro-and electrochemical properties

The structure of the polypyridyl ligand determines the redox and spectroscopical properties of the ruthenium complex, which can be modified by the introduction of appropriate chelating ligands.[48] Generally, two strategies are used to tune these properties: (a) the modification of the LUMO energy level by introducing a ligand with a low-lying π* molecular orbital involved in the MLCT or (b) by destabilisation of the t_{2g} metal orbital (HOMO energy level), which is affected by the donor or acceptor properties of the ligands.[49]

The modification of the HOMO and LUMO energy levels has a direct effect over the MLCT transitions of the ruthenium complexes, and consequently induces a change in the absorption spectra of the molecule. Controllable adjustments of the excited state energy levels can be performed with an appropriate selection of the ligands involved in the MLCT (*e.g.* $[Ru(2,2'\text{-bipyridine})_3]^{2+}$ and $[Ru(2,2'\text{-bipyridine})_2(2,2'\text{-biquinoline})]^{2+}$). However, smaller changes in the LUMO energy levels are done by the simply introduction of substituents in the aromatic rings of the ligands (*e.g.* $[Ru(2,2'\text{-bipyridine})_3]^{2+}$ and $[Ru(4,4'\text{-dimethyl-}2,2'\text{-bipyridine})_3]^{2+}$). Furthermore, considerable changes in the spectral properties of the ruthenium complexes can be achieved upon substitution of a ligand not involved in the MLCT transition by a non-chromophoric donor ligand, which destabilises the metal t_{2g} orbitals (*e.g.* $[Ru(2,2'\text{-bipyridine})(2,2'\text{-biquinoline})_2]^{2+}$ and $[Ru(2,2'\text{-biquinoline})_2(CN)_2]$) (Figure 2.10).[31]

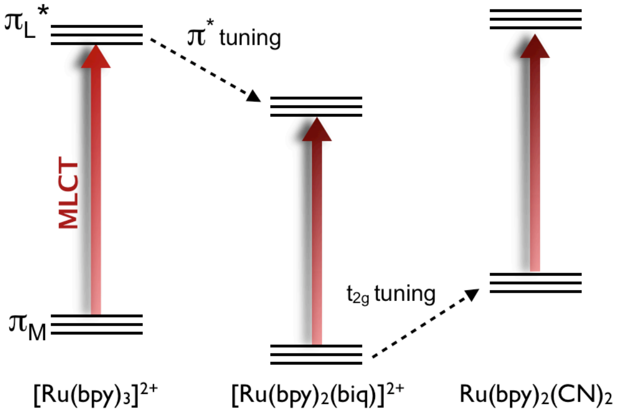

Figure 2.10. Tuning of HOMO (t_{2g}) and LUMO (π^*) orbital energy in various ruthenium polypyridyl complexes

2.4. Stereochemistry of ruthenium polypyridyl complexes

Another characteristic of octahedral metal complexes such as $Ru^{(II)}$ with bidentate ligands is their stereoisomerism.[50] For homoleptic tris(bidentate) complexes with symmetrical ligands (NN), two enantiomers are possible, called Δ and Λ (Figure 2.11a). Two geometrical isomers (facial (*fac*) and meridional (*mer*)) are possible for complexes with non-symmetrical bidentate chelate ligands (R-NN) (Figure 2.11b). However, the number of isomers increases to four and eight, respectively, when two $[Ru(\mathbf{R_1\text{-}NN_1})(\mathbf{R_2\text{-}NN_2})(\mathbf{NN})]$ or three $[Ru(\mathbf{R_1\text{-}NN_1})(\mathbf{R_2\text{-}NN_2})(\mathbf{R_3\text{-}NN_3})]$ unsymmetrical substituted ligands are linked to the ruthenium metal center (R_1-NN_1, R_2-NN_2 and R_3-NN_3 are different unsymmetrical nitrogen containing bidentate chelate ligands). For bis(bidentate) complexes two geometrical isomers can be formed (*cis/trans*) as well as two enantiomers of the *cis* form (Figure 2.11c). Furthermore, the number of possible isomers increases exponentially with the number of metal ions in the synthesis of polynuclear complexes.

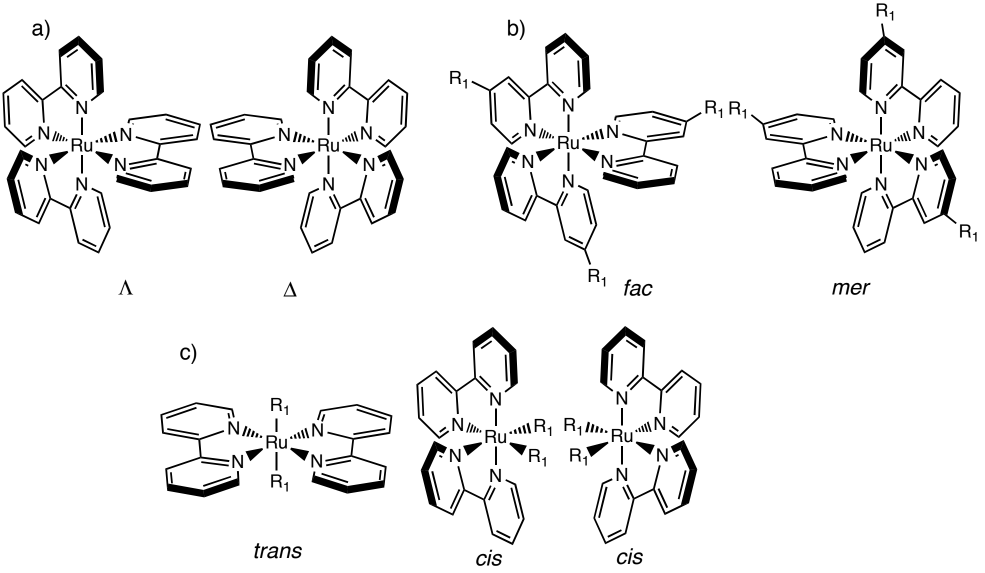

Figure 2.11. (a) Λ and Δ geometrical isomers of $Ru^{(II)}$ symmetrical tris(bidentate) complexes, (b) fac and mer isomers of $Ru^{(II)}$ tris(bidentate) complexes containing an unsymmetrical ligand, and (c) trans and two cis isomers of bis(bidentate) ruthenium complexes

In order to avoid stereochemical problems, several approaches have been used in the enantioselective synthesis of ruthenium complexes, such as the use of tridentate instead of bidentate ligands,[51] the utilisation of chiral building blocks to synthesise complexes with a predetermined stereochemistry,[52] and the light-induced isomerism in ruthenium complexes.[53]

The stereochemical problems are solved when tridentate ligands such as tpy are used, which are coordinated to the ruthenium metal center in a meridional form creating an achiral center. Furthermore, the introduction of a substituent in the 4' position of the terpyridine does not increase the number of geometrical isomers (Figure 2.12).[54]

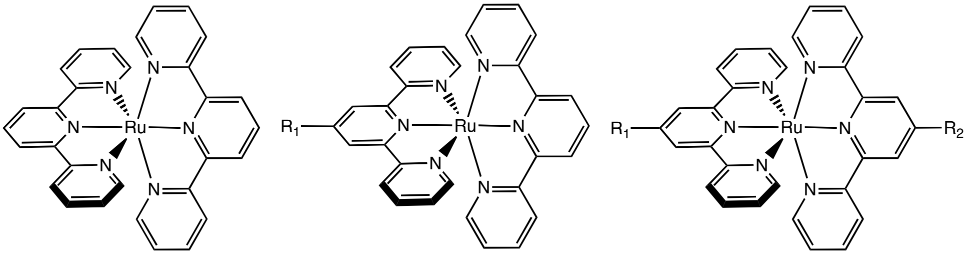

Figure 2.12. Ruthenium tris(bidentate) polypyridyl complexes without, with one, and with two substituents in the 4' position (from left to right)

2.5. Synthesis of ruthenium polypyridyl complexes

Ruthenium polypyridyl complexes have an extensive and well-known synthetic chemistry.[55] Their compounds show high stability and flexibility with a wide range of mono-, bi-, tri- and tetradentate ligands. Furthermore, ligands can be exchanged sequentially, removing some of them while maintaining the presence of others as well as the stereochemical integrity.

One of the most common synthetic precursor for ruthenium mononuclear polypyridyl complexes is the commercially available $RuCl_3{\cdot}xH_2O$. Some important intermediates in the synthesis of homo- and heteroleptic complexes such as $[Ru(CO)_2Cl_2]_n$,[56] Ru(dimethylsulfoxide)$_4$Cl$_2$ ($Ru(DMSO)_4Cl_2$),[57] $[Ru(\eta^6\text{-arene})Cl_2]_2$,[58] [Ru(1,5-cyclooctadiene)Cl$_2$]$_n$ ($[Ru(COD)Cl_2]_n$)[59] can be synthesised in one step from $RuCl_3{\cdot}xH_2O$. Several synthetic routes for the synthesis of homoleptic and heteroleptic polypyridyl ruthenium complexes are detailed below.

2.5.1. Synthesis of tris(bidentate) ruthenium complexes

The ruthenium (II) metal ion can accommodate three nitrogen-containing bidentate chelate ligands (NN), resulting in the possibility of the formation of homoleptic complexes ($[Ru(\mathbf{NN_1})_3]^{2+}$), bis-heteroleptic complexes ($[Ru(\mathbf{NN_1})_2(\mathbf{NN_2})]^{2+}$ and tris-heteroleptic complexes ($[Ru(\mathbf{NN_1})(\mathbf{NN_2})(\mathbf{NN_3})]^{2+}$).

2.5.1.1. Synthesis of ruthenium homoleptic complexes

The first synthesis of an homoleptic ruthenium compound reported in 1936 corresponds to the complex $[Ru(bpy)_3]Cl_2$.[60] Refluxing $RuCl_3{\cdot}xH_2O$ with an excess of a bipyridyl compound ($\mathbf{NN_1}$) results in the formation of ruthenium homoleptic tris(bidentate) ligand. This synthesis was extended to the incorporation of a wide range of bidentate ligands with the addition of a reducing agent such as phosphinic acid or hydroxylamine hydrochloride to the reaction mixture.[61,62]

Although the most simple reaction to obtain ruthenium tris-bipyridyl complexes is based on ruthenium (III) chloride, homoleptic compounds can also be prepared from other precursors such as $[Ru(\eta^6\text{-arene})Cl_2]_2$,[58] $[Ru(CO)_2Cl_2]_n$,[63] $Ru(DMSO)_4Cl_2$[64] or $[Ru(COD)Cl_2]_n$[65] involving a two-step reaction (Figure 2.13).

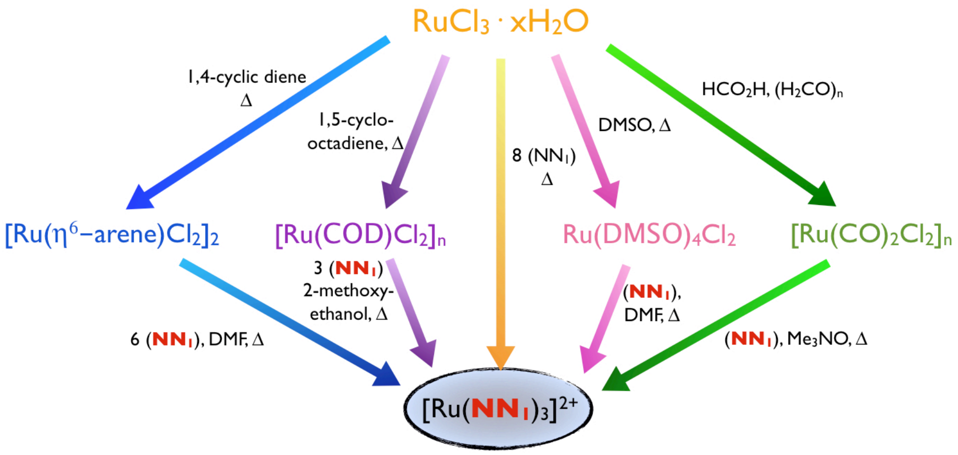

Figure 2.13. Synthetic routes of homoleptic ruthenium complexes containing three bidentate ligands. (NN_1) is a bidentate chelate ligand

An interesting alternative to the previous synthetic routes, which offers a reduction in the reaction time, consists of the microwave assisted reaction of different precursors such as $RuCl_3{\cdot}xH_2O$[66] or $[Ru(p\text{-}cymene)Cl_2]_2$[67].

2.5.1.2. Synthesis of ruthenium bis-heteroleptic complexes

In some cases, the coordination of different chelate ligands to the metal ion is necessary in order to modify the spectroscopic and electrochemical properties of the ruthenium complex for a specific application. Synthetic routes for ruthenium complexes of type $[Ru(NN_1)_2(NN_2)]^{2+}$ are based on the sequential introduction of ligands to a ruthenium precursor.

A widely used synthetic approach involves the introduction of two chelate ligands by the direct reaction of $RuCl_3{\cdot}xH_2O$ with two equivalents of the bidentate ligand, obtaining a $[Ru(NN_1)_2Cl_2]$ complex. Other precursors used in the synthesis of such complexes are $Ru(COD)Cl_2$[68] and $Ru(DMSO)_4Cl_2$[69], with the disadvantage of involving more than one synthetic steps. Subsequent introduction of a third diimine to the $[Ru(NN_1)_2Cl_2]$ complex in an appropriate medium results in the formation of $[Ru(NN_1)_2(NN_2)]^{2+}$ (Figure 2.14).[70]

Another synthetic method to obtain ruthenium bis-homoleptic complexes is based on the sequential introduction of three chelate ligands to the $[Ru(CO)_2Cl_2]_n$ oligomer.[71]

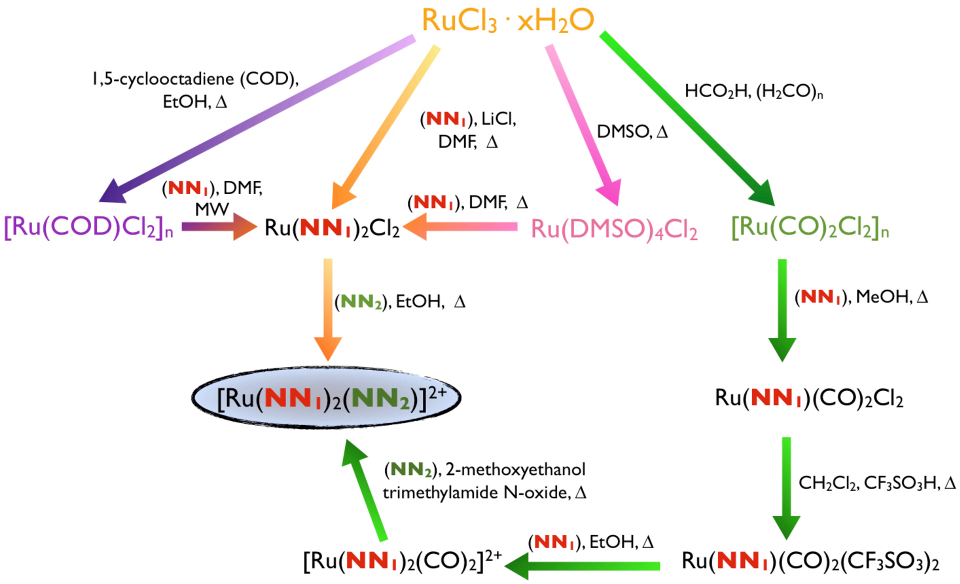

Figure 2.14. Synthetic routes of bis-heteroleptic ruthenium complexes containing three bidentate ligands. (NN_1) and (NN_2) are different bidentate chelate ligands

2.5.1.3. Synthesis of ruthenium tris-heteroleptic complexes

Several synthetic methodologies have been developed for the preparation of ruthenium tris-heteroleptic complexes. All of these synthetic routes are based on the sequential introduction of chelate ligands by substitution of labile ligands.

Two synthetic routes for the synthesis of $[Ru(NN_1)(NN_2)(NN_3)]^{2+}$ complexes using $[Ru(CO)_2Cl_2]_n$ as starting material have been extensively studied (Figure 2.15). The first step in both methodologies is the introduction of one chelate ligand. The subsequent decarbonylation steps differ. In the first method the labile CO ligands are substituted by the application of heat,[72] while in the second decarbonylation takes place by irradiation with UV light.[73]

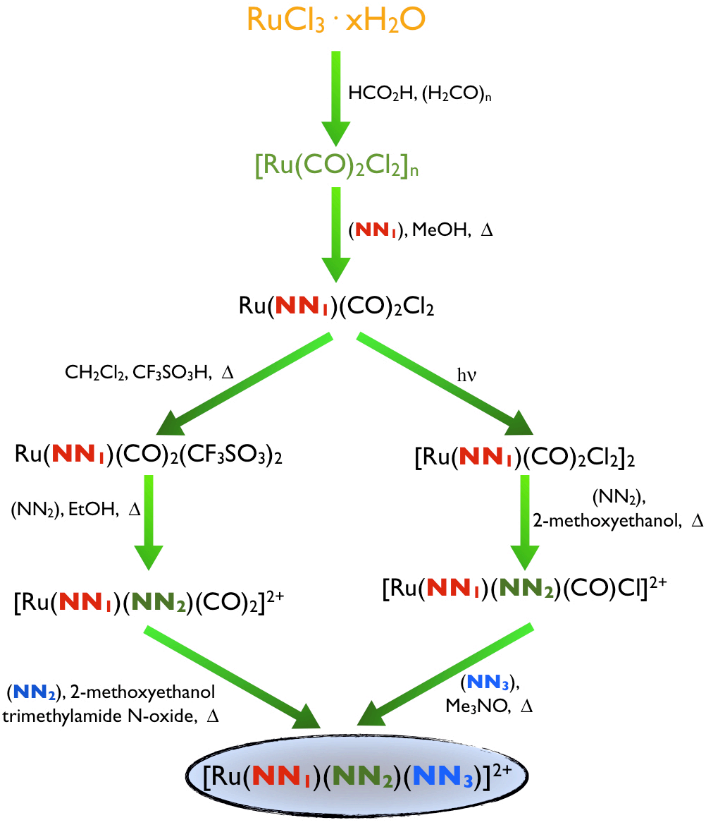

Figure 2.15. Synthetic routes of tris-heteroleptic ruthenium complexes containing three bidentate ligands using carbonyl complexes as a precursor. (NN_1), (NN_2) and (NN_3) are different bidentate chelate ligands

Other widely studied synthetic routes are based on synthesising $Ru(NN_1)(NN_2)Cl_2$ intermediates, using different precursors such as $RuCl_3{\cdot}xH_2O$,[70] $Ru(DMSO)_4Cl_2$[74] or $[Ru(\eta^6\text{-arene})Cl_2]_2$[58] as starting material and subsequent sequential introduction of chelate ligands under different reaction conditions (Figure 2.16).

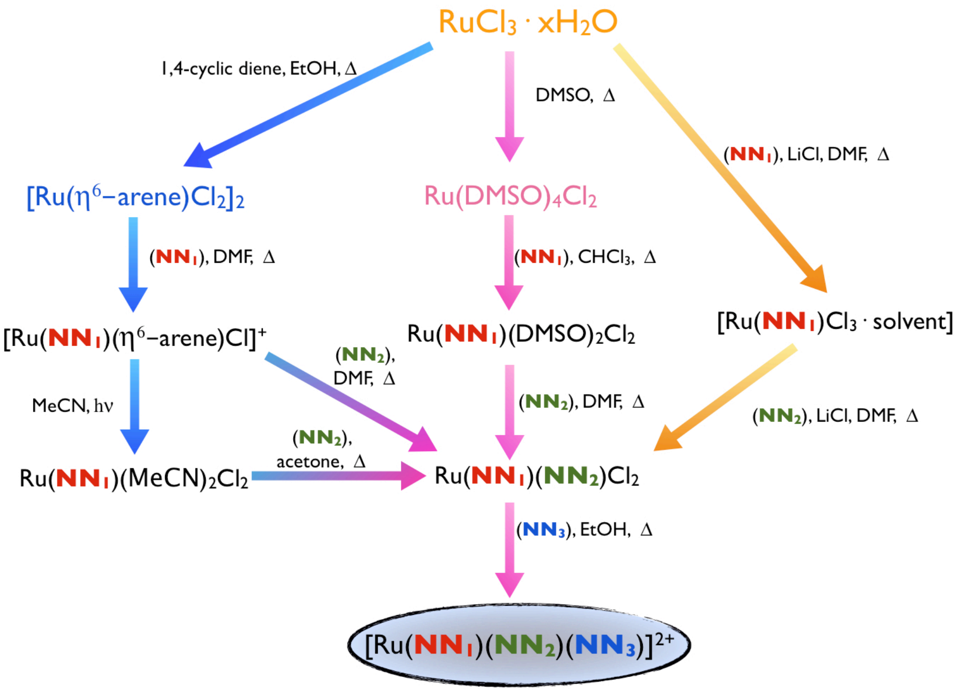

Figure 2.16. Synthetic routes of tris-heteroleptic ruthenium complexes containing three bidentate ligands using different precursors. (NN_1), (NN_2) and (NN_3) are different bidentate chelate ligands

2.5.2. Synthesis of bis(tridentate) ruthenium complexes

Complexation of ruthenium metal ions with two tridentate ligands leads to the formation of a complex with a distorted octahedral geometry.[54] Synthetic routes involve a two-step sequence, with the sequential introduction of two equal or different tridentate ligands.

The most widely used synthetic method uses $RuCl_3{\cdot}3H_2O$ as a precursor. The introduction of the first ligand results in the formation of $Ru(NNN_1)Cl_3$, where (NNN) is a nitrogen containing tridentate ligand. A reducing agent for the $Ru^{(III)} \rightarrow Ru^{(II)}$ conversion is necessary when the second ligand is coordinated to the metal ion.[42] This synthetic approach allows the synthesis of both homoleptic and heteroleptic ruthenium complexes by applying the same ligand twice or two different ligands. Furthermore, this synthesis can be carried out within a microwave, saving an enormous amount of time (Figure 2.17).[75]

An alternative procedure for ligands that can easily decompose is the synthesis under mild conditions of bis(tridentate) ruthenium complexes using $Ru(DMSO)_4Cl_2$ as starting material.[76]

A third synthetic strategy is available for obtaining symmetric bis(tridentate) complexes by reacting [Ru(η^6-arene)Cl$_2$]$_2$ with two equivalents of the ligand.[77]

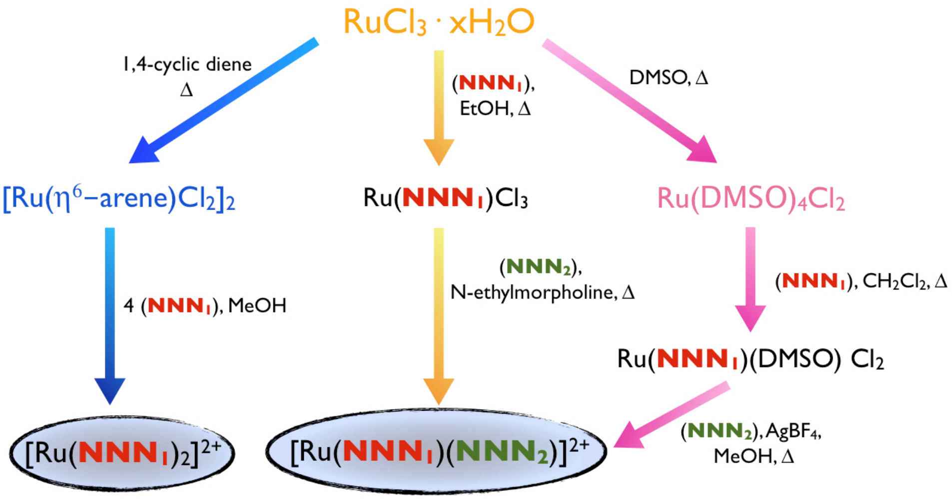

Figure 2.17. Synthetic routes of tris-heteroleptic ruthenium complexes containing three bidentate ligands using different precursors. (NNN$_1$) and (NNN$_2$) are different tridentate chelate ligands

2.6. Main uses and applications of ruthenium polypyridyl complexes

Ruthenium polypyridyl complexes have a wide range of applications in different areas due to their unique spectroscopical and electrochemical properties.[32] The popularity of these compounds arises from the ability to tune their properties by the introduction of different substituents, enabling the rational design of ruthenium complexes with the desired properties. Furthermore, chemical manipulation of the substituents allows the anchoring of these complexes onto a variety of surfaces.

2.6.1. Solar energy conversion

The potential of ruthenium polypyridyl complexes to act as photosensitisers in the conversion of solar energy into electrical energy has become an attractive subject of study.[27,48,78] Through appropriate molecular design, ruthenium polypyridyl complexes can exhibit a wide range of colours absorbing in different regions of the UV-visible spectrum, as well as having very different redox properties.

The breakthrough was achieved in 1991 with the first paper published by O'Regan and Grätzel, reporting a new type of solar cell based on the sensitisation of a wide band gap mesoporous semicondutor.[79] Since then, dye sensitised solar cells have been extensively investigated.

The application of ruthenium polypyridyl complexes as photosensitisers is discussed in further detail in Chapter 3.

2.6.2. Water splitting and CO_2 reduction

The goal of artificial photosynthesis is to mimic the conversion of water and sunlight carried out by plants and other photosynthetic organisms to obtain environmentally friendly energy sources.[80] An interesting reaction which results in the formation of carbon free fuels (H_2) is the splitting of water.

Light induced homogeneous (or partially homogeneous) water splitting devices at a molecular level involve at least three essential components: a photosensitiser, a water oxidant catalyst and a hydrogen reduction catalyst.[81] Ruthenium complexes play an important role when used as water oxidation catalysts and dyes due to their ease of characterisation.[82] To date, dimeric and monomeric ruthenium aqua polypyridyl complexes are the most well studied and characterised oxidation catalysts due to their capacity to lose and gain electrons and protons and their high number of stable oxidation states.[83-85] On the other hand, ruthenium photosensitisers are polypyridyl complexes able to absorb visible light with an oxidation potential higher than the oxidation potential of the oxidation catalyst.

An interesting approach for the conversion of water into hydrogen and oxygen is the incorporation of this catalytic system into a complete functional device called a solar fuel cell or dye sensitised photoelectrochemical cell (DSPEC) (Figure 2.18).[86] This device is based on a modification of the dye sensitised solar cell, where the oxidation and reduction reactions take place at the cathode and anode electrodes of an electrochemical cell.

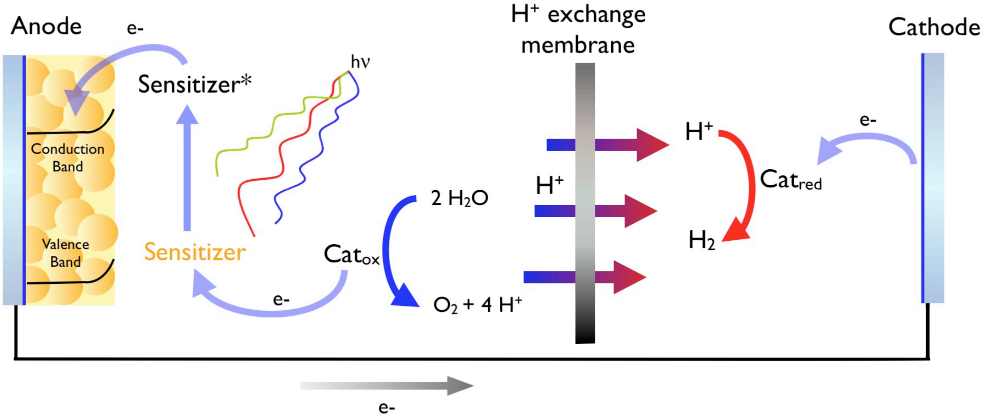

Figure 2.18. Schematic diagram for a DSPEC cell for water oxidation

The reduction of CO_2 can be carried out through a light-driven reaction, with electrons and protons derived from the water oxidation reaction. The reduction reaction of CO_2 into more complex chemicals can also be integrated into complete functional devices in a similar schematic diagram to that used for DSPECs. A ruthenium hydride complex able to insert CO_2 molecules into the metal-hydride bond can be used as a CO_2 reduction catalyst.[87]

2.6.3. Light driven molecular devices and machines

A molecular device is an assembly of molecular components designed to perform a particular function, while a molecular machine is a particular type of molecular device able to transform an external stimulation into mechanical-like movement. The energy supply for molecular devices and machines can arise from chemical, photochemical or electrochemical stimuli. However, stimulation by light is one of the most interesting way to power systems of this type since the system is not altered by the addition of chemical reagents.[88] For this reason, luminescence or photo-redox active metal complexes have been used as essential components for the construction of molecular devices and machines.[30]

Examples of molecular devices are molecular wires, molecular switches and molecular antenna receptors. Molecular wires are molecular-based devices which allow the electron or charge transfers between a donor and an acceptor units over long distances and in a determined direction. [89] Molecular switches can allow or prohibit the electron or energy transfer between two components of the molecular device, an acceptor and a donor unit, by reversible modifications on the structure or conformation of the linker.[90] In these two types of molecular devices, the ruthenium polypyridyl complexes are used as chromophoric agents able to transfer an electron to the acceptor moiety of the molecular device when they are irradiated with light. On the other hand, dendrimers are organised systems in which several chromophoric components absorb the incident light and direct the excitation energy towards a common acceptor component.[91,92] In this type of devices, ruthenium complexes can act as the chromophoric agent, transferring the energy to another metal center; or as the core energy trap, where several aromatic units of the dendrimer absorb UV light and transfer the energy to the ruthenium metal center.

Molecular machines transform an external energy into a large displacement of some components of the system.[93] The most important movements performed by molecular machines for practical applications are lineal and rotary movements, changes in their molecular structure, translocation of components and contractions and extensions. Particularly interesting molecular machines are those where the ruthenium complexes can be used as photosensitisers able to impulse motions through electron or charge transfers to the acceptor moieties of the molecular machines.[94]

2.6.4. Light emitting devices

Organometallic complexes possessing a heavy transition metal element are strong phosphorescent emitters, making them suitable for their employment in light emitting devices.[95] These kind of devices are very interesting for display and lighting applications.

Organic light emitting diodes (OLEDs) are based on an emissive aromatic organic layer between two electrodes. When an electric potential is applied, the organic layer is oxidised at the anode and reduced at the cathode, and the recombination between the electrons and holes at the organic layer generates an exciton with an energy similar to the difference between the HOMO and LUMO of the organic molecules.

Ruthenium complexes, such as the tris-(bidentate) $[Ru(NN)_3]^{2+}$ can be used in light emitting devices in the form of a single emitting layer,[96, 97] polymerised,[98] or incorporated into an inert solid matrix[99]. However, the emission of light is due to the recombination reaction between the oxidised $[Ru(NN)_3]^{3+}$ and the reduced $[Ru(NN)_3]^{+}$ forms of the ruthenium complex.[100]

2.6.5. Optical molecular chemosensors

Chemosensors are molecules which display a specific response to a particular analyte species. Optical chemosensors offer a variation in their absorption or emission spectra, intensity or lifetime in the presence of specific species.

Ruthenium polypyridyl complexes have been extensively used for the detection of O_2, since diatomic oxygen is a well known luminescence quencher.[101] In addition, these compounds can be functionalised with specific groups capable of recognising selective anions (halogens, CH_3COO^-, $H_2PO_4^-$), cations (H^+, metal ions), small molecules (CO_2, NH_3) and biomolecules making them suitable for the optical detection of analytes.[102] Furthermore, ruthenium complexes can be immobilised onto a permeable solid matrix (*e.g.* zeolites, polymers, sol-gel type supports, etc.) through covalent or non-covalent bonds. The anchorage of a chemosensor onto a solid surface allows the preparation and commercialisation of portable devices.

2.6.6. Interaction with biomolecules

Transition metal complexes which are stable, inert and water-soluble are extensively used in chemotherapy and in the development of highly sensitive diagnostic agents.[103] Specifically, ruthenium complexes show a long-lived luminescence in the visible region of the spectra, which enables them to be used in detection and imaging studies. Furthermore, the sensitivity of their absorption and emission spectra, intensity and lifetime to different biomolecule microenvironments such as DNA or proteins make these complexes attractive candidates for biomolecule sensing.[104]

By changing the ligands of the ruthenium complex, the nature and the strength of binding with biomolecules can be modified. For this reason, ruthenium polypyridyl complexes used as chemosensors can interact with biomolecules trough covalent or non-covalent bonds.

"Probe" is the name assigned to those complexes that bind the biomolecules through non-covalent interactions, such as electrostatic attraction between the cationic metal complexes and polyanionic nucleic acids, hydrophobic interactions between the ligands and the biomolecules or intercalation of the ruthenium complexes containing an extended aromatic planar ligand into the biomolecules.

On the other hand, ruthenium complexes that interact with biomolecules through covalent bonds are called "labels". These metal complexes can be introduced as a luminescence linkers between two different biomolecule moieties, or can be functionalised with a specific reactive group to bind the biomolecules.

2.7. References

1. Henry, G. D., *Tetrahedron* **2004,** *60* (29), 6043-6061.
2. Dumur, F., Dumas, E., Mayer, C., *Targ. Heterocycl. Syst.* **2007,** *130*, 70-103.
3. Kaes, C.; Katz, A.; Hosseini, M. W., *Chem. Rev.* **2000,** *100* (10), 3553-3590.
4. Summers, L. A., *Adv. Heterocycl. Chem.* **1984,** *35*, 281-374.
5. Constable, E. C., *Adv. Inorg. Chem. Radiochem.* **1986,** *30*, 69-121.
6. Newkome, G. R.; Patri, A. K.; Holder, E.; Schubert, U. S., *Eur. J. Org. Chem.* **2004,** (2), 235-254.
7. Collin, J. P.; Guillerez, S.; Sauvage, J. P., *J. Chem. Soc., Chem. Commun.* **1989,** (12), 776-778.
8. Summers, L. A., *Adv. Heterocycl. Chem.* **1978,** *22*, 1-69.
9. Luman, C. R.; Castellano, F. N., *Compr. Coord. Chem. II* **2004,** *1*, 25-39.
10. Brandt, W. W.; Dwyer, F. P.; Gyarfas, E. D., *Chem. Rev.* **1954,** *54* (6), 959-1017.
11. Goller, A.; Grummt, U. W., *Chem. Phys. Lett.* **2000,** *321* (5,6), 399-405.
12. Bessel, C. A.; See, R. F.; Jameson, D. L.; Churchill, M. R.; Takeuchi, K. J., *J. Chem. Soc.-Dalton Trans.* **1992,** (22), 3223-3228.
13. Donnay, G.; Donnay, J. D. H.; Harding, M. J. C., *Acta Crystallogr.* **1965,** *19* (4), 688-689.
14. Hapke, M.; Brandt, L.; Lutzen, A., *Chem. Soc. Rev.* **2008,** *37* (12), 2782-2797.
15. Sammes, P. G.; Yahioglu, G., *Chem. Soc. Rev.* **1994,** *23* (5), 327-334.
16. Thompson, A. M. W. C., *Coord. Chem. Rev.* **1997,** *160*, 1-52.
17. Nakamoto, K., *J. Phys. Chem.* **1960,** *64* (10), 1420-1425.
18. Henry, M. S.; Hoffman, M. Z., *J. Phys. Chem.* **1979,** *83* (5), 618-625.
19. Albano, G.; Balzani, V.; Constable, E. C.; Maestri, M.; Smith, D. R., *Inorg. Chim. Acta* **1998,** *277* (2), 225-231.
20. Bandyopadhyay, B. N.; Harriman, A., *J. Chem. Soc., Faraday Trans. 1* **1977,** *73*, 663-674.
21. Leroy-Lhez, S.; Fages, F., *C. R. Chim.* **2005,** *8* (8), 1204-1212.
22. Sugihara, H.; Hiratani, K., *Coord. Chem. Rev.* **1996,** *148*, 285-299.
23. Smith, G. F., *Anal. Chem.* **1954,** *26* (10), 1534-1538.
24. Reynal, A.; Etxebarria, J.; Nieto, N.; Serres, S.; Palomares, E.; Vidal-Ferran, A., *Eur. J. Inorg. Chem.* **2010,** *2010* (9), 1360-1365.
25. Steel, P. J., *Coord. Chem. Rev.* **1990,** *106*, 227-265.
26. Constable, E. C., *Chem. Soc. Rev.* **2007,** *36* (2), 246-253.
27. Polo, A. S.; Itokazu, M. K.; Murakami Iha, N. Y., *Coord. Chem. Rev.* **2004,** *248* (13-14), 1343-1361.
28. Lo, K. K.-W.; Hui, W.-K.; Chung, C.-K.; Tsang, K. H.-K.; Ng, D. C.-M.; Zhu, N.; Cheung, K.-K., *Coord. Chem. Rev.* **2005,** *249* (13-14), 1434-1450.
29. Chelucci, G.; Thummel, R. P., *Chem. Rev.* **2002,** *102* (9), 3129-3170.
30. Balzani, V.; Bergamini, G.; Ceroni, P., *Coord. Chem. Rev.* **2008,** *252* (23+24), 2456-2469.
31. Juris, A.; Balzani, V.; Barigelletti, F.; Campagna, S.; Belser, P.; Von Zelewsky, A., *Coord. Chem. Rev.* **1988,** *84*, 85-277.
32. Vos, J. G.; Kelly, J. M., *Dalton Trans.* **2006,** (41), 4869-4883.

34. Griffith, W. P., *Chem. Soc. Rev.* **1992,** *21* (3), 179-185.
35. Balzani, V.; Bergamini, G.; Campagna, S.; Puntoriero, F., *Top. Curr. Chem.* **2007,** *280* (Photochemistry and photophysics of coordination compounds I: Overview and general concepts), 1-36.
36. Campagna, S.; Puntoriero, F.; Nastasi, F.; Bergamini, G.; Balzani, V., *Top. Curr. Chem.* **2007,** *280* (Photochemistry and Photophysics of Coordination Compounds I: Ruthenium), 117-214.
37. Campagna, S.; Puntoriero, F.; Nastasi, F.; Bergamini, G.; Balzani, V., *Top. Curr. Chem.* **2007,** *280* (Photochemistry and Photophysics of Coordination Compounds I), 117-214.
38. Balzani, V.; Juris, A.; Venturi, M.; Campagna, S.; Serroni, S., *Chem. Rev.* **1996,** *96* (2), 759-833.
39. Crosby, G. A., *Acc. Chem. Res.* **1975,** *8* (7), 231-238.
40. Kalyanasundaram, K.; Nazeeruddin, M. K., *Chem. Phys. Lett.* **1992,** *193* (4), 292-297.
41. Hofmeier, H.; Schubert, U. S., *Chem. Soc. Rev.* **2004,** *33* (6), 373-399.
42. Maestri, M.; Armaroli, N.; Balzani, V.; Constable, E. C.; Thompson, A. M. W. C., *Inorg. Chem.* **1995,** *34* (10), 2759-2767.
43. Wang, X.-y.; Del Guerzo, A.; Schmehl, R. H., *J. Photochem. Photobiol., C.* **2004,** *5* (1), 55-77.
44. Medlycott, E. A.; Hanan, G. S., *Chem. Soc. Rev.* **2005,** *34* (2), 133-142.
45. Tokel-Takvoryan, N. E.; Hemingway, R. E.; Bard, A. J., *J. Am. Chem. Soc.* **1973,** *95* (20), 6582-6589.
46. Lever, A. B. P., *Inorg. Chem.* **1990,** *29* (6), 1271-1285.
47. Fielder, S. S.; Osborne, M. C.; Lever, A. B. P.; Pietro, W. J., *J. Am. Chem. Soc.* **1995,** *117* (26), 6990-6993.
48. Islam, A.; Sugihara, H.; Arakawa, H., *J. Photochem. Photobiol., A* **2003,** *158* (2-3), 131-138.
49. Anderson, P. A.; Strouse, G. F.; Treadway, J. A.; Keene, F. R.; Meyer, T. J., *Inorg. Chem.* **1994,** *33* (18), 3863-3864.
50. Keene, F. R., *Coord. Chem. Rev.* **1997,** *166*, 121-159.
51. Constable, E. C.; Thompson, A., *J. Chem. Soc.-Dalton Trans.* **1992,** (24), 3467-3475.
52. Muerner, H.; Belser, P.; von Zelewsky, A., *J. Am. Chem. Soc.* **1996,** *118* (34), 7989-7994.
53. Nazeeruddin, M. K.; Zakeeruddin, S. M.; Humphry-Baker, R.; Gorelsky, S. I.; Lever, A. B. P.; Gratzel, M., *Coord. Chem. Rev.* **2000,** *208*, 213-225.
54. Sauvage, J. P.; Collin, J. P.; Chambron, J. C.; Guillerez, S.; Coudret, C.; Balzani, V.; Barigelletti, F.; De Cola, L.; Flamigni, L., *Chem. Rev.* **1994,** *94* (4), 993-1019.
55. Spiccia, L.; Deacon, G. B.; Kepert, C. M., *Coord. Chem. Rev.* **2004,** *248* (13-14), 1329-1341.
56. Anderson, P. A.; Deacon, G. B.; Haarmann, K. H.; Keene, F. R.; Meyer, T. J.; Reitsma, D. A.; Skelton, B. W.; Strouse, G. F.; Thomas, N. C.; et al., *Inorg. Chem.* **1995,** *34* (24), 6145-6157.
57. Evans, I. P.; Spencer, A.; Wilkinson, G., *J. Chem. Soc., Dalton Trans.* **1973,** (2), 204-209.
58. Freedman, D. A.; Evju, J. K.; Pomije, M. K.; Mann, K. R., *Inorg. Chem.* **2001,** *40* (22), 5711-5715.

60. Burstall, F. H., *J. Chem. Soc.* **1936**, 173-175.
61. Lin, C. T.; Boettcher, W.; Chou, M.; Creutz, C.; Sutin, N., *J. Am. Chem. Soc.* **1976**, *98* (21), 6536-6544.
62. Crosby, G. A.; Watts, R. J., *J. Am. Chem. Soc.* **1971**, *93* (13), 3184-3188.
63. Thomas, N. C.; Deacon, G. B., *Inorg. Synth.* **1989**, *25*, 107-110.
64. Haberecht, M., Schnorr, J. M., Andreitchenko, E. V., Clark, C. G., Wagner, M., Müllen, K., *Angew. Chem., Int. Ed.* **2008**, *47* (9), 1662-1667.
65. Walker, G. W.; Nocera, D. G.; Swavey, S.; Brewer, K. J., *Inorg. Synth.* **2004**, *34*, 66-68.
66. Xiao, X.; Sakamoto, J.; Tanabe, M.; Yamazaki, S.; Yamabe, S.; Matsumura-Inoue, T., *J. Electroanal. Chem.* **2002**, *527* (1-2), 33-40.
67. Bolink, H. J.; Cappelli, L.; Coronado, E.; Graetzel, M.; Nazeeruddin, M. K., *J. Am. Chem. Soc.* **2006**, *128* (1), 46-47.
68. Rau, S.; Bernhard, S.; Grübing, A.; Schebesta, S.; Lamm, K.; Vieth, J.; Görls, H.; Walther, D.; Rudolph, M.; Grummt, U. W.; Birkner, E., *Inorg. Chim. Acta* **2004**, *357*, 4496-4503.
69. Johansson, O.; Wolpher, H.; Borgstrom, M.; Hammarstrom, L.; Bergquist, J.; Sun, L.; Akermark, B., *Chem. Commun.* **2004**, (2), 194-195.
70. Hesek, D.; Inoue, Y.; Everitt, S. R. L.; Ishida, H.; Kunieda, M.; Drew, M. G. B., *Inorg. Chem.* **2000**, *39* (2), 308-316.
71. Rutherford, T. J.; Reitsma, D. A.; Keene, F. R., *J. Chem. Soc., Dalton Trans.* **1994**, (24), 3659-3666.
72. Strouse, G. F.; Anderson, P. A.; Schoonover, J. R.; Meyer, T. J.; Keene, F. R., *Inorg. Chem.* **1992**, *31* (14), 3004-3006.
73. Deacon, G. B.; Kepert, C. M.; Sahely, N.; Skelton, B. W.; Spiccia, L.; Thomas, N. C.; White, A. H., *J. Chem. Soc., Dalton Trans.* **1999**, (3), 275-278.
74. Zakeeruddin, S. M.; Nazeeruddin, M. K.; Humphry-Baker, R.; Graetzel, M.; Shklover, V., *Inorg. Chem.* **1998**, *37* (20), 5251-5259.
75. Greene, D. L.; Mingos, D. M. P., *Transition Met. Chem.* **1991**, *16* (1), 71-72.
76. Ziessel, R.; Grosshenny, V.; Hissler, M.; Stroh, C., *Inorg. Chem.* **2004**, *43* (14), 4262-4271.
77. Lalrempuia, R.; Rao Kollipara, M., *Polyhedron* **2003**, *22* (23), 3155-3160.
78. Kalyanasundaram, K.; Gratzel, M., *Coord. Chem. Rev.* **1998**, *177*, 347-414.
79. O'Regan, B.; Grätzel, M., *Nature* **1991**, *353* (6346), 737-740.
80. Meyer, T. J., *Acc. Chem. Res.* **1989**, *22* (5), 163-170.
81. Brimblecombe, R.; Dismukes, G. C.; Swiegers, G. F.; Spiccia, L., *Dalton Trans.* **2009**, (43), 9374-9384.
82. Sala, X.; Romero, I.; Rodriguez, M.; Escriche, L.; Llobet, A., *Angew. Chem., Int. Ed.* **2009**, *48* (16), 2842-2852.
83. Gersten, S. W.; Samuels, G. J.; Meyer, T. J., *J. Am. Chem. Soc.* **1982**, *104* (14), 4029-4030.
84. Sens, C.; Romero, I.; Rodríguez, M.; Llobet, A.; Parella, T.; Benet-Buchholz, J., *J. Am. Chem. Soc.* **2004**, *126* (25), 7798-7799.
85. Zong, R.; Thummel, R. P., *J. Am. Chem. Soc.* **2005**, *127* (37), 12802-12803.
86. Herrero, C.; Lassalle-Kaiser, B.; Leibl, W.; Rutherford, A. W.; Aukauloo, A., *Coord. Chem. Rev.* **2008**, *252* (3-4), 456-468.
87. Jessop, P. G.; Joó, F.; Tai, C. C., *Coord. Chem. Rev.* **2004**, *248* (21-24), 2425-2442.

88. Ballardini, R.; Balzani, V.; Credi, A.; Gandolfi, M. T.; Venturi, M., *Acc. Chem. Res.* **2001,** *34* (6), 445-455.
89. Grosshenny, V.; Harriman, A.; Hissler, M.; Ziessel, R., *Platinum Met. Rev.* **1996,** *40* (1), 26-35.
90. Otsuki, J.; Akasaka, T.; Araki, K., *Coord. Chem. Rev.* **2008,** *252* (1+2), 32-56.
91. Serroni, S.; Campagna, S.; Puntoriero, F.; Loiseau, F.; Ricevuto, V.; Passalacqua, R.; Galletta, M., *C. R. Chim.* **2003,** *6* (8-10), 883-893.
92. Voegtle, F.; Plevoets, M.; Nieger, M.; Azzellini, G. C.; Credi, A.; De Cola, L.; De Marchis, V.; Venturi, M.; Balzani, V., *J. Am. Chem. Soc.* **1999,** *121* (26), 6290-6298.
93. Balzani, V.; Venturi, M.; Credi, A., *Molecular Devices and Machines: A Journey into the Nano World*. 2003.
94. Bonnet, S.; Collin, J.-P., *Chem. Soc. Rev.* **2008,** *37* (6), 1207-1217.
95. Yersin, H., *Top. Curr. Chem.* **2004,** *241* (Transition Metal and Rare Earth Compounds), 1-26.
96. Handy, E. S.; Pal, A. J.; Rubner, M. F., *J. Am. Chem. Soc.* **1999,** *121* (14), 3525-3528.
97. Buda, M.; Kalyuzhny, G.; Bard, A. J., *J. Am. Chem. Soc.* **2002,** *124* (21), 6090-6098.
98. Mak, C. S. K.; Chan, W. K., *Highly Efficient OLEDs with Phosphorescent Materials, Wiley-VCH* **2008**, 329-362.
99. Gong, X.; Ng, P. K.; Chan, W. K., *Adv. Mater.* **1998,** *10* (16), 1337-1340.
100. Leprêtre, J. C.; Deronzier, A.; Stéphan, O., *Synth. Met.* **2002,** *131* (1-3), 175-183.
101. Demas, J. N.; DeGraff, B. A., *J. Chem. Educ.* **1997,** *74* (6), 690-695.
102. Demas, J. N.; DeGraff, B. A., *Coord. Chem. Rev.* **2001,** *211*, 317-351.
103. Lo, K. K.-W., *Struct. Bond.* **2007,** *123* (Luminescent transition metal complexes as biological labels and probes), 205-245.
104. Xiong, Y.; Ji, L.-N., *Coord. Chem. Rev.* **1999,** *185-186*, 711-733.

Chapter 3. Experimental methods

The general device preparation steps, reagents and equipment used in the work presented in this thesis are explained in this section. However, specific characteristics of the particular experimental conditions and fabrication procedures of each sample are further commented in the corresponding article.

TABLE OF CONTENTS

3.1. Dye synthesis and characterisation

3.1.1. General reagents and solvents

All of the chemical products were purchased from Sigma-Aldrich without further purification unless otherwise stated. **N719** and the **Black Dye** were purchased from Solaronix. The **C101** complex was received as a courtesy from the FP7-EU project (ROBUST). Commonly used solvents were purchased from SdS.

3.1.2. General instrumentation

Proton and carbon NMR spectra, NOESY and COSY experiments were measured on a Bruker Avance 400 Ultrashield NMR spectrometer. The deuterated solvents are indicated and the chemical shifts (δ) are given in ppm, referenced to the solvent residual peak. Coupling constants (*J*) are given in Hz.

A Waters LCT Premier liquid chromatograph coupled to a time-of-flight mass spectrometer (HPLC/MS-TOF) with electrospray ionisation (ESI) was used to measure the mass spectra of the samples.

Fourier transform infrared spectra (FTIR) were obtained with an FTIR ThermoNicolet 5700 spectrometer, with a spectral range from 4000 to 400 cm^{-1}. UV-visible and fluorescence spectra were recorded in 1 cm path length quartz cell in a Shimadzu UV spectrophotometer 1700 and Aminco-Bowman Series 2 luminescence spectrometer, respectively. The absorption spectra of sensitised films were measured by directly attaching the films to the cuvette holder.

The electrochemical data were obtained by employing a conventional three-electrode cell connected to a CH Instruments 660c potentiostat-galvanostat. For cyclic voltammetry, a platinum working electrode, a calomel reference electrode (saturated calomel electrode, SCE), and a platinum wire as the auxiliary electrode were used. During cyclic voltammetry of most ruthenium polypyridyl complexes, the metal is oxidised and one ligand is reduced. A reversible oxidation wave which involves a metal centered orbital, and various reduction waves localised on the ligands can be observed. However, since the reduction of the ligands occurs in the far negative potential range, the oxidation potentials of the excited state ($E_{1/2}Ru^{II/III^*}$, V) can be approximated to the oxidation potentials of the ground state ($E_{1/2}Ru^{II/III}$, V) and to the excited state zero-zero energies ($E_{0,0}$, J) using Equation 3.1, where q is the elementary charge (C) and the 0-0 energy calculated from the highest energy side of the emission band.

$$E_{1/2}(Ru^{II/III*}) = E_{1/2}(Ru^{II/III}) - E_{0,0}/q \qquad \text{(Equation 3.1)}$$

3.1.3. Synthesis of organic ligands

3.1.3.1. Synthesis of 4,4'-dicarboxy-2,2'-bipyridine

The ligand 4,4'-dicarboxy-bipyridine was synthesised as previously reported. 4,4'-dimethyl-2,2'-bipyridine (0.5 g, 3 mmol) was dissolved in 27 mL of H_2SO_4 4 M. The solution was cooled to -5 °C in an ice-salt bath. $KMnO_4$ (1.07 g, 6.8 mmol) was added in six portions while stirring. After half an hour another $KMnO_4$ portion (1.07 g, 6.8 mmol) was added in a similar form. The reaction mixture was heated in a silicon oil bath and refluxed for 18 h. The mixture was cooled to room temperature and was filtered with a buchner funnel. The white precipitate was dissolved in 30 mL of 1 M Na_2CO_3. The insoluble part was removed by filtration at atmospheric pressure. A 4 M 1:1 solution of HNO_3 and HCl was added to lower the pH of the filtered solution to pH 2. A white precipitate appeared and was collected by filtration with a sintered glass funnel. Yield: 75%. ^{1}H-NMR (400 MHz, D_2O/NaOD) δ: 7.49 (d, J=5.1 Hz, 2H), 7.99 (s, 2H), 8.39 (d, J=5.1 Hz, 2H).

3.1.4. Synthesis of the ruthenium polypyridyl complexes

The synthesis of all complexes was carried out in a one-pot reaction following the procedure published in the literature by Kasuga *et al.* (Figure 3.1).[1]

Ruthenium polypyridyl complexes were purified by size exclusion chromatography. The reaction crude (50 mg) was dissolved in 2.5 mL of methanol (MeOH) and 2 eq of tetrabutylammonium hydroxide (40 % wt in MeOH) were added. The solution was filtered through a 45 µm filter and purified through a Sephadex LH-20 column (2.5 x 30 cm) using methanol as the mobile phase. The main red band was collected and the solvent was evaporated under vacuum. Small aliquots of 0.01 M HNO_3 were added until a brown precipitate appeared, which was collected by filtration. Ruthenium diastereoisomers were separated by reverse phase C_{18} semipreparative HPLC (Waters Delta 600 pump), using a mixture of H_2O (0.1 % trifluoroacetic acid, TFA)/acetonitrile (0.1 % TFA) (1:1).

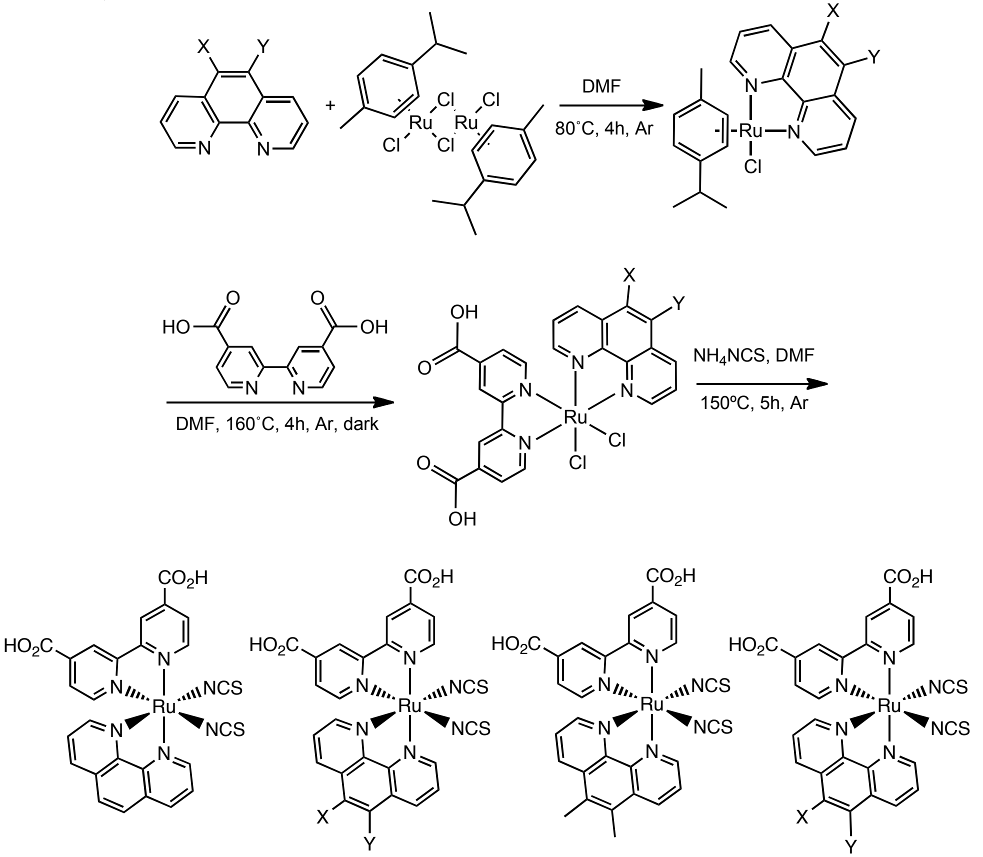

AR20

AR24a: X = H, Y = NH$_2$
AR24b: X = NH$_2$, Y =H

AR25

AR27a: X = H, Y = NO$_2$
AR27b: X = NO$_2$, Y =H

Figure 3.1. Synthetic route of the preparation of heteroleptic ruthenium complexes

3.2. Theoretical calculations

The theoretical calculations of the different photosensitisers used in this thesis were performed by Prof. Anton Vidal. The geometries of the different complexes were calculated with Gaussian 03, revision C.02,[2] using the B3LYP functional. 6-31(d) basis sets were used for sulfur, nitrogen, carbon and hydrogen atoms, whereas the Stuttgart-Dresden effective core potential (ECP)[3] and corresponding basis set were used for ruthenium. HOMO and LUMO orbitals were calculated from the optimised geometries.

3.3. Device preparation

3.3.1. Nanoparticle synthesis and film preparation

The synthesis of highly transparent 20 nm TiO_2 nanoparticles is based on the hydrolysis of a titanium alkoxide precursor, followed by peptisation under acidic conditions and autoclaving at high temperature. The TiO_2 nanoparticles used in this thesis work were synthesized in the laboratory of Prof. Emilio Palomares by Dr. Eugenia Martínez, Amparo Forneli and Antonio Sánchez following the procedure detailed by Palomares and coworkers.[4] Titanium isopropoxide (40 mL, 0.13 mol) was added to glacial acetic acid (9.12 g) under argon atmosphere while stirring. The reaction mixture was cooled in an ice-bath and 0.1 M nitric acid (240 mL) was added with vigourous stirring. The mixture was heated in an oil bath at 80 °C for 8 h and, after cooling, was filtered through a 0.45 µm syringe filter. The resulting product was diluted to 5 % weight of TiO_2 by adding water and was then autoclaved at 220 °C for 12 h. The aqueous phase was removed by centrifugation and the solid nanoparticles were isolated and rinsed two times with ethanol. An ultrasonic horn was used to break the aggregates and the solvent was removed under vacuum. The solid nanoparticles were diluted to 15 % TiO_2 weight, using ethyl cellulose and terpineol, and the paste was homogenised using a ball mill. This procedure results in the preparation of highly transparent approximately 20 nm partially anatase nanoparticles.

The Al_2O_3 paste was prepared by Josep Albero from commercially available aqueous solution of 20 nm Al_2O_3 nanoparticles (Alfa Aesar).

Furthermore, for highly efficient devices, TiO_2 pastes with a nanoparticle diameter of 20 and 400 nm were purchased from Dyesol.

In the present work, three different types of nanocrystalline films were used: (1) films for the spectroscopical measurements of the dye anchored onto the TiO_2 surface, (2) films used for measuring the photophysical properties of cell devices, and (3) films used for efficiency measurements of solar cells (Film 3). All of the glass slides were rinsed in the same way prior to use, in order to guarantee good contact with the semiconductor nanoparticles. The cleaning process involved the sequential sonication of the glass slides for 15 min in detergent solution, distilled water and ethanol, followed by calcination at 500 °C. Finally the slides are exposed to ozone in a UV-O_3 cleaning system (UVOCS Inc. T10X10/OES/E) for 20 min.

3.3.1.1. Films used for the spectroscopical characterisation of dyes (Film 1)

For the measurements focused on the optical characteristics of dyes, the glass substrate used was transparent non-conductive glass (cover slide) of 7.5 cm x 2.5 cm size. The deposition of TiO_2 or Al_2O_3 nanoparticles onto the glass substrates for the preparation of films used in the measurement of the spectroscopical properties of the dye and the photophysical characteristics of the devices was performed by the "Doctor Blade" technique (Figure 3.2). This technique consists of the spreading of the TiO_2 or Al_2O_3 paste onto the glass surface by using a glass rod, with both edges protected by strips of tape. The number of tape layers define the thickness of the film but, typically, for spectroscopical measurements the films had a thickness of about 4 μm, which is provided by one layer of tape. After deposition of the nanoparticles, the tape was carefully removed and the films were heated for 10 min at 120 ºC. Then, the homogeneous layers were gradually heated to 500 ºC to obtain the desired anatase crystalline form and remove water and organic molecules present in the TiO_2 or Al_2O_3 pastes. The thickness of the films were corroborated with a profilometer (Ambios Technology XP-1). Finally, the film was cut in small pieces of 2.5 cm x 1.5 cm in order to be sensitised with a dye.

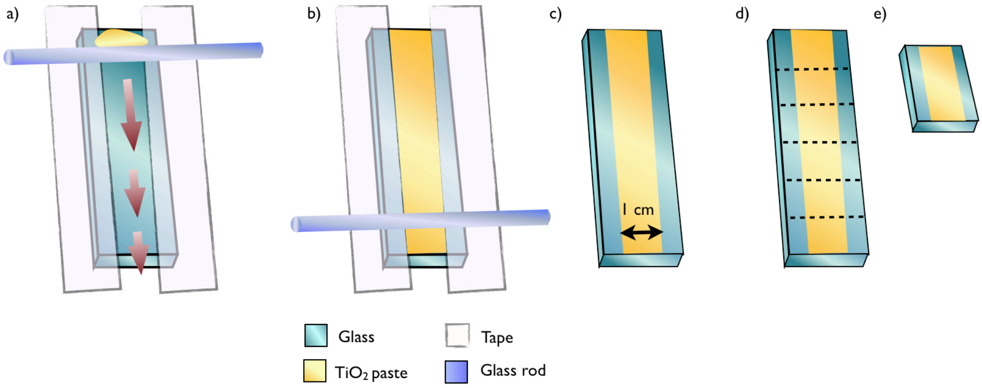

Figure 3.2. Scheme of the different steps of the Doctor Blade technique for the preparation of TiO_2 films for photophysical measurements

3.3.1.2. Films used for the photophysical characterisation of complete devices (Film 2)

For the experimental measurements of the photophysical properties of complete devices, 4 μm thick transparent films were prepared. The TiO_2 or Al_2O_3 nanoparticles were deposited onto the conductive side of the FTO glass (Hartford Glass Inc. with $\Omega\cdot15$ cm^{-2} resistance) of 7.5 cm x 2.5 cm size using the same procedure as for non-conductive glasses.

3.3.1.3. Films used for the characterisation of complete functional devices (Film 3)

The preparation of TiO$_2$ thin films for highly efficient DSSC differ from the other procedures explained above. Firstly, the FTO conductive glass (Nippon Sheet Glass Co, with a resistance of 10 $\Omega\cdot$cm^{-2} and Hartford Glass Inc. with 15 $\Omega\cdot$cm^{-2} resistance) was cut into pieces of 2.5 cm x 1.5 cm and then rinsed using the same procedure as for the other glass slides. After the cleaning process, the glass slides were introduced into a 40 mM TiCl$_4$ solution and heated for 15 min at 70 °C. The introduction of a dense TiO$_2$ layer by thermal treatment of FTO with TiCl$_4$ (thickness 100 - 200 nm) prevents the electrolyte from reaching the back contact of the conductive glass surface and so reduces electron recombination. The TiO$_2$ nanoparticles were deposited onto the conductive side of the glasses through the "Doctor Blade" technique using a tape which contained a round hole with a surface area of 0.152 cm^2 (Figure 3.3). After removing the tape, the films were heated at 120 °C for 10 min and then gradually heated to 500 °C.

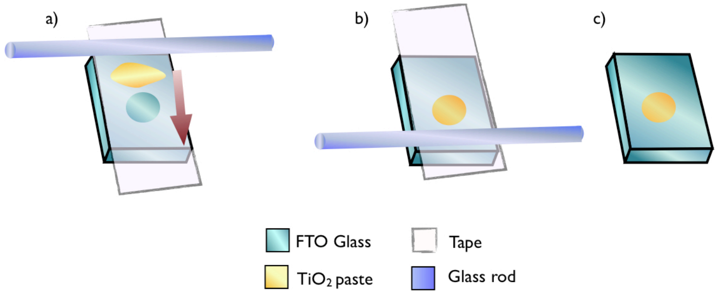

Figure 3.3. Scheme of the different steps of the Doctor Blade technique for the preparation of TiO$_2$ films for device preparation

The thickness of the films were measured with a profilometer and the processes of TiO$_2$ deposition and calcination were repeated until a transparent layer with a thickness of between 8 and 12 μm was obtained. A 4 μm layer of 400 nm TiO$_2$ nanoparticles was then applied on top of the film using the same deposition technique and heated to 500 °C. This layer of white nanoparticles acts as an internal light scattering reflector. After this process, the films were introduced into a 40 mM TiCl$_4$ solution and heated at 70 °C for 15 min.Finally the films were heated to 500 °C for 30 min and then cooled to room temperature. The films were used immediately or stored under anhydrous conditions.

3.3.1.4. Characterisation of mesoporous nanocrystalline films

Mesoporous nanocrystalline titanium dioxide films were characterised by microscopy and elemental analysis techniques (Figure 3.4). Surface characterisation measurements were performed by Amparo Forneli, Josep Albero and myself.

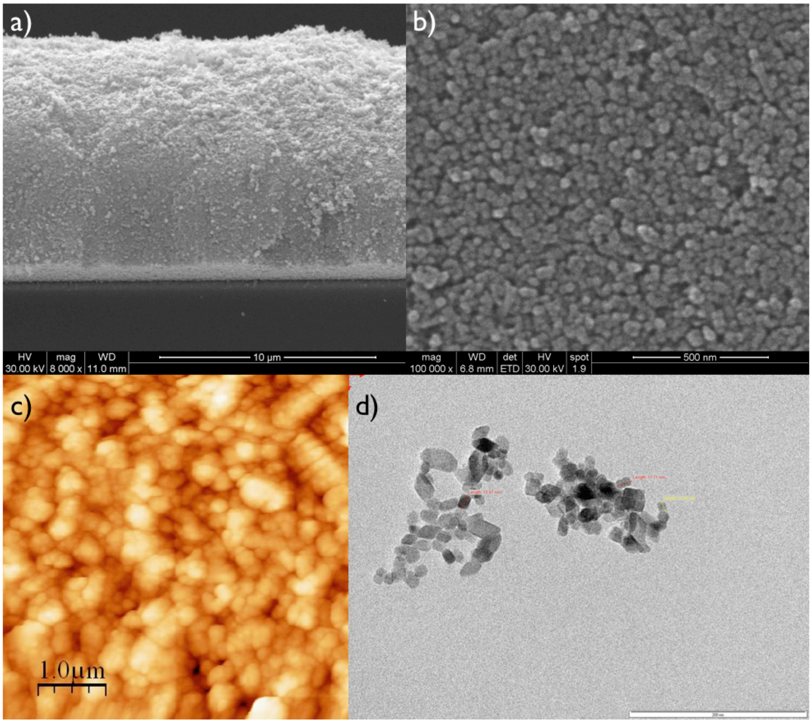

Figure 3.4. (a) Front view SEM, (b) cross view SEM, (c) AFM and (d) TEM images of mesoporous nanocrystalline TiO_2 films

The topography, thickness of the film and dispersion of the nanoparticles onto the film were determined by scanning electron microscopy (SEM) (JEOL JSM 6400 microscope). TiO_2 nanocrystalline films were covered with a thin layer of gold to make the sample conducting. Atomic force microscopy (AFM) (Imaging Pico SPMII) and transmission electron microscopy (TEM) (JEOL 1011 microscope) were used to confirm the size of TiO_2 nanoparticles on the film. X-ray powder diffraction measurements (Bruker-Siemens Smart CCD diffractometer) were used to ascertain the crystalline form and the size of the TiO_2 nanoparticles. X-ray diffraction peaks corresponded to the standard peaks of anatase form, with a nanoparticle diameter of 19 nm. BET analysis (Autosorb 1-MP Quatachrome apparatus) showed a surface area of 100 $m^2 \cdot g^{-1}$ and an average pore size of 13 nm.

3.3.2. Dye sensitisation

Dye sensitisation was carried out by introducing the films into the different dye solutions and leaving them in the dark for a period of time. Although different solvents and additives were used for each photosensitiser in order to optimise the preparation of the sensitised films, the procedure is very similar for all the samples prepared.

The dye solutions were prepared by dissolving the necessary amount of dye to obtain a concentration of between 10^{-3} and 10^{-4} M in an appropriate solvent such as acetonitrile (MeCN), *tert*-butanol (^{t}BuOH), ethanol (EtOH) or dimethylformamide (DMF). In some samples, a concentration of between $3 \cdot 10^{-4}$ and $3 \cdot 10^{-3}$ M of a coadsorbent such as chenodeoxycholic acid or citric acid was added to the dye solutions.

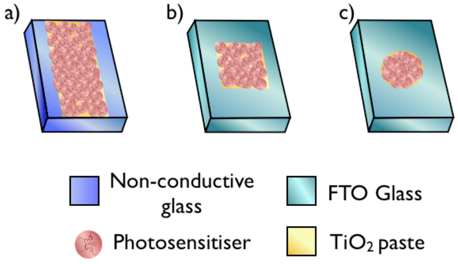

Figure 3.5. Scheme of (a) a dye sensitised film for spectroscopical measurements of the dye (Film 1), (b) 1 cm² dye sensitised film for photophysical measurements of the devices (Film 2), and (b) 0.152 cm² dye sensitised film for highly efficient solar cell (Film 3)

For the preparation of films used in spectroscopical measurements of the dye (Film 1) (Figure 3.5a) and for the measurement of photophysical properties of the devices (Film 2) (Figure 3.5b), the time of sensitisation was adjusted to obtain an absorbance at the maximum of the metal to ligand charge transfer band of the dye corresponding to 0.6 arbitrary units. However, after the anchoring process, the surface of the films used in the preparation of devices for photophysical experiments of complete devices was adjusted to 1 cm^2 by scratching away the excess film. For the preparation of efficient devices, the films were immersed overnight into the dye solutions (Film 3) (Figure 3.5c).

After dye sensitising, the films were rinsed with the same solvent as that used in the sensitisation solution in order to remove any unanchored dye molecules from the surface of the nanocrystalline films. The films were air dried and used immediately.

3.3.3. Preparation of the counter electrode

The counter electrodes were prepared with FTO conductive glass with a resistance of 15 $\Omega\cdot cm^{-2}$ cut in small pieces of 2.5 cm x 1.5 cm size. For highly efficient solar cells, a hole was made in the counter electrode with a drill, while for 1 cm^2 devices prepared for photophysical measurements two holes were made in the same slide. Then, the small pieces of glass were rinsed following the same procedure as explained for the working electrode in section 3.3.1. A drop of a $5\cdot10^{-3}$ M H_2PtCl_6 anhydrous solution in ethanol was spread with a Pasteur pipette on the conductive FTO side and the electrodes were heated to 390 °C for 30 minutes. Once the glasses were cooled at room temperature, they were used instantly or placed in a desiccator.

3.3.4. Preparation of the electrolyte

The composition of the electrolyte solution differs depending on the measurements being performed on the devices. Electrolytes used in the photophysical properties of the devices did not contain *tert*-butylpyridine (TBP), while the high efficient devices contained electrolytes with TBP. The electrolyte solutions were prepared by dissolving the necessary amount of reagents in a acetonitrile/valeronitrile (85:15) solution.

3.3.5. Assembly and sealing of the dye sensitised solar cell

Once the electrodes were prepared, the working and the counter electrodes were assembled in a sandwich form. In between the two electrodes a frame of a polymer that melts at 100 °C (Surlyn) was placed around the nanocrystalline film (Figure 3.6a). The two electrodes were sealed by applying high temperature and pressure (Figure 3.6b). Then the electrolyte was introduced into the device through the hole previously made at the counter electrode with a syringe (Figure 3.6c). For 1 cm^2 solar cells, the electrolyte entered through one of the holes, while the second hole allowed the air to escape. However, for devices that only had one hole, the electrolyte was introduced by applying vacuum. The holes were sealed by melting a small piece of Surlyn and a cover slide. Finally, silver paint was applied to the cell contacts in order to reduce the resistance to the current flow (Figure 3.6d).

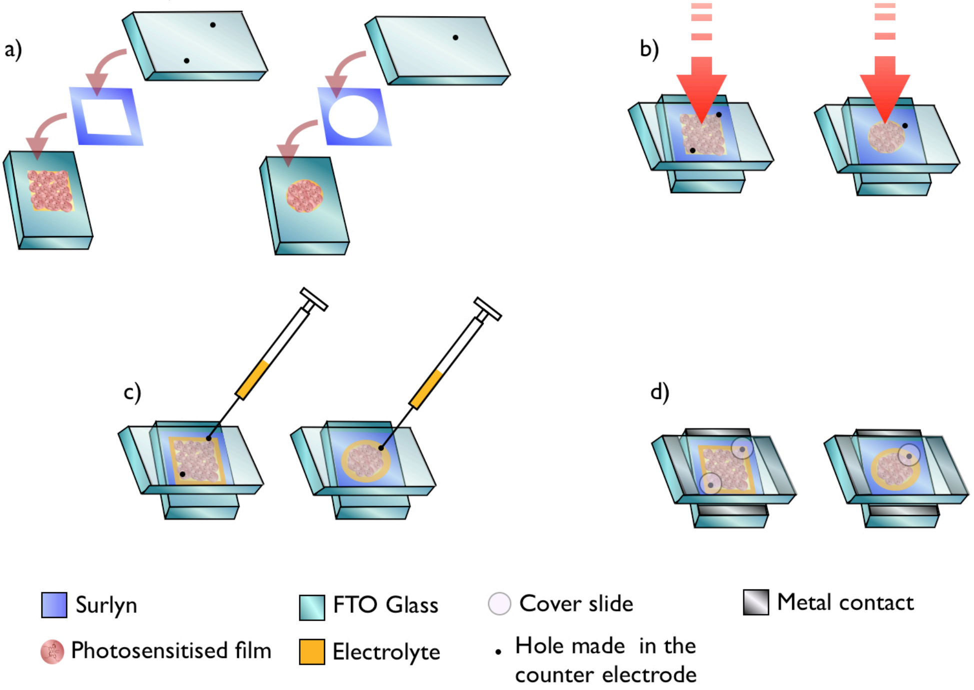

Figure 3.6. Scheme showing the assembly process of a dye sensitised solar cell

The measurements of the photophysical and efficiency properties were performed immediately after sealing. However, the cells remained stable for a few months.

3.4. Device characterisation

3.4.2. Time correlated-single photon counting measurements

Time correlated single photon counting (TC-SPC) is an optical technique which allows the study of the luminescence decay times of radiative materials. The operational basis is the detection of single photons as a function of time.[5] The lifetime of the excited state is the average time that the molecule takes to come back to the ground state from its excited state. The picosecond to microsecond emission lifetime measurements were carried out with a Lifespec-red picosecond to microsecond fluorescence lifetime spectrometer from Edinburgh Instruments. As excitation sources, two pulsed diode lasers, with 405 or 635 nm nominal wavelengths, were used. The instrument response measured at the FWHM (full-width at half-maximum) was below 350 ps.

With this technique, the lifetime of the photosensitiser can be measured both in solution or anchored onto the surface of a mesoporous nanocrystalline film such as Al_2O_3 or TiO_2. Furthermore, the comparison of the lifetime decay of a dye in a complete device and the decay of the photosensitiser attached to the surface of an insulator allows the estimation of the electron injection yield.

The TC-SPC decay can be fitted to an exponential decay (Equation 3.2), where $I(t)$ is the time-dependent luminescence intensity, A_n values are pre-exponential factors, t is the time and τ is the lifetime. The slow component of the lifetime in ruthenium complexes is thought to be due to the decay of the dye excited state from the triplet state.

$$I(t) = A_0 + \sum_{i=1}^{i=n} A_i \cdot e^{-t/\tau_i} \qquad \text{(Equation 3.2)}$$

3.4.3. Laser-transient absorption spectroscopy

Laser-transient absorbance spectroscopy (L-TAS) provides information about the lifetime and decay dynamics of short life transient species. With this technique, the absorbance of a sample is measured after excitation by a pulse of light and measured as a function of time, giving information about its decay kinetics over a wide time scale (from µs to s).

Nanosecond to microsecond transient absorption spectroscopy measurements were carried out with a home-built system as reported before.[6] The L-TAS equipment was assembled by Dr. Javier Pérez-Hernández.

The sample was irradiated with a short intense pulse of light generated by a nitrogen laser pumped dye laser. The nitrogen laser excitation source provided a pulse width of 1 ns at 337 nm with a pulse energy of 1.45 mJ at a frequency of 1 Hz (GL-3300 nitrogen laser from Microbeam, TG330 function generation from Thurlby Thandar). An appropriate dye laser was connected to the nitrogen laser to provide different wavelength excitation sources (360 - 750 nm) (Figure 3.7).

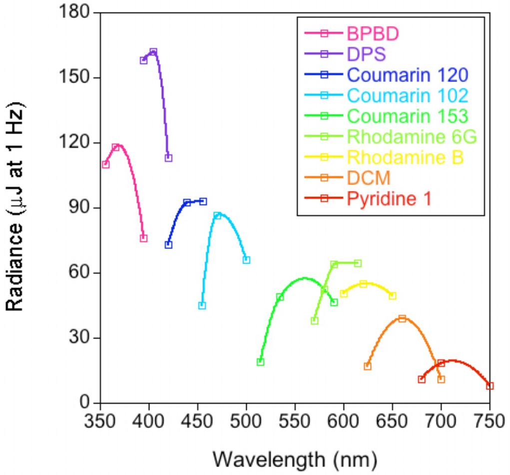

Figure 3.7. Emission spectra of the laser dyes used in the L-TAS system. Abbreviatures: BPBD: 2-(4-biphenylyl)-5-(4-tert-butylphenyl)-1,3,4-oxadiazol, DPS: 4,4'-diphenylstilbene, Coumarin 120: 7-amino-4-methylcoumarin, Coumarin 102: 2,3,5,6-1H,4H-tetrahydro-8-methylquinolizino-[9,9a,1-gh] coumarin, Coumarin 153: 2,3,5,6-1H,4H-tetrahydro-8-trifluormethylquinolizino-[9,9a,1-gh]coumarin, Rhodamine 6G: ethyl 2-[6-(ethylamino)-3-(ethylimino)-2,7-dimethyl-3H-xanthen-9-yl]benzoate hydrochloride, Rhodamine B: 2-[6-(diethylamino)-3-(diethylimino)-3H-xanthen-9-yl]benzoic acid, DCM: 4-dicyanmethylene-2-methyl-6-(p-dimethylaminostyryl)-4H-pyran, Pyridine 1: 1-ethyl-2-(4-(p-dimethylamonophenyl)-1,3-butadienyl)-pyridinium perchlorate

A second less intense light source provided by an halogen lamp (150 W), known as the probe, passes through the sample. An appropriate set of lenses and monochromators were used to focus and control the irradiation wavelength of the halogen lamp. The change in optical density (ΔO.D.) of the probe source was determined in order to monitor the change in the absorption spectra of the sample. The optical detector was a silicon photodiode equipped with a set of filters (Costronics) and coupled to an oscilloscope (Tecktronics TDS 2022) (Figure 3.8).

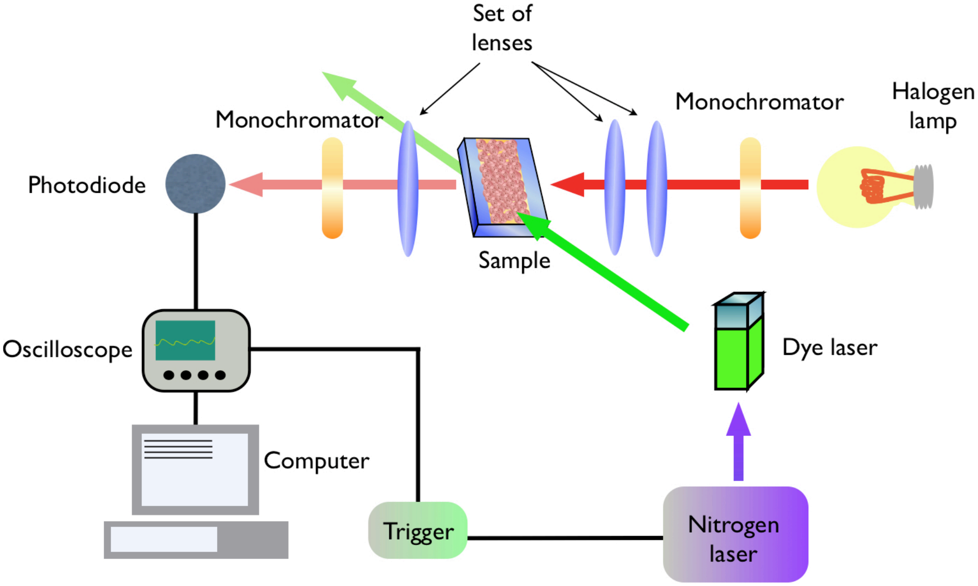

Figure 3.8. Scheme of the laser-transient absorption spectroscopy system

Two different types of measurements were performed using the L-TAS system. The first experiment involved the measurement of the recombination dynamics between the photoinjected electrons in the conduction band of the photosensitiser and the oxidised dye on the nanoparticle surface. Following the measurement of the transient absorption spectrum of the sensitised TiO_2 film (by measuring signal sizes of the sample at a given time at approximately 20 nm intervals over the absorption range 400 - 1000 nm) the change in the optical density of the dye cation at its maximum absorption wavelength was recorded as a function of time. The second experiment involved the measurement of complete devices, which gives an idea of both the regeneration of the dye cation by the redox couple and also the recombination kinetics between the photoinjected electrons in the conduction band of the semiconductor and the oxidised form of the redox couple present in the electrolyte. The latter measurement was performed by monitoring the change in optical density as a function of time at a probe wavelength fixed at 1000 nm using the monochromators.

Transient decays can be fitted to an stretched exponential function (Equation 3.3), where A_o and A_t are constants, t is time (s), τ is the relaxation time (s) and α is a value between 0 and 1 called the stretching parameter.[7]

$$\Delta O.D. = A_0 + A_1 \cdot e^{-\left(t/\tau\right)^{\alpha}} \qquad \text{(Equation 3.3)}$$

3.4.4. Charge extraction measurements

Charge extraction is a technique that provides information about the electron transport, trapping and recombination reactions in DSSCs under operating conditions.[8, 9] With this technique, electrons are accumulated in the semiconductor upon photoexcitation of the dye at open circuit. The extraction of these electrons by short-circuiting the cell is then measured as a function of time.

Charge extraction measurements were carried out using a home-built system (Figure 3.9). This equipment was assembled by Dr. Brian O'Regan, Dr. Javier Pérez-Hernández and Antonio Sánchez-Díaz.

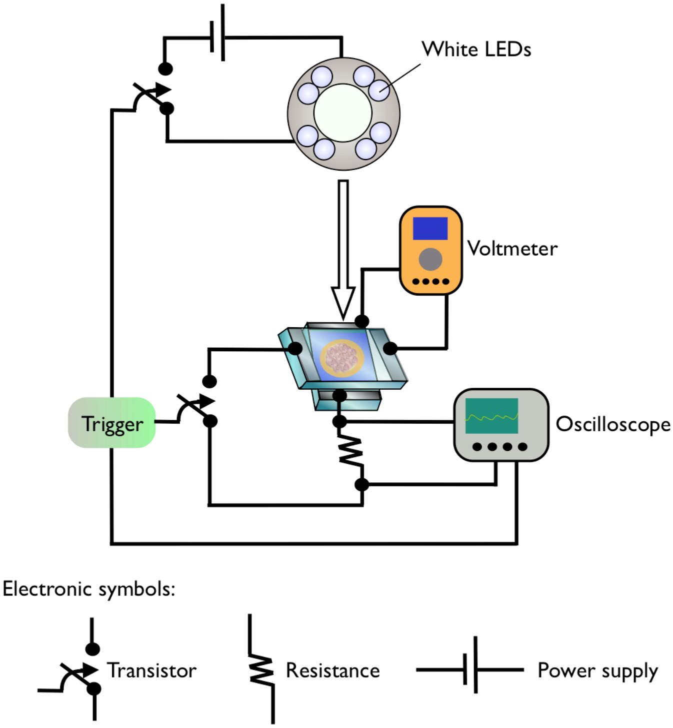

Figure 3.9. Scheme of the charge extraction system

The charge extraction data were acquired after a 4 s pulse generated by an array of white LEDs (Luxeon Lumileds). The trigger (TGP110 from Thurlby Thandar Instruments) is used to generate a pulse, which controls the LEDs, the switch which changes the short/open circuit regime of the cell and the oscilloscope. Upon illumination at open circuit, the photoexcited dye injects electrons into the semiconductor. The charges are accumulated in the TiO_2 and the voltage of the cell reaches its maximum value at the imposed white light conditions. After the pulse, the LEDs are turned off in 300 ps and the cell is switched from open to short circuit simultaneously. At short circuit, the accumulated charges at the TiO_2 are extracted, while the photovoltage decreases (Figure 3.10). Different light intensities were applied to achieve different open circuit voltages of the cell. The photovoltage decay between a resistance of 6.8 Ω was monitored using a Tektronics oscilloscope TDS 2022 and recorded using the Tektronics data acquisition software.

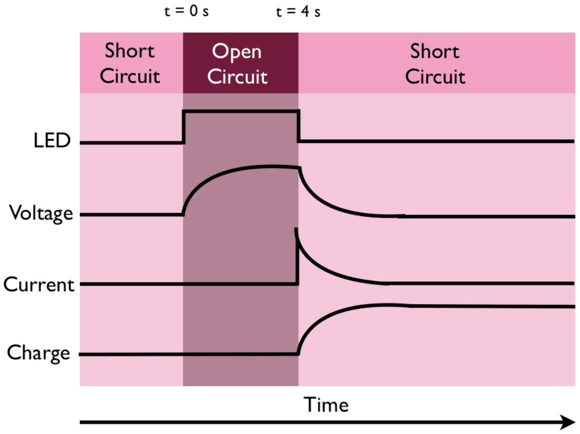

Figure 3.10. Behavior of the voltage, current and charge during the charge extraction experiments

The accumulated charge Q (C) can be calculated from the photovoltage decay experimental points as shown in Equation 3.4, where R (Ω) is the resistance, $V(t)$ is the measured voltage as function of time expressed in volts and I (A) is the photocurrent intensity as function of time.

$$Q = \frac{1}{R}\int_{t=0}^{t=t} V(t)\,dt = \int_{t=0}^{t=t} I(t)\,dt \qquad \text{(Equation 3.4)}$$

The electron density ($e^-_{density}$, e^-/cm^3) is used to define the amount of electrons accumulated in the semiconductor. It can be calculated from Equation 3.5, where Q is the accumulated charge calculated previously (C), q_e is the charge of one electron ($1.609 \cdot 10^{-19}$ C/e^-), d is the film thickness (cm), A is the surface area of the film (cm^2) and p is the porosity of the TiO_2 film. The porosity was calculated from BET theory,[10] obtaining a value of 0.6, expressed on a per unit basis.

$$e^{-}_{density} = \frac{Q}{q_e \cdot d \cdot A \cdot (1-p)} \qquad \text{(Equation 3.5)}$$

The electron density at the different open circuit voltage values of a cell can be then represented in a plot. The experimental points can be fitted to an exponential curve, as detailed in Equation 3.6. A_0 and A_1 are constants and k is a parameter which defines the curvature of the distribution.[11]

$$e^{-}_{density} = A_0 + A_1 \cdot e^{k \cdot V} \qquad \text{(Equation 3.6)}$$

3.4.5. Transient photovoltage measurements

Transient photovoltage measurements (TPV), also known as V_{oc} decay, is a technique which provides information about the electron recombination between the photoinjected electrons in the TiO_2 conduction band and the redox couple present in the electrolyte under operating conditions. [12] With this technique, the voltage of the cell is measured as function of time while it is illuminated by constant white light diodes and a short pulse generated by red-emitting diodes.

TPV measurements were carried out using a home-built system (Figure 3.11), which were assembled by Dr. Brian O'Regan, Dr. Javier Pérez-Hernández and Antonio Sánchez-Díaz.

Photovoltage transients are measured by applying a constant light bias using white LEDs (Luxeon Lumileds) to an open-circuited solar cell followed by shorter pulses from red LEDs. The V_{oc} decays are strongly dependant upon the charge density in the semiconductor. For this reason, in order to obtain a correct comparison in a study, photovoltage transient data of different devices is not compared at the same voltage, rather it is compared where similar charge densities are present in the films and this is done by changing the light intensity of the white LEDs. The charge density of the films is measured with the charge extraction technique explained in section 3.4.4.

Upon photoexcitation of the dye using 8 white LEDs under open circuit conditions, the rate of electron injection into the TiO_2 reaches an equilibrium with the recombination processes (e^--TiO_2/electrolyte$^+$ and e^--TiO_2/dye$^+$). However, when a 100 µs pulse of red light provided by 4 red LEDs is applied, injection of electrons into the conduction band of the semiconductor increases. This short pulse is modulated to cause a small increase in cell voltage of 10 mV, which is only a minor deviation from the 'equilibrium' conditions imposed by the white LEDs. The extra electrons in the TiO_2 recombine with the redox couple present in the electrolyte, and the resulting photovoltage transient is recorded. These transients can be recorded at several voltages in order to investigate their lifetime as a function of applied bias to the DSSC and thereby electron occupancy within the TiO_2 film. The photovoltage decay kinetics are measured with an oscilloscope (TDS 2022 Tecktronics).

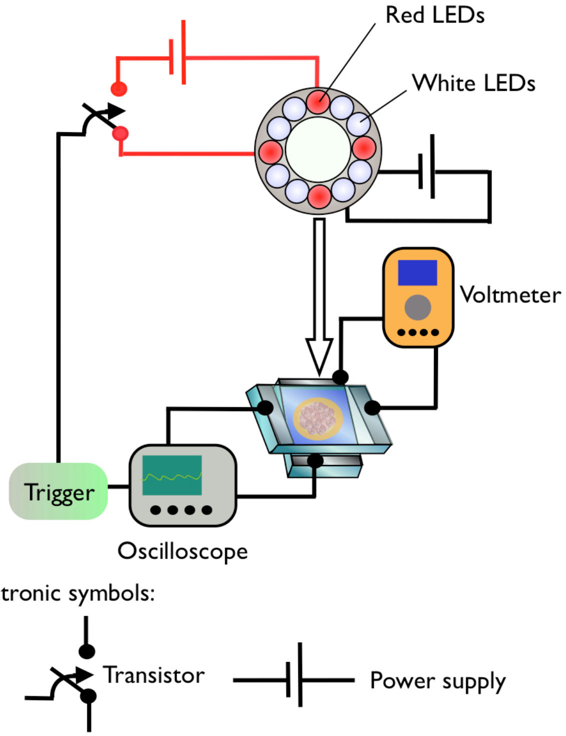

Figure 3.11. Scheme representing the transient photovoltage measurement system

The data obtained with this technique can be fitted to an exponential equation (Equation 3.7), where the voltage (V) is plotted as a function of time. V_{oc} (V) is the voltage at open circuit, V_{1} (V) is the voltage generated by the pulse and τ (s) is the recombination lifetime.

$$V(t) = V_{oc} + V_1 \cdot e^{-\left(t/\tau\right)} \qquad \text{(Equation 3.7)}$$

The lifetime τ (s) of the e^{-}-TiO_2 recombination reaction is usually plotted in a logarithmic scale, using a Power-law function as fitting equation, where A and k are constants (Equation 3.8).

$$\tau = 10^{A} \cdot \left(e^{-}_{density}\right)^{k} \qquad \text{(Equation 3.8)}$$

3.4.6. Incident photon to current efficiency

As explained in section 1.3.2, IPCE measures the performance of a DSSC giving the percentage of electrons generated in the cell following illumination with a given number of incident photons at a particular wavelength. The IPCE equipment consists of an Oriel 150 W xenon lamp as the light source and the wavelength is automatically changed with a PTIM-101 monochromator. A 4 inch integrating sphere was incorporated into the system to allow homogenous light irradiation over the entire surface of the cell. A Keithley 2400 monitored the photocurrent generated by the cell.

3.4.7. Photocurrent *vs* photovoltage curves

The overall efficiency of a cell is determined by the measurement of the photocurrent *vs* photovoltage curve (Figure 3.12). This technique consists of the measurement of the photocurrent generated by a solar cell under light irradiation when a gradually increasing photovoltage is applied to the cell. The device is illuminated by a solar simulator, which is a light source able to reproduce the solar spectrum. Appropriate filters are used to achieve AM 1.5 spectral illumination.

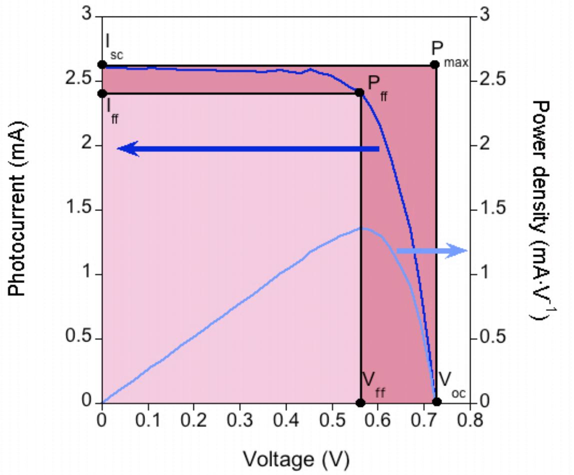

Figure 3.12. Current-voltage (I-V) and power-voltage (P-V) curves from a DSSC device made using the N719 dye

3.5. References

1. Onozawa-Komatsuzaki, N.; Kitao, O.; Yanagida, M.; Himeda, Y.; Sugihara, H.; Kasuga, K., *New J. Chem.* **2006,** *30* (5), 689-697.
2. Frisch, M. J., et al., *Gaussian 03, Revision C.02* **2004**, Gaussian, Inc.: Wallingford, CT.
3. Andrae, D.; Häussermann, U.; Dolg, M.; Stoll, H.; Preuss, H., *Theor. Chim. Acta* **1990,** *77* (2), 123-141.
4. Palomares, E.; Vilar, R.; Green, A.; Durrant, J. R., *Adv. Funct. Mater.* **2004,** *14* (2), 111-115.
5. Bollinger, L. M.; Thomas, G. E., *Rev. Sci. Instrum.* **1961,** *32* (9), 1044-1050.
6. Tachibana, Y.; Moser, J. E.; Gratzel, M.; Klug, D. R.; Durrant, J. R., *J. Phys. Chem.* **1996,** *100* (51), 20056-20062.
7. Nelson, J.; Haque, S. A.; Klug, D. R.; Durrant, J. R., *Phys. Rev. B* **2001,** *63* (20), 205321.
8. Duffy, N. W.; Peter, L. M.; Rajapakse, R. M. G.; Wijayantha, K. G. U., *J. Phys. Chem. B* **2000,** *104* (38), 8916-8919.
9. Duffy, N. W.; Peter, L. M.; Rajapakse, R. M. G.; Wijayantha, K. G. U., *Electrochem. Commun.* **2000,** *2* (9), 658-662.
10. Brunauer, S.; Emmett, P. H.; Teller, E., *J. Am. Chem. Soc.* **1938,** *60* (2), 309-319.
11. O'Regan, B. C.; Scully, S.; Mayer, A. C.; Palomares, E.; Durrant, J., *J. Phys. Chem. B* **2005,** *109* (10), 4616-4623.
12. O'Regan, B. C.; Bakker, K.; Kroeze, J.; Smit, H.; Sommeling, P.; Durrant, J. R., *J. Phys. Chem. B* **2006,** *110* (34), 17155-17160.

Chapter 4. Relationship between dye molecular structure and DSSC performance

The aim of this Chapter is to investigate the influence of dye sensitiser structure on the performance of dye sensitised solar cells. The first two studies included in Chapter 4 detail the synthesis, electrochemical and photochemical properties of novel polypyridyl complexes containing different electron donating and electron withdrawing groups. Their performance in DSSC devices is also studied. The third study from this Chapter involves a thorough comparison of DSSC devices made using the most efficient dyes reported up to now.

This Chapter is based on the following publications:

Reynal, A., Forneli, A., Martínez-Ferrero, E., Sánchez-Díaz, A., Vidal-Ferran, A., Palomares, E., Eur. J. Inorg. Chem., 2008, 1955-1958.

Reynal, A., Forneli, A., Martínez-Ferrero, E., Sánchez-Díaz, A., Vidal-Ferran, A., O'Regan, B., Palomares, E., J. Am. Chem. Soc., 2008, 130, 13558-13567.

Reynal, A., Forneli, A., Palomares, E., Energy Env. Sci., 2010, 3(6), 805-812.

TABLE OF CONTENTS

4.1. Introduction

The role of the photosensitiser in molecular photovoltaic devices is to act as a light harvesting antenna and to inject photoexcited electrons into the conduction band of the semiconductor. Besides the numerous chromophoric molecules studied, the most efficient sensitisers used so far in DSSCs are ruthenium polypyridyl complexes.[1]

The first papers published in the field of dye sensitised solar cells based on nanocrystalline TiO_2 used a trinuclear ruthenium complex as photosensitiser (Figure 4.1).[2, 3] However, considerable improvements in the overall performance of the devices has been achieved in recent years by successive modifications to the dye structure.[4]

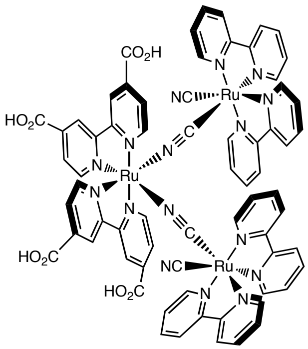

Figure 4.1. Molecular structure of the first trinuclear ruthenium complex used in DSSCs

The molecular structure of the dye affects not only their absorption, photophysical and redox properties, but also the electron transfer processes occurring at the TiO_2/dye/electrolyte surface. These parameters strongly determine the overall efficiency of the device.

The use of photosensitisers such as $Ru^{(II)}$ polypyridyl complexes with low molar extinction coefficients requires that DSSC devices have thicker TiO_2 films in order to have enough dye present to capture as many as possible of the incident photons. However, this results in a decreased V_{oc} due to an enhancement of the surface area, which provides additional e^--TiO_2/electrolyte$^+$ recombination sites.[5, 6] For this reason, some developments in the design of new ruthenium polypyridyl photosensitizers have arisen from efforts aimed at improving their optical absorption. One of the best routes to improve the light harvesting capability of ruthenium complexes is through the extension of the pyridyl ligands with the introduction of π−conjugated donor or acceptor systems (Figure 4.2).[7-13]

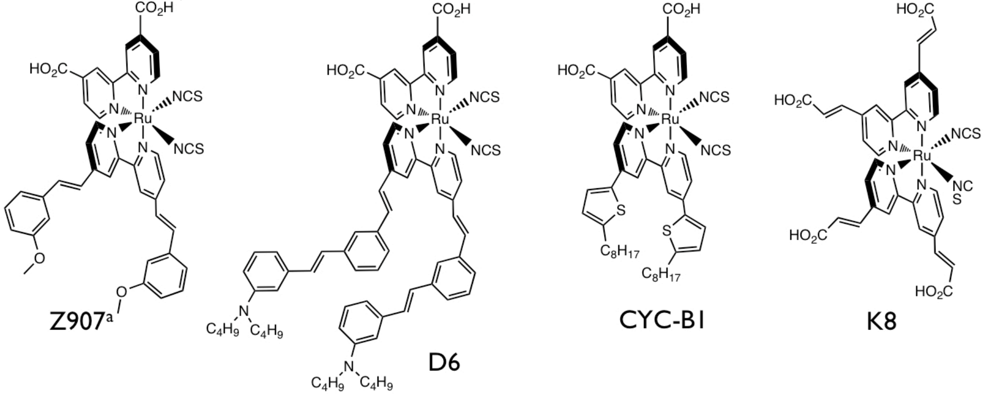

Figure 4.2. Molecular structure of highly π-conjugated ruthenium polypyridyl complexes. [a] In some of the publications regarding DSSCs, dyes are referred to by codes. These codes will also be used in this thesis

Ideally, the photosensitiser absorption spectrum should overlap as far as possible with that of the solar spectrum. Sequential tuning of the HOMO and LUMO energy levels through the incorporation of strong σ-electron donor or low-lying π* groups can be performed in order to extend the absorption spectrum of the dye to the near IR region (Figure 4.3).[14] These modifications involve a decrease in the band gap, but the position of the HOMO and LUMO energy levels of the dye have to be such as to maintain sufficient driving force to allow for both efficient electron injection into the TiO_2 and dye regeneration by the iodide/triiodide redox couple.

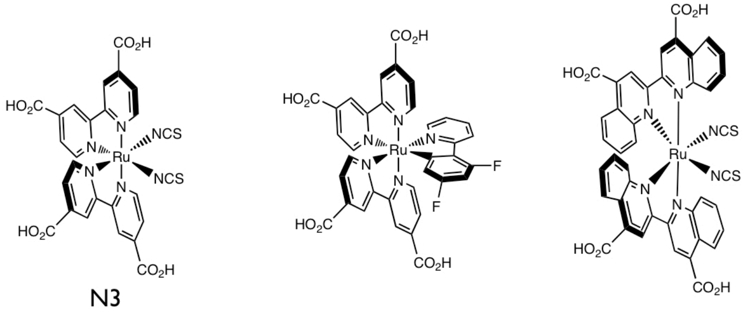

Figure 4.3. Molecular structure of ruthenium polypyridyl complexes containing ligands which are able to shift absorption spectra towards the near IR

One of the most commonly used approaches to produce a red-shift to the absorption spectra of $Ru^{(II)}$ polypyridyl complexes is through the destabilisation of the HOMO energy level with the introduction of thiocyanate ancillary ligands,[15] or, more recently, using cyclometalated ligands.[16-18]

Another way to decrease the HOMO-LUMO gap has been achieved with the introduction of ligands containing low-lying π*orbitals.[19]

An important issue for molecular photovoltaics is to achieve fast and efficient electron injection into the metal oxide. This can be obtained by a strong attachment of the dye onto the surface of the semiconductor, as well as by a sufficiently high LUMO energy level of the photosensitiser. In addition, the LUMO energy level should be located in the ligands containing the groups anchored onto the TiO_2 surface, in order to obtain an effective coupling between the dye and the metal oxide orbitals. Covalent bonds between the anchoring groups of the ruthenium polypyridyl complex and the hydroxyl groups present on the surface of the TiO_2 nanoparticles allow for strong electron coupling between the photosensitiser and the semiconductor.[20] Different anchoring groups have been tested, but the most common anchoring group in ruthenium complexes are carboxylic acids (Figure 4.4). Carboxylic acid groups can be easily hydrolysed in the presence of water or basic media resulting in dye desorption from the TiO_2 surface. A strategy to prevent the hydrolysation of the link between the dye and the TiO_2 is the substitution of carboxylic acid groups by more stable linkers such as phosphonic acid .[21, 22]

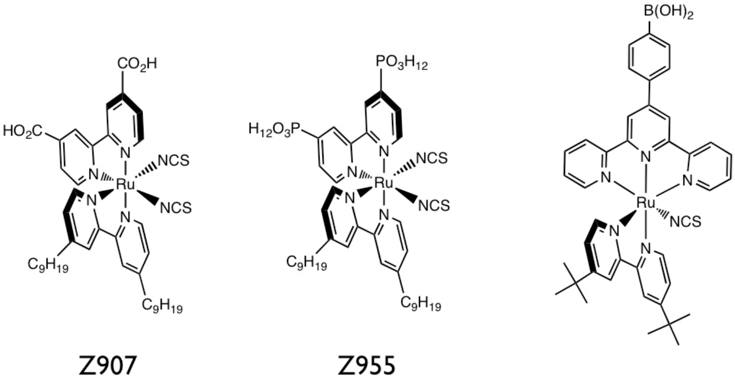

Figure 4.4. Molecular structure of ruthenium polypyridyl complexes containing different anchoring groups

Furthermore, dyes attached to the surface of metal oxides can be desorbed by the presence of water in the electrolyte, which is obviously a concern for the long term stability of DSSCs. The incorporation of hydrophobic alkyl chains to the pyridyl ligand can decrease dye desorption and increase cell stability by preventing the accumulation of water molecules near the TiO_2 surface (Figure 4.5).[23-25]

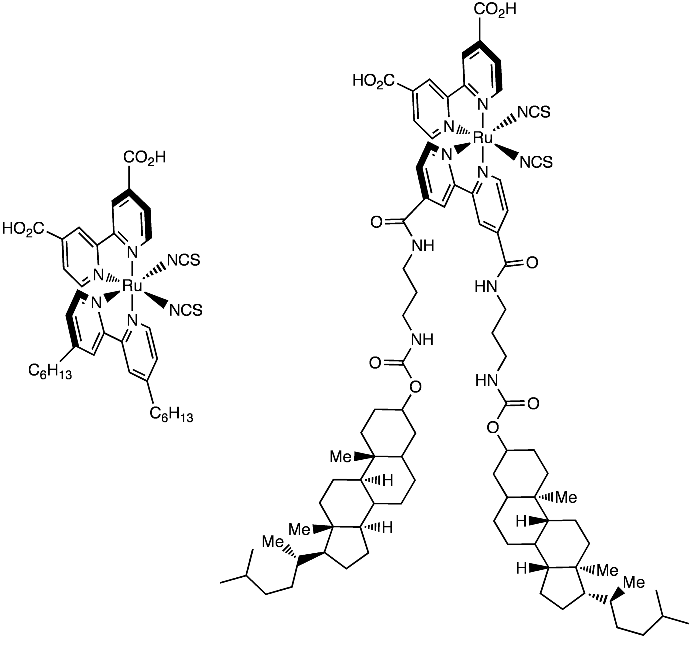

Figure 4.5. Molecular structure of two amphiphilic ruthenium polypyridyl complexes

The spatial charge separation between the oxidised dye and the surface of the semiconductor has an important effect on the charge recombination dynamics between the photoinjected electrons in the conduction band of the TiO_2 and the oxidised dye.[26] Increasing this distance and minimising recombination can be achieved by the attachment of electron donor groups [27, 28] or rigid spacers [29] to the polypyridyl ligands able to locate the cationic charges at long distances from the TiO_2 surface (Figure 4.6).

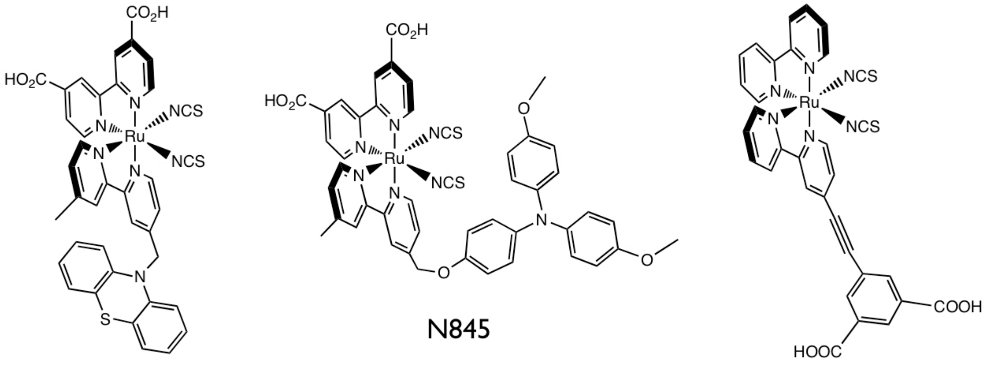

N845

Figure 4.6. Ruthenium polypyridyl complexes which increase the distance between dye cation and TiO_2 surface by the introduction of electron-donor groups or rigid spacers into dye structure

The recombination reaction between the photoinjected electrons and the oxidised electrolyte strongly affects the V_{oc} of the device and, thus, the final overall efficiency. The incorporation of long alkyl chains and the degree of protonation of the ruthenium photosensitisers are key factors in the reduction of the e^--TiO_2/electrolyte$^+$ recombination reaction. Amphiphilic dyes can block the approach of the oxidised electrolyte to the semiconductor surface, while the control of the degree of protonation of the acid anchoring groups prevents the downward shift of the semiconductor conduction band edge caused by surface protonation. The protons of ruthenium polypyridyl sensitisers can be substituted by tetrabutylammonium cations (TBA), sodium cations or other counter ions (Figure 4.7).[30, 31]

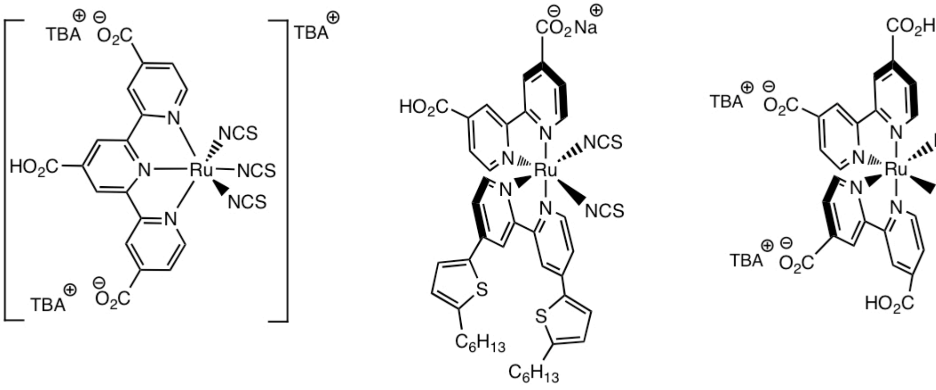

Black Dye C101 N719

Figure 4.7. Ruthenium polypyridyl complexes with various counter ions

The V_{oc} in DSSCs seems strongly related to the dye molecular structure. Small changes in certain atoms or substituent groups of the dye molecular structure have shown strong effects on the V_{oc}.[32, 33] The role of the structure of the dye in this context is still not clear. For this reason, several studies were performed by introducing small modifications to a ruthenium polypyridyl complex (Articles A and B). Furthermore, the quantitative parameters of the cells sensitised with the most efficient dyes published to date were measured (Article C).

4.2. Article A. A phenanthroline heteroleptic ruthenium complex and its application to dye sensitised solar cells

Eur. J. Inorg. Chem. 2008, 1955

Anna Reynal,[a] Amparo Forneli,[a] Eugenia Martínez-Ferrero,[a] Antonio Sánchez-Díaz,[a] Anton Vidal-Ferran,[a,b] Emilio Palomares*[a,b]

[a] Institute of Chemical Research of Catalonia (ICIQ), Avda. Països Catalans, 16. Tarragona. 43007 (Spain). Fax: +34 977920241, e-mail address: epalomares@iciq.es, [b] ICREA

Keywords: Dyes / Solar cells / Ruthenium / Heteroleptic complexes / Charge recombination / Electron transfer

4.2.1. Abstract

We report here the synthesis and characterisation of a new heteroleptic ruthenium(II) complex and its applications as efficient light-harvesting sensitiser in functional dye sensitised solar cells. The relation between the interfacial charge-transfer processes that govern the device performance and the cell efficiency under illumination are also discussed.

4.2.2. Introduction

Bis(bipyridine)ruthenium complexes have been widely studied as efficient light-harvesting molecules when adsorbed onto the surface of mesoporous semiconductor thin films, which are used as working electrodes on dye-sensitised solar cells.[4] Despite the low molecular extinction coefficient and the lack of absorbance in the near infrared region of the solar spectrum when compared to, for example, phthalocyanines, they have the best light-to-energy conversion efficiencies to date. During the last 10 years the molecule known as **N719** [chemical name: bis(tetrabutylammonium) *cis*-bis(isothiocyanato)bis(2,2'-bipyridyl-4,4'-dicarboxilato)ruthenium(II)] has been the paradigm of a molecular dye because of its high solar-to-electricity efficiency achieved when used as sensitiser in DSSC.[34] Hence, an interesting challenge for many researchers has been the design and synthesis of new ruthenium(II) complexes with enhanced properties such as slow back-electron transfer from the photoinjected electrons at the mesoporous semiconductor either with the oxidised dye or the electrolyte[35] as well as the dye long-term stability under device operation.[13] To this end, a successful strategy has been the design and synthesis of ruthenium(II) heteroleptic compounds where one of the 4,4'-dicarboxy-2,2'-bipyridines has been replaced by a more appropriate ligand. As an example, Nazeeruddin *et al.* showed that the presence of a bipyridine on the ruthenium(II) complex bearing long alkyl chains (common name: Z907, chemical name: *cis*-[bis(2,2'-bipyridyl-4,4'-dicarboxylic acid)(4,4'-dinonyl-2,2'-bipyridyl)bis(isothiocyanato)ruthenium(II)]) improves not only the device stability but also its performance under illumination at full sun light (100 mW·cm^{-2} 1.5 AM G).[23] The same strategy has been applied by Zakeeruddin and co-workers with K77 dye ([*cis*-{4,4-bis[2-(4-tert-butoxyphenyl)ethenyl]-2,2'-bipyridyl}bis(2,2'-bipyridyl-4,4'-dicarboxylic acid)bis(isothiocyanato)ruthenium(II)]) which, in combination with a non-volatile electrolyte, exhibits a unique performance by combining high efficiency and stability.[36] Thelakkat and co-workers have also reported the use of tris(phenylamine)-substituted bipyridines in Ru^{II} complexes as efficient sensitisers for solid-state DSSC when using an organic hole conductor as a solid electrolyte.[37]

In this communication we would like to report the synthesis and characterisation of a new heteroleptic ruthenium(II) complex with one of the bipyridine ligands replaced by a more conjugated ligand such as the 5,6-dimethyl-1,10-phenanthroline. Scheme 4.1 illustrates the molecular structure of the ruthenium(II) heteroleptic complex. Moreover, we have also carried out a study of the interfacial charge-transfer kinetics of the molecule when anchored onto the surface of nanocrystalline TiO_2 semiconductor particles.

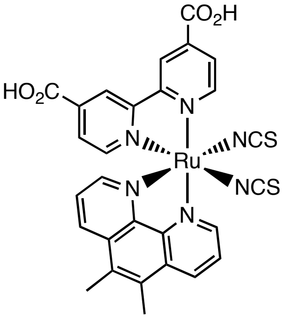

Scheme 4.1. Molecular structure of AR25 (chemical name: cis-bis(2,2'-bipyridyl-4,4'-dicarboxylic acid)(5,6-dimethyl-1,10-phenanthroline)bis(isothiocyanato)ruthenium(II))

4.2.3. Results and discussion

The **AR25** shows a typical UV/Vis spectrum with a metal-to-ligand charge transfer band centred at λ = 518 nm with a molecular extinction coefficient of 6578 dm^3·M^{-1}·cm^{-1}. Figure 4.8 illustrates the absorption spectra of the complex in solution and adsorbed onto a transparent mesoporous TiO_2

or negligible presence of dye molecular aggregates. Moreover, in solution, after excitation at the maximum of the MLCT band, a broad emission band can be observed with a maximum at $\lambda = 746$ nm. The large Stokes shift is due to the nature of the excited state, which –as reported before for other ruthenium(II) complexes[38]– is a triplet energy state. It is worthy to note that the **AR25** emission is strongly quenched when its molecules are anchored to nanocrystalline TiO_2 particles (Figure 4.9). Hence, we can conclude that the electron injection process from the excited state into the semiconductor conduction band is responsible for the immediate disappearance of luminescence upon light excitation. Furthermore, the excited-state emission lifetime for the complex is strongly shortened when anchored to the mesoporous TiO_2 film. The emission lifetime for **AR25** in solution (we used dimethylformamide as solvent) gives in our hands a decay that was fitted to two kinetic components, $\tau_1 = 9.57$ ns (18.9 %) and $\tau_2 = 56.67$ ns (81.1 %) whereas for the **AR25**/TiO_2 samples $\tau_1 = 2.23$ ns (48.5 %) and $\tau_2 = 12.61$ ns (51.5 %).

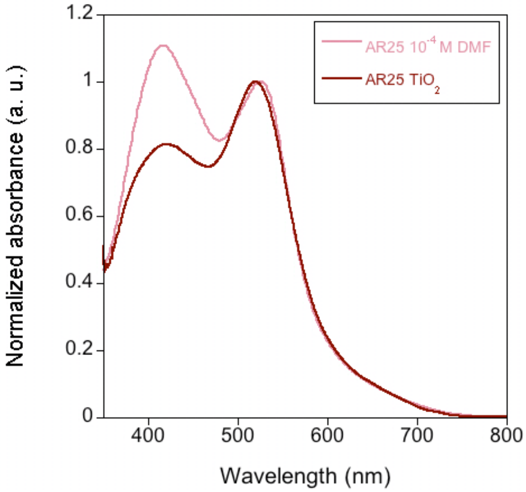

Figure 4.8. UV/Vis spectra of AR25 in DMF ($1\cdot10^{-4}$M, —) and adsorbed onto a 4 μm thick transparent TiO_2 film (—)

The electrochemical properties of the ruthenium(II) complex **AR25** were also analysed using cyclic voltammetry in dry DMF as solvent with 0.1 M tetrabutylammonium hexafluorophosphate as electrolyte. The CV allowed the observation of a quasi-reversible couple at 0.79 V *vs* SCE assigned to the $Ru^{II/III}$ redox couple.

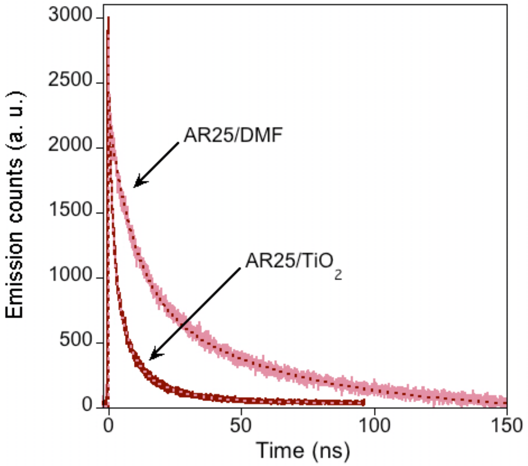

Figure 4.9. Emission decay kinetics measured using time correlated-single photon counting under normal conditions for AR25 in DMF (10^{-4} M) and adsorbed onto a 4 μm thick transparent TiO_2 film. Dashed lines correspond to the adjusted fit decay. The excitation wavelength was λ_{ex} = 405 nm, and the emission was monitored at λ_{em} = 745 nm

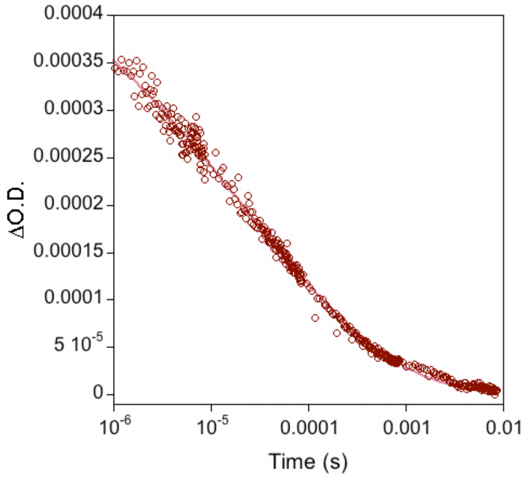

Figure 4.10. Transient absorption decay kinetics for a 4 μm thick transparent mesoporous film sensitised with AR25. The solid line corresponds to the fitting to a stretched exponential function: $\Delta O.D. = e^{\left[-\left(t/\tau\right)\right]^{\alpha}}$ *. The excitation wavelength was λ_{ex} = 535 nm and the probe wavelength was λ_{pr} = 800 nm*

Once the electrochemical and the emission properties of the ruthenium complex were measured, we turned to the light induced charge transfer kinetics between the sensitiser and the semiconductor nanocrystalline TiO_2 particles. As we have reported before,[39] we have utilised laser-transient absorption spectroscopy to investigate the electron-recombination dynamics. Figure 4.10

shows typical decay kinetics for the **AR25**/TiO_2 samples. We assigned the transient decay signal to the recombination of the photoinjected electrons, upon laser excitation, into the semiconductor conduction band and the oxidised dye species. The recorded excited spectra show a broad absorption band with a maximum centered at 800 nm, which has previously been assigned to the cation species of similar ruthenium(II) complexes such as the above-mentioned **N719** molecule.[40] The measurement of the electron-recombination lifetime at the half maximum of the signal is 35 μs.

Finally, we carried out measurements on complete functional devices. We measured the incident photon-to-current conversion efficiency spectra for devices sensitised with **AR25** using as electrolyte a solution containing the redox couple iodine/iodide. Figure 4.11 illustrates the IPCE spectra for an **AR25**/DSSC.

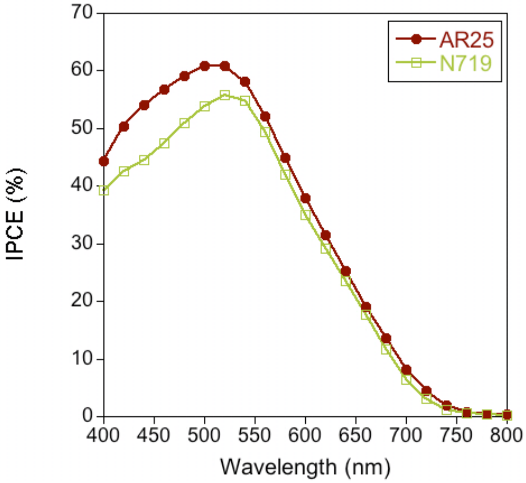

Figure 4.11. IPCE spectra for DSSC sensitised using AR25 and the homoleptic dye N719

In our hands, the IPCE spectrum for **AR25** devices showed higher intensity at the maximum absorption wavelength at λ = 550 nm when irradiated with simulated sunlight. The corresponding photocurrent *vs* voltage characteristic curves were also measured to give an overall efficiency of 2.6 % under irradiation at 1 sun (100 $mW\cdot cm^{-2}$) with simulated AM-1.5G solar spectrum (Figure 4.12). Under the same conditions, we examined DSSC sensitised with the **N719** dye, and the overall efficiency was 3.6 %. The main difference between both devices was in the open circuit voltage. While for the former ruthenium(II) complex a V_{oc} = 0.69 V was obtained, for the latter a V_{oc} = 0.78 V was observed. We also noted that the devices made using **AR25** as sensitiser usually showed lower fill factors when compared to devices made using the **N719** complex (38.5 % and 47.6 %, respectively). We believe that the higher recombination on **AR25** devices limits the photocurrent and the overall performance of the solar cell. Further work focussed on the control of such wasteful reactions is being carried out.

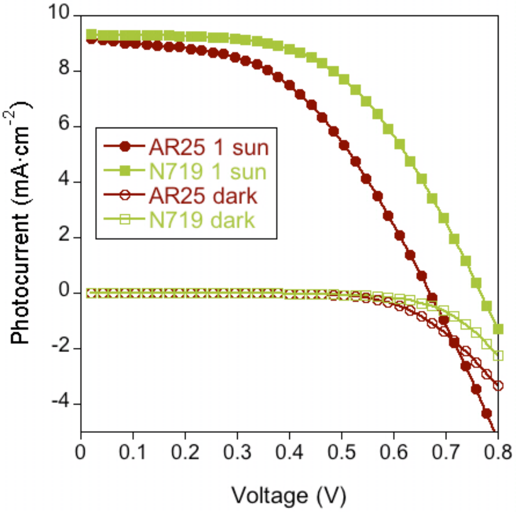

Figure 4.12. Photocurrent vs voltage curve (I-V curve) for a 1 cm^2 AR25 DSSC (circles) and N719 DSSC (squares). Measurements were performed at 1 sun (full signal) and dark conditions (empty signal)

4.2.4. Conclusions

We presented a new ruthenium(II) heteroleptic complex which shows the appropriated redox electrochemistry to be used as sensitiser in dye-sensitised solar cells. Furthermore, we have characterised the charge transfer processes occurring at the interface between the **AR25** dye and the nanocrystalline TiO_2 nanoparticles showing that the photo-induced electron injection is particularly efficient despite the low-lying π* level character of the phenanthroline moiety as coordinating ligand,[41] and the electron recombination processes is at least one order of magnitude slower than the regeneration reactions, which normally occur on the nanosecond time scale; this makes feasible the possibility to optimise the devices and achieve higher light-to-energy efficiencies in the same order of magnitude than the most popular dye, **N719**. The high photocurrent observed using **AR25** makes the dye an interesting candidate for "molecular cocktails" where several dyes with light absorptions in different regions of the solar spectrum are combined to achieve the desired panchromatic sensitisation of DSSC.

4.2.5. Experimental section

4.2.5.1. Synthesis of AR25

The synthesis of *cis*-bis(2,2'-bipyridyl-4,4'-dicarboxylic acid)(5,6-dimethyl-1,10-phenanthroline)bis(isothiocyanato)ruthenium(II) [Ru(dcbpy)(dmphen)(NCS)$_2$] (**AR25**) was carried out according to that reported by Kasuga *et al.*,[42] but by adding 5,6-dimethyl-1,10-phenantroline (81.6 mg, 0.4 mmol) instead of 1,10-phenantroline. Yield: 56.6 %. ^{1}H-RMN (400 MHz, DMF-d$_7$) δ: 9.75 (d, *J* = 5,8 Hz, 1H), 9.68 (d, *J* = 5.3 Hz, 1H), 9.26 (d, *J* = 1.3 Hz, 1H), 9.06 (d, *J* = 1.3 Hz, 1H), 9.04 (d, *J* = 8.5 Hz, 1H), 8.66 (d, *J* = 8.6 Hz, 1H), 8.44 (dd, *J* = 5.8, 1.3 Hz, 1H), 8.35 (dd, *J* = 8.5, 5.3 Hz, 1H), 8.11 (d, *J* = 5.3 Hz, 1H), 7.92 (d, *J* = 5.9 Hz, 1H), 7.63 (dd, *J* = 8.5, 5.3 Hz, 1H), 7.56 (dd, *J* = 5.9, 1.3 Hz, 1H), 2.92 (s, 3H), 2.81 (s, 3H). ESI-MS: m/z 670 (M + H).

4.2.5.2. Optical, electrochemical and spectroscopical measurements

The UV/Vis and fluorescence spectra were recorded using a 1 cm pathlength quartz cell with a Shimadzu UV spectrophotometer 1700 and an Aminco–Bowman series 2 luminescence spectrometer with temperature controller. The electrochemical data was obtained employing a conventional three-electrode cell connected to a CH Instruments 660c potentiostat-galvanostat. For the cyclic voltammetry, we used a platinum working electrode, a calomel reference electrode and a platinum wire as auxiliary electrode. The picoseconds to microseconds emission lifetime measurements were carried out with a Lifespec picosecond fluorescence lifetime spectrometer from Edinburgh Instruments. As excitation source, the diode laser with 405 nm nominal wavelength was used. The instrument response measurement at the half width a high maximum was below 350 ps. Laser-transient absorption measurements were carried out with a home-built system as reported before.[43] ^{1}H and ^{13}C NMR spectra, NOESY and COSY experiments were measured with a Bruker 400 MHz spectrometer. A Waters LCT Premier liquid chromatograph coupled to a time-of-flight mass spectrometer with electrospray ionisation was used to measure mass spectra. The FTIR spectra were obtained with an FTIR ThermoNicolet 5700 spectrometer.

4.2.5.3. Nanoparticle synthesis and film preparation

The nanocrystalline TiO$_2$ particles were synthesised as reported before.[44] In brief: Titanium isopropoxide (40 mL, 0.13 mol) was added to glacial acetic acid (9.12 g) under argon while stirring. The reaction mixture was cooled in an ice-bath, and 0.1 M nitric acid (240 mL) was added while vigourously stirring. The mixture was heated in an oil bath at 80 °C during 8 h. and, after cooling, was filtered through a 0.45 µm syringe filter. The resulting product was diluted to 5 wt % of TiO_2 by adding water and then autoclaved at 220 °C for 12 h. The aqueous phase was removed by centrifugation, and the solid nanoparticles were isolated and rinsed twice with ethanol. An ultrasonic horn was used to break the aggregates, and the solvent was removed under vacuum. The solid nanoparticles were diluted to 15 wt % in TiO_2, using ethyl cellulose and terpineol, and the paste was homogenised by using a ball mill.

4.2.5.4. Device preparation and characterisation

DSSCs were made using 4 µm thin films consisting of 20 nm TiO_2 nanoparticles deposited onto a conducting glass substrate (Hafford Glass Inc., 15 $\Omega \cdot cm^{-2}$ resistance) by using the well-known doctor-blade technique. The active area was 0.152 cm^2. The prepared electrodes were gradually heated under airflow at 325 °C for 5 min, 375 °C for 5 min, 450 °C for 15 min, and 500 °C for 15 min. Then, they were submerged into $40 \cdot 10^{-3}$ M $TiCl_4$ aqueous solution at 70 °C for 15 min, washed with ethanol, heated again at 500 °C for 30 min, and cooled to 50 °C before soaking the films in a $5 \cdot 10^{-4}$ M **AR25** solution in acetonitrile/*tert*-butyl alcohol (1:1) overnight. The counter electrodes were prepared by spreading a solution of H_2PtCl_6 in ethanol onto a conducting glass substrate with a small hole to allow the introduction of the liquid electrolyte, under vacuum. The liquid electrolyte was prepared by using 0.6 M DMPII (1-propyl- 2,3-dimethylimidazolium iodide), 0.05 M I_2, and 0.1 M LiI in acetonitrile/valeronitrile (85:15). The photovoltaic measurements were carried out with a 150 W xenon lamp from Oriel Instruments with the appropriated set of filters for the correct simulation of the AM-1.5G solar spectrum. The incident light power was calibrated by using a silicon photodiode previously calibrated at 1000 $W \cdot m^{-2}$ at AM-1.5G.

4.2.6. Acknowledgements

E. P. would like to thank the Spanish Ministerio de Educación y Ciencia (MEC) for the funding through the CONSOLIDER HOPE- CSD-0007-2007 and the CTQ2007-60746/BQU project. E. M. F. also thanks the MEC for her Juan de la Cierva Fellowship.

4.3. Article B. Interfacial charge recombination between e$^-$-TiO$_2$ and the I$^-$/I$_3^-$ electrolyte in ruthenium heteroleptic complexes: dye molecular structure-open circuit voltage relationship

J. Am. Chem. Soc. 2008, 130, 13558

Anna Reynal,[a] Amparo Forneli,[a] Eugenia Martínez-Ferrero,[a] Antonio Sánchez-Díaz,[a] Anton Vidal-Ferran,[a,b] Brian O'Regan,[c] Emilio Palomares*[a,b]

[a] Institute of Chemical Research of Catalonia (ICIQ), Avda. Països Catalans, 16, Tarragona, Spain. E-mail: epalomares@iciq.es, [b] ICREA, [c] Imperial College of London, Chemistry Department, South Kensington, Exhibition Road, SW7 2AZ London, United Kingdom.

4.3.1. Abstract

A series of heteroleptic ruthenium(II) polypyridyl complexes containing phenanthroline ligands have been designed, synthesised, and characterised. The spectroscopic and electrochemical properties of the complexes have been studied in solution and adsorbed onto semiconductor nanocrystalline metal oxide particles. The results show that for two of the ruthenium complexes, bearing electron-donating (-NH$_2$) or electron-withdrawing (-NO$_2$) groups, the presence of the redox-active I$^-$/I$_3^-$ electrolyte produces important changes in the interfacial charge transfer processes that limit the device performance. For example, those dyes enhanced the electron recombination reaction between the photoinjected electrons at TiO$_2$ and the oxidised redox electrolyte. In an effort to understand the details of such striking observations, we have monitored the charge transfer reactions taking place at the different interfaces of the devices using time resolved single photon counting, laser transient spectroscopy, and light-induced photovoltage measurements.

4.3.2. Introduction

Ruthenium(II) polypyridyl complexes have been widely investigated as efficient light harvesting molecules in dye sensitised solar cells.[4, 34, 45] In fact, devices made using as the sensitiser the complex *cis*-bis(isothiocyanato)bis(2,2'-bipyridyl-4,4'-dicarboxylato)ruthenium(II) bis(tetra-butylammonium), also known as **N719** (Scheme 4.2), have achieved certified efficiencies for light-to-energy conversion of 11 % under illumination at 1 sun (100 mW·cm^{-2}).[46] Several groups have designed and synthesised a wide range of ruthenium(II) complexes, but still bis(2,2'-bipyridyl-4,4'-dicarboxylato)-based ruthenium complexes or their derivates have superior performance when compared in similar conditions, although a few exceptions have been demonstrated in recent years.[47-49] However, although it has been possible to achieve a higher photocurrent for devices made using those alternative dyes (for example, the "**Black Dye**",[49] chemical name tris(isothiocyanato)ruthenium(II) 2,2':6',2"-terpyridine-4,4',4"-tricarboxylic acid, tris(tetra-butylammonium) salt, usually a decrease in the cell open circuit voltage has been observed.

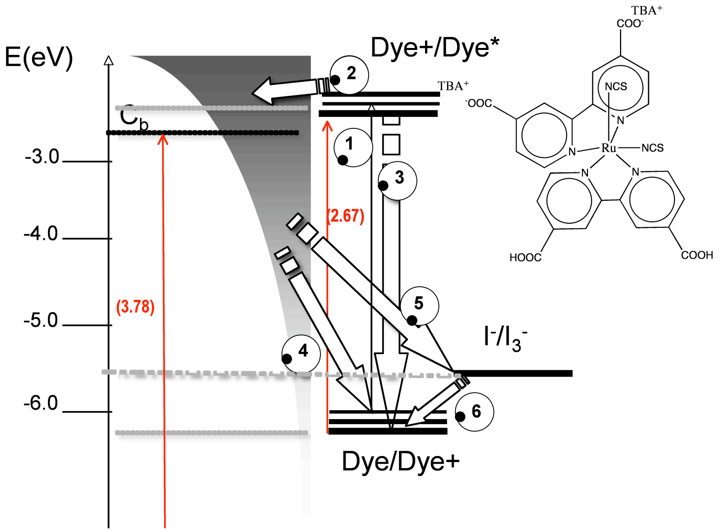

Scheme 4.2. Charge transfer reactions taking place at the different interfaces of a DSSC and the molecular structure of N719. The numbers in parentheses are the energy gap for TiO_2 and the N719 dye, and the gray shadow represents the density of electron states. Values in parentheses are the energy versus vacuum level as calculated using reference [50]. Reaction 1: light absorption and formation of the dye excited state (solid black arrow). Reaction 2: photoinduced electron injection from the excited dye to the TiO_2 conduction band. Reaction 3: luminescence emission from the dye excited state. Reaction 4: electron recombination between photoinjected electrons at TiO_2 and the oxidised dye. Reaction 5: electron recombination between photoinjected electrons at TiO_2 and the oxidised electrolyte. Reaction 6: dye ground-state regeneration by the electrolyte

A detailed study of the charge transfer reactions taking place at the different interfaces of a DSSC sensitised with **N719** shows that electron transfer reactions are very much optimised.[35, 40, 51-53] For example, in a typical DSSC using an iodine/iodide liquid electrolyte, upon light absorption (Scheme 4.2, reaction 1) electron injection occurs in < 1 ps to hundreds of picoseconds (Scheme 4.2, reaction 2). This is usually much faster than the nanosecond scale lifetime of excited ruthenium complexes in pure solution (Scheme 4.2, reaction 3). This normally gives an electron injection yield higher than 90 %. Similarly, the oxidised dye is regenerated by the iodine/iodide electrolyte in 0.1 - 10 μs (Scheme 4.2, reaction 6), well before the back electron transfer reaction between the photoinjected electrons and the oxidised dye, which takes place in the range of hundreds of microseconds or even a few milliseconds (Scheme 4.2, reaction 4).

Several authors have studied the different causes that affect the V_{oc} of the DSSC.[54-64] Most of the results are based on the well-established knowledge of the Nernstian behaviour[63-67] of the TiO_2 semiconductor in the presence of surface dipoles. For example, the use of *tert*-butylpyridine, a base, provokes a positive shift of the TiO_2 conduction band and, therefore, an increase in the cell open circuit voltage.[63, 68, 69] On the contrary, the presence of acid dipoles has the inverse effect. Moreover, using conformal coatings on the surface of the nanocrystalline TiO_2 particles with different basic or acidic metal oxides also influences the cell voltage[70, 71] and, thus, the overall device efficiency. Furthermore, systematic work has been carried out on controlling the number of protons in the dye molecules to tune the photocurrent and the voltage of the cell too, and, for example, the mentioned **N179** has its more acidic version, with four protons, named N3, that shows upon illumination at a higher photocurrent but a lower V_{oc}.[30] Only recently, it has been demonstrated that several dyes, which show poor light-to-energy conversion performance, when employed as sensitisers in a DSSC, do increase the rate of electron recombination between the photoinjected electrons and the oxidised electrolyte, affecting not only the photocurrent but also the cell voltage.[72] As a matter of fact, the molecular structures of those dyes have in common the presence of extended π-conjugated systems which lie close to the nanoparticle metal oxide surface when anchored.[73] Several authors have previously studied either homoleptic or heteroleptic phenanthroline-based ruthenium(II) complexes and have observed modest light-to-electricity conversion efficiencies when compared to those of devices made using **N719** as a sensitiser although the generated photocurrent was comparable to that of the devices made using **N719**.[31, 42, 74-78] Several hypotheses have been proposed, which are mainly related to a shift of the energy levels of the dye lowest unoccupied molecular orbital or the highest occupied molecular orbital due to the introduction of a lower energy π* molecular orbital and, therefore, inefficient photoinduced electron transfer from the dye excited state to the semiconductor conduction band (Scheme 4.2, reaction 2) or inefficient regeneration of the dye ground state by the electrolyte, respectively, or both (Scheme 4.2, reaction 6).[77, 79] However, there is still an ongoing discussion about the influence of those extended π-conjugated systems on the interfacial electron transfer reactions at the device. For example, Arakawa and co-workers observed in $Ru^{(II)}$ complexes bearing 4,4'-dicarboxy-2,2'-biquinoline ligands an increase in the dark current (e^--TiO_2/electrolyte$^+$) (Scheme 4.2, reaction 5) when compared to that of the standard **N719** DSSC.[74, 80] Moreover, Thummel *et al.*

have recently reported the synthesis of new homoleptic 1,8-naphthyridine-based $Ru^{(II)}$ complexes that show modest incident photon-to-current efficiencies, and they have assigned those results to the low yield of photoinduced electron injection of the complexes into the semiconductor.[81] Furthermore, it has been postulated that some organic dyes based on thiophene groups show a clear dependence between their structure and the V_{oc}; increasing the number or thiophene bridge units on the organic dye increases drastically the dark current.[82, 83] Hence, it seems there is a general trend between extending the π-conjugated ligand and the cell voltage.

Taking into account all these observations mentioned above, we have designed a series of heteroleptic ruthenium(II) complexes where one of the 4,4'-dicarboxy-2,2'-bipyridine ligands has been substituted by a phenanthroline moiety (Figure 4.13) with the aim to achieve high photocurrents and study the effect of the dye molecular structure on the cell voltage. Moreover, the phenanthroline ligand has been modified with the introduction of electron-donating or electron-withdrawing groups to achieve the desired control over the molecular orbitals. While electron-donating groups should decrease the energy gap (HOMO-LUMO gap), the introduction of electron-withdrawing groups should have the opposite effect, and thus, we expect a variation in the DSSC performance.

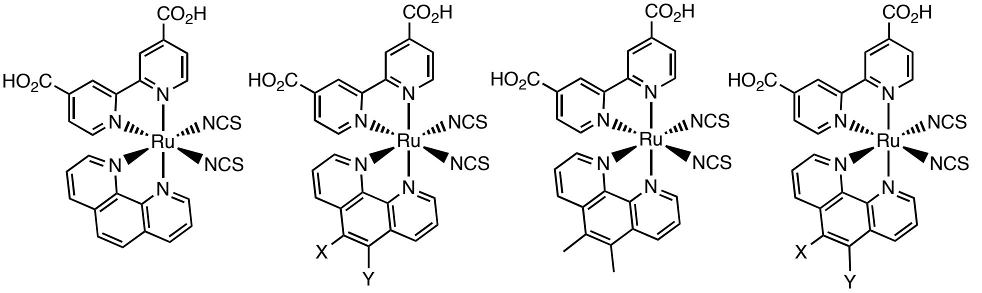

AR20

AR24a: X = H, Y = NH_2
AR24b: X = NH_2, Y =H

AR25

AR27a: X = H, Y = NO_2
AR27b: X = NO_2, Y =H

Figure 4.13. Molecular structures for the $Ru^{(II)}$ complexes utilised in the present study

4.3.3. Experimental section

The syntheses of all complexes were carried out following the procedure in a previous paper published in the literature by Kasuga *et al.*[42] All the chemical products were purchased from Sigma-Aldrich and used without further purification if not otherwise stated.

4.3.3.1. Synthesis of *cis*-(4,4'-dicarboxy-2,2'-bipyridine) (1,10-phenantroline)dithiocyanate ruthenium (II) ($[Ru(dcbpy)(phen)(NCS)_2]$) (AR20)

Dichloro(*p*-cymene)ruthenium(II) dimer (120 mg, 0.2 mmol) was dissolved in 30 mL of dimethylformamide in a three-necked round bottomed flask completely covered with aluminium foil. The flask was purged with argon during 15 minutes. 1,10-phenanthroline (70.6 mg, 0.4 mmol) was added while stirring. The reaction mixture was heated at 60 ºC for 4 h. After this time 4,4'-dicarboxy-2,2'-bipyridine (95.62 mg, 0.4 mmol) was added, and the reaction mixture was heated at 160 ºC for 4 h under argon and in absence of light to avoid *cis* to *trans* isomerisation. Then, ammonium thiocyanate (0.99 g, 13 mmol) was added and the reaction mixture was maintained at 150 ºC for 5 h. After the reaction crude was kept cold at room temperature, the solvent was removed under vacuum. Then 5 mL of milli-Q water were added to remove the ammonium thiocyanate excess. A brown precipitate appeared, and it was collected by filtration with a sintered glass crucible. The product was washed three times with water and diethyl ether and dried under vacuum. Then, the product was dissolved in a mixture of 2.5 mL of methanol and 0.5 mL of tetrabutylammonium hydroxide (40 % weight) in order to form the tetrabutylammonium salt of the ruthenium complex. This solution was purified by size exclusion chromatography using a LH-20 Sephadex column (2,5 x 30 cm) and methanol as the mobile phase. The main red band was collected and the solvent was evaporated under vacuum. A few drops of 0.01 HNO_3 were added to the resulting semi-solid product until a brown precipitate appeared. It was collected with a sintered glass crucible and dried under vacuum. Yield: 81.5 %.

^1H-NMR (400 MHz, DMF-d_7) δ: 9.94 (d, *J* = 5.8 Hz, 1H), 9.92 (d, *J* = 5.3 Hz, 1H), 9.43 (s, 1H), 9.24 (s, 1H), 9.15 (d, *J* = 8.3 Hz, 1H), 8.78 (d, *J* = 7.3 Hz, 1H), 8.63 (d, *J* = 5.8 Hz, 1H), 8.61 (d, *J* = 8.8 Hz, 1H), 8.56 (dd, *J* = 8.3, 5.3 Hz, 1H), 8.49 (d, *J* = 8.8 Hz, 1H), 8.38 (d, *J* = 5.3 Hz, 1H), 8.14 (d, *J* = 5.9 Hz, 1H), 7.85 (dd, *J* = 8.3, 5.3 Hz, 1H), 7.75 (d, *J* = 5.9 Hz, 1H). ESI-MS: m/z 643 (M+H).

4.3.3.2. Synthesis of *cis*-(4,4'-dicarboxy-2,2'-bipyridine)(5-amino-1,10-phenantroline)dithiocyanate ruthenium (II) ($[Ru(dcbpy)(aphen)(NCS)_2]$ (AR24)

The synthesis of $[Ru(dcbpy)(aphen)(NCS)_2]$ was carried following a procedure like that of compound **AR20** except that 5-amino-1,10-phenanthroline (83 mg, 0.4 mmol) was added instead of 1,10-phenanthroline. The solid obtained was analysed by ^1H and COSY NMR spectroscopy, and two diastereoisomers were observed in a 1:1 proportion. Yield: 54.6 %. The different products were separated by reverse phase C_{18} semipreparative HPLC, using a mixture of H_2O (0.1 % TFA)/MeCN (0.1 % TFA) (73:23) as the mobile phase. Two compounds were isolated with a retention time (t_R) of 16.36 and 18.8 min, respectively, and finally, the solvent was removed under vacuum. Yield: 46.67 %.

Compound **AR24a** (t_R: 16.36 min): ^{1}H-RMN (400 MHz, MeOD) δ: 9.72 (d, *J* = 5.3 Hz, 1H), 9.56 (d, *J* = 5.9 Hz, 1H), 9.00 (s, 1H), 8.91 (d, *J* = 8.6 Hz 1H), 8.81 (s, 1H), 8.22 (d, *J* = 5.7 Hz, 1H), 8.14 (dd, *J* = 8.6, 5.3 Hz, 1H), 7.97 (d, *J* = 8.3 Hz, 1H), 7.46 (d, *J* = 5.3 Hz, 1H), 7.45 (m, 2H), 7.29 (dd, *J* = 8.3, 5.3 Hz, 1H), 7.07 (s, 1H). ESI-MS: m/z 658 (M+H). Compound **AR24b** (t_R: 18.8 min): ^{1}H-RMN (400 MHz, MeOD) δ: 9.74 (d, *J* = 5.6 Hz, 1H), 9.32 (d, *J* = 5.1 Hz, 1H), 9.01 (s, 1H), 8.88 (s, 1H), 8.54 (d, *J* = 8.5 Hz, 1H), 8.32 (m, 1H), 8.31 (d, *J* = 8.3 Hz, 1H), 7.92 (dd, *J* = 8.3, 5.1 Hz, 1H), 7.86 (d, *J* = 5.2 Hz, 1H), 7.71 (d, *J* = 5.9 Hz, 1H), 7.54 (d, *J* = 5.9 Hz, 1H), 7.45 (dd, *J* = 8.5, 5.3 Hz, 1H), 7.15 (s, 1H). ESI-MS: m/z 658 (M+H).

4.3.3.3. Synthesis of *cis*-(4,4'-dicarboxy-2,2'-bipyridine)(5,6-dimethyl-1,10-phenantroline)dithiocyanate ruthenium (II) [Ru(dcbpy)(dmphen)$(NCS)_2$] (AR25)

The synthesis of **AR25** was carried following the procedure as detailed for the synthesis of compound **AR20**, adding 5,6-dimethyl-1,10-phenantroline (81.6 mg, 0.4 mmol) instead of 1,10-phenantroline. Yield: 56.6 %.

^{1}H-RMN (400 MHz, DMF-d_7) δ: 9.75 (d, *J* = 5,8 Hz, 1H), 9.68 (d, *J* = 5.3 Hz, 1H), 9.26 (d, *J* = 1.3 Hz, 1H), 9.06 (d, *J* = 1.3 Hz, 1H), 9.04 (d, *J* = 8.5 Hz, 1H), 8.66 (d, *J* = 8.6 Hz, 1H), 8.44 (dd, *J* = 5.8, 1.3 Hz, 1H), 8.35 (dd, *J* = 8.5, 5.3 Hz, 1H), 8.11 (d, *J* = 5.3 Hz, 1H), 7.92 (d, *J* = 5.9 Hz, 1H), 7.63 (dd, *J* = 8.5, 5.3 Hz, 1H), 7.56 (dd, *J* = 5.9, 1.3 Hz, 1H), 2.92 (s, 3H), 2.81 (s, 3H). ESI-MS: m/z 670 (M + H).

4.3.3.4. Synthesis of *cis*-(4,4'-dicarboxy-2,2'-bipyridine)(5-nitro-1,10-phenantroline)dithiocyanate ruthenium (II) [Ru(dcbpy)(nophen)$(NCS)_2$] (AR27)

The synthesis of **AR27** was carried following the procedure as detailed for the synthesis of compound **AR20**, adding 5-nitro-1,10-phenantroline (81.6 mg, 0.4 mmol) instead of 1,10-phenantroline. Two stereoisomers were observed by proton and COSY NMR experiments in 1:1

HPLC, using MeCN (0.1 % TFA)/H_2O (0.1 % TFA) (70:30) as the eluent. Two compounds were isolated with a retention time of 16.03 and 18.47 min, respectively. Yield: 55.8 %.

Compound **AR27a** (t_R = 16.03 min): ^{1}H-RMN (400 MHz, MeOD) δ: 9.16 (dd, *J* = 5.3, 1.0 Hz, 1H), 8.96 (d, *J* = 5.6 Hz, 1H), 8.86 (s, 1H), 8.59 (s, 1H), 8.57 (dd, *J* = 8.3, 1.0 Hz, 1H), 8.41 (s, 1H), 8.34 (dd, *J* = 8.6, 0.7 Hz, 1H), 7.91 (dd, *J* = 8.3, 5.3 Hz, 1H), 7.54 (d, *J* = 5.6 Hz, 1H), 7.18 (m, 2H), 6.91 (d, *J* = 5.6 Hz, 1H). ESI-MS: m/z 688 (M + H). Compound **AR27b** (t_R = 18.47 min): ^{1}H-RMN (400 MHz, MeOD) δ: 9.26 (dd, *J* = 5.3, 1.2 Hz, 1H), 9.10 (d, *J* = 5.8 Hz, 1H), 8.73 (d, *J* = 8.7, 1.1 Hz, 1H), 8.59 (s, 1H), 8.51 (d, *J* = 1.1 Hz, 1H), 8.33 (d, *J* = 1.3 Hz 1H), 8.08 (dd, *J* = 8.2, 1.2 Hz, 1H), 7.83 (dd, *J* = 8.7, 5.3 Hz, 1H), 7.81 (dd, *J* = 5.8, 1.1 Hz, 1H), 7.54 (dd, *J* = 5.3, 1.1 Hz, 1H), 7.18 (d, *J* = 5.8 Hz, 1H), 7.07 (dd, *J* = 8.2, 5.4 Hz, 1H), 6.91 (dd, *J* = 5.8, 1.3 Hz, 1H). ESI-MS: m/z 688 (M + H).

4.3.3.5. Optical, electrochemical and spectroscopic measurements

The UV-vis and fluorescence spectra were recorded using a 1 cm path length quartz cell on a Shimadzu UV spectrophotometer 1700 and an Aminco-Bowman series 2 luminescence spectrometer with a temperature controller, respectively. The electrochemical data were obtained employing a conventional three-electrode cell connected to a CH Instruments 660c potentiostat-galvanostat. For cyclic voltammetry, we used a platinum working electrode, a calomel reference electrode (saturated calomel electrode), and a platinum wire as the auxiliary electrode. The picosecond to microsecond emission lifetime measurements were carried out with a Lifespec picosecond fluorescence lifetime spectrometer from Edinburgh Instruments. As excitation sources two diode lasers, with 405 and 635 nm nominal wavelengths, were used. The instrument response measured at the full-width at half-maximum was below 350 ps. Laser transient absorption spectroscopy measurements were carried out with a home-built system as reported before.[43]

Charge extraction and photovoltage measurements were carried out using a home-built system. In brief, the charge extraction data were acquired using a pulse generated by an array of white LEDs. The decay was monitored using a Tektronics oscilloscope TDS 2022 and recorded using the Tektronics data acquisition software. We applied different light intensities to achieve different open circuit voltages of the cell, and immediately after the light pulse the device was short-circuited to extract the charge, which was controlled with a switch. For the photovoltage transients, the pulse was generated with red-emitting diodes while the cell was illuminated with the same array of white light diodes. Proton NMR spectra, NOESY and COSY experiments, were measured on a Bruker

400 MHz spectrometer. A Waters LCT Premier liquid chromatograph coupled with a time-of-flight mass spectrometer with electrospray ionisation was used to measure the mass spectra.

4.3.3.6. Nanoparticle synthesis and film preparation

The nanocrystalline TiO_2 particles were synthesised as reported before.[44] In brief, titanium isopropoxide (40 mL, 0.13 mol) was added to glacial acetic acid (9.12 g) under an argon atmosphere with stirring. The reaction mixture was cooled in an ice bath, and 0.1 M nitric acid (240 mL) was added with vigourous stirring. The mixture was heated in an oil bath at 80 °C for 8 h and, after cooling, was filtered through a 0.45 µm syringe filter. The resulting product was diluted to 5 % by weight of TiO_2 by adding water and then was autoclaved at 220 °C for 12 h. The aqueous phase was removed by centrifugation, and the solid nanoparticles were isolated and rinsed twice with ethanol. An ultrasonic horn was used to break the aggregates, and the solvent was removed under vacuum. The solid nanoparticles were diluted to 15 % by TiO_2 weight, using ethyl cellulose and terpineol, and the paste was homogenised by ball milling. The Al_2O_3 mesoporous films were synthesised using commercially available Al_2O_3 nanoparticles.

4.3.3.7. Device preparation and characterisation

In the present work we have utilised two different types of devices due to their characterisation. Highly transparent thin film devices were utilised for time-correlated single photon counting and L-TAS experiments. These devices were made using 4 µm thick films and sensitised with the ruthenium complexes until the absorbance at the metal-to-ligand charge transfer band of the sensitised film was 0.6 absorption unit. On the other hand, for optimised efficiencies all the devices studied during this work were made using 16 µm thick films consisting of a layer of 12 µm of 19 nm TiO_2 nanoparticles and a layer of 4 µm of 300 nm TiO_2 nanoparticles (scatter layer). In both cases, the films were deposited onto a conducting glass substrate (Hafford Glass Inc., with 15 $\Omega\cdot cm^{-2}$ resistance) using the well-known doctor blade technique. For the thin film devices the area was 1 cm^2, while in the case of the thick film DSSC the active area was 0.152 cm^2. The counter electrodes were made by spreading a solution of H_2PtCl_6 in ethanol onto a conducting glass substrate with a small hole to allow the introduction of the liquid electrolyte using a vacuum. Two liquid electrolytes were used depending on the measurements; AF19 is composed of 0.6 M DMPII, 0.04 M I_2, and 0.025 M LiI in MeCN/valeronitrile (85:15), and AF4 was made using 0.6 M DMPII , 0.04 M I_2, 0.025 M LiI and 0.28 M TBP in MeCN/valeronitrile (85:15). The photovoltaic measurements were carried out with a 150 W xenon lamp from Oriel Instruments with the appropriate set of filters for the correct simulation of the AM 1.5-G solar spectrum. The incident light power was calibrated using a silicon photodiode previously calibrated at 1000 W·m^{-2} at AM 1.5-G.

4.3.3.8. Theoretical calculations

The geometries of the different complexes were calculated with Gaussian 03, revision C.02,[84] using the B3LYP functional. 6-31G(d) basis sets were used for sulfur, oxygen, nitrogen, carbon, and hydrogen atoms, whereas the Stuttgart-Dresden effective core potential (ECP)[85] and corresponding basis set were used for ruthenium. HOMO and LUMO orbitals were calculated from the optimised geometries.

4.3.4. Results and discussion

4.3.4.1. Spectroscopic properties. UV-vis absorption spectra and photoluminescence measurements

Figure 4.14 illustrates the UV-vis spectra of **AR20**, **AR24a**, **AR24b**, **AR25**, **AR27a**, **AR27b** and **N719** in dimethylformamide. The absorption band in the visible region has been previously assigned to the MLCT in ruthenium(II) complexes.[38]

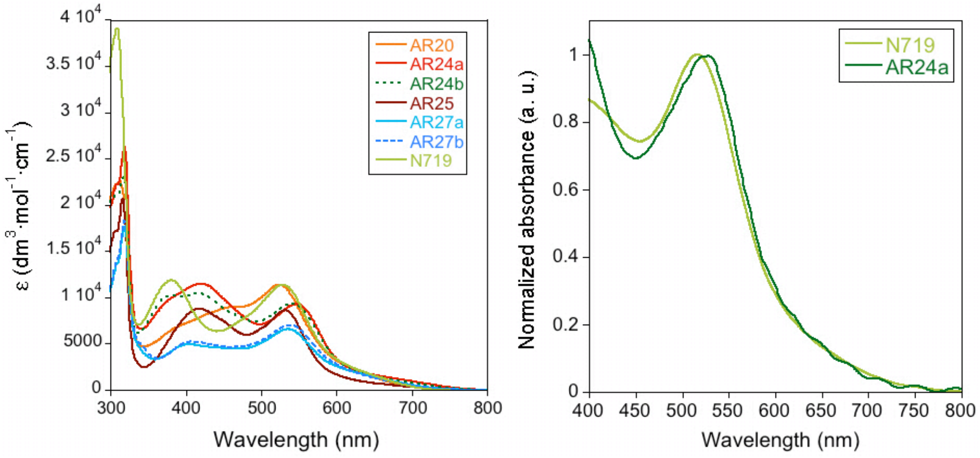

Figure 4.14. UV-Vis absorption spectra if all the Ru$^{(II)}$ complexes described above in DMF (left) and adsorbed onto a 4 µm thick TiO$_2$ transparent mesoporous film (right). The sensitisation was 30 min at 50 °C (the concentration of the dye solution was 1·10^{-4} M)

Table 4.1 shows the most important parameters for all the ruthenium complexes. As can be observed, in the case of **AR24** and **AR27** the amino and the nitro groups on the phenanthroline induce a red shift of the maximum. It is worth noting that the visible spectra of the dyes adsorbed onto TiO_2 transparent thin mesoporous films retain the red shift as in solution (Figure 4.14, right). However, we note that the lower energy of the visible transition for the **AR24** dye appears to be in contradiction to the expected increase in the optical gap.[38]

Ruthenium complex	π-π* (ε)	MLCT (ε)
AR20	415 (7830)[a]	522 (11360)
AR24a	420 (11500)	546 (9242)
AR24b	415 (10441)	545 (9312)
AR25	415 (8820)	531 (8606)
AR27a	403 (5220)	538 (6984)
AR27b	400 (4938)	535 (6560)
N719	378 (11852)	527 (11360)

Table 4.1. UV-Vis absorption parameters (nm) for the ruthenium(II) complexes described above. [a] *The numbers in parentheses correspond to the molecular extinction coefficient ($dm^3 \cdot mol^{-1} \cdot cm^{-1}$)*

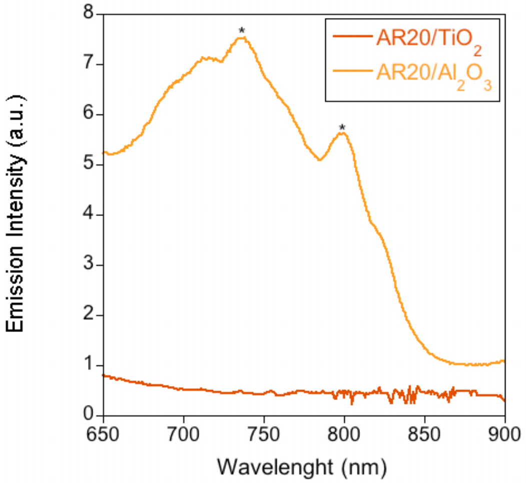

Figure 4.15. Photoluminescence spectra of AR20-sensitised films recorded under normal conditions (λ_{ex} = 500 nm). The asterisks indicate optical artifacts from the luminescence spectrophotometer

The photoluminescence properties of the dyes in solution and adsorbed onto transparent mesoporous thin films have also been measured. The emission of the dye sensitised films is dramatically quenched for the TiO_2 samples when compared to that of Al_2O_3-sensitised films, which, in principle, suggests the existence of efficient light-induced electron injection from the dye excited state into the TiO_2 semiconductor conduction band. Absorption of the dye to an oxide surface could in principle reduce the emission without the presence of electron injection. For this reason it is better to compare the luminescence of the dye on TiO_2 to the luminescence on another substrate such as Al_2O_3, where the conduction band edge is above the LUMO of the molecule. The results indicate that dye-sensitised Al_2O_3 films show typical photoluminescence at room temperature when excited at the MLCT band as in solution. Figure 4.15 illustrates, as an example, the AR20/Al_2O_3 emission spectra, and the most relevant photoluminescence properties for all dyes are listed in Table 4.2. In the case of AR27 we were only able to measure the emission kinetics in solution since we could not resolve the decay on either TiO_2 or Al_2O_3 as it was faster than our instrument response. This observation can be understood, if we take into account that the AR27 complex fulfills the band gap law. In brief, the smaller the energy gap, the lower the complex emission quantum yield and the faster its emission decay dynamics.

Complex	Emission (λ_{max}, nm)	$E_{0,0}$[a] (eV)	Solution lifetime[b] (ns)	Al_2O_3 film emission lifetime[d] (ns)	DSSC emission lifetime (ns)	Estimated electron injection yield (%)
AR20	724	193	3.82 (3) 51.92 (97)	11.90 (10) 34.49 (90)	1.44 (40.3) 7.70 (56.7)	85
AR24a	777	189	10.05 (33.2) 47.65 (66.8)	11.16 (40.2) 36.86 (59.8)	2.34 (50.6) 12.53 (49.4)	70
AR24b	774	19	11.03 (38.3) 54.03 (61.6)	11.56 (43.2) 32.97 (56.8)	2.51 (41.6) 20.98 (58.4)	70
AR25	746	192	9.57 (18.9) 56.67 (81.1)	11.96 (20.6) 37.36 (79.4)	2.23 (48.5) 12.61 (51.5)	90
AR27a	760	1.52[c]	3.41 (7.76) 12.8 (92.2)			
AR27b	760	1.53[c]	1.57 (6.3) 12.95 (93.7)			

Table 4.2. Photophysical parameters for the ruthenium(II) complexes described above in DMF solution. [a] The 0-0 energy was calculated using the tangent from the higher energy side of the emission band except for AR27. [b] The number in parentheses are the percentage for each parameter. [c] Estimated from the electrochemical data. [d] The emission lifetime for the AR27 complex is shorter than the instrument response of our TC-SPC system (Instrument response = 350 ps)

To determine the photoinduced electron transfer yield of those dyes into TiO_2, we have carried out further experiments to study the dyes in complete devices. It has been previously shown that TCSPC is a convenient technique that can be used to estimate not only the yield of the electron injection in a qualitative way, but also the rate of electron injection dynamics in the DSSC.[86, 87] However, it is necessary, as a control, to determine the native excited lifetime (τ) of the molecules adsorbed onto the nanoparticle surface. Thus, as explained before, we employed Al_2O_3 mesoporous sensitised films as a control.

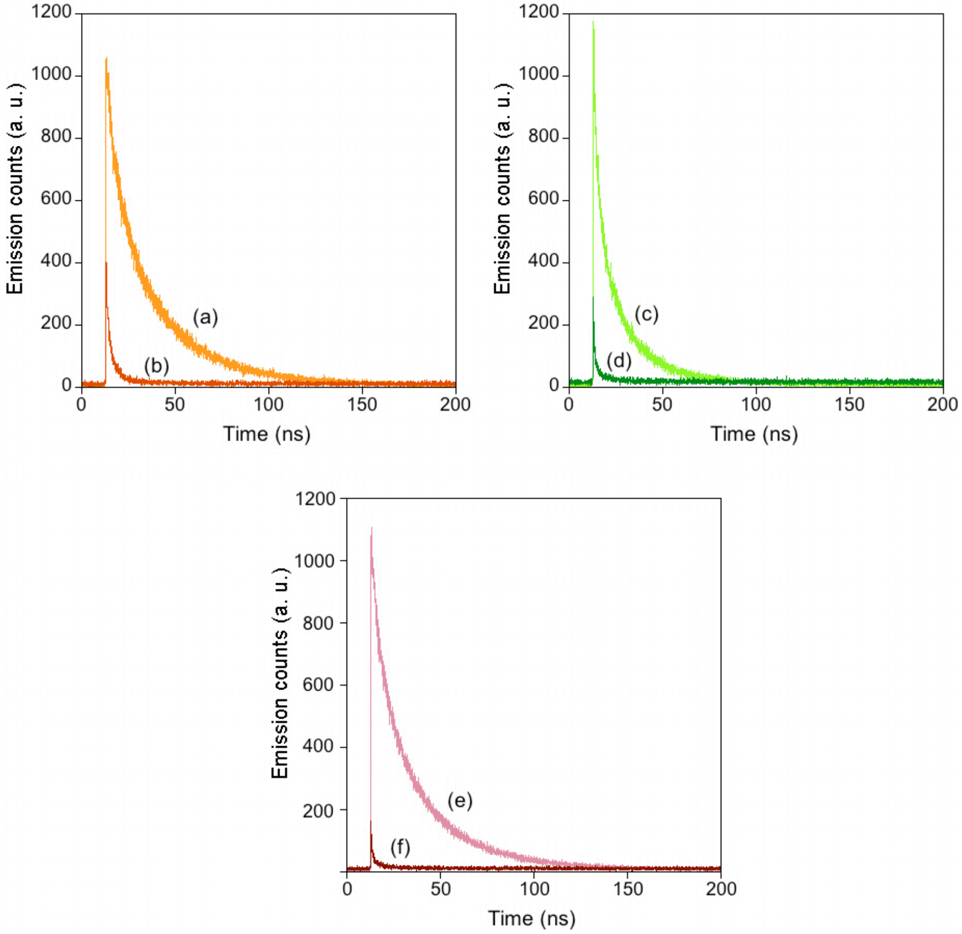

Figure 4.16. Photoluminescence emission decays for (a) AR20/Al_2O_3, (b) AR20/DSSC, (c) AR24b/Al_2O_3, (d) AR24b/DSSC, (e) AR25/Al_2O_3, (f) AR25/DSSC

As detailed in Table 4.2, in the absence of electrolyte, either in solution or adsorbed onto Al_2O_3 thin films, the emission kinetics were fitted to a biexponential decay, and a slow component was observed in all decays. Several authors have reported that the slow component of the dye excited lifetime decay arises from the nature of the dye's triplet excited state.[38, 88] More interesting is the difference in emission decay amplitude when the dye-sensitised Al_2O_3 films are compared with the photovoltaic devices. For a fixed acquisition time of 900 s we can observe (Figure 4.16) faster emission decay kinetics for complete devices and a decrease in the signal amplitude and the area under the curve. In fact, we evaluate the electron injection yield by comparison of the decay curves between both sets of samples (Al_2O_3 *vs* DSSC). As can be observed in Figure 4.16, in all cases the photoinduced electron injection is efficient, and in the case of **AR25**, the yield is near 90 %. Those values are similar to those previously reported for **N719**. Furthermore, using the same mathematical procedure as published by Koops *et al.*,[86] we have estimated that the photoinduced electron injection reaction takes place faster than in 175 ps, which is in good agreement with previously published data for ruthenium(II) complexes used in a complete DSSC.[89, 90]

4.3.4.2. L-TAS and electrochemical measurements

Transient absorbance measurements were performed either on dye sensitised 4 μm thick transparent mesoporous TiO_2 or in complete functional devices and are shown in Figures 4.17 and 4.18.

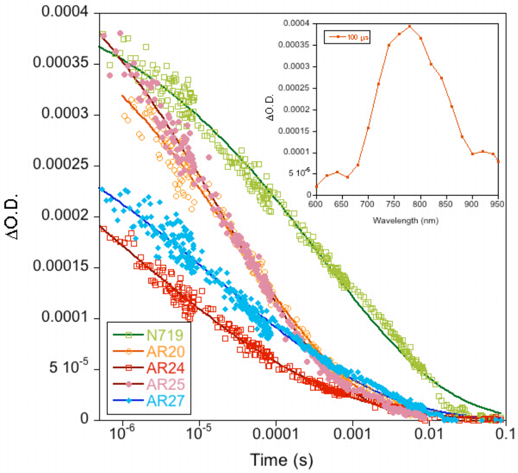

Figure 4.17. Absorbance transient for 4 μm thick transparent dye-sensitised TiO_2 films (MLCT λ_{abs} = 0.3). The excitation wavelength was 620 nm, and the probe wavelength was 800 nm. The solid lines correspond to the stretched exponential fit. The inset illustrates the AR20 cation spectra after excitation at 535 nm

Consistent with previous reports, we associated the decay of the dye-TiO_2 sample with the photoinduced electron recombination kinetics between the electrons at TiO_2 and the oxidised dye at the nanoparticle surface (Scheme 4.2, reaction 4).[91, 92] Moreover, in good agreement with previous papers, the electron recombination kinetics can be fitted to a classic stretched exponential which is consistent with the presence of a large distribution of recombination sites within the mesoporous film with different energetic characteristics. These differences in the local environment not only lead to a variation of the recombination kinetics but also have been observed for the electron injection dynamics.[35, 51, 52, 91] Back electron transfer half-times ($\tau_{1/2}$), measured at full width at half-maximum, for the heteroleptic $Ru^{(II)}$ complexes are summarised in Table 4.3.

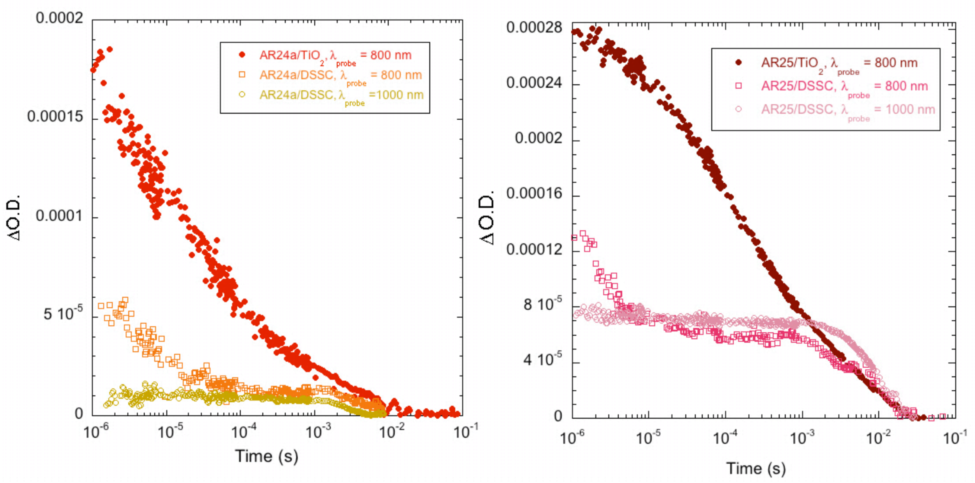

Figure 4.18. Electron recombination dynamics for a 4 μm thick transparent film: (left) AR24a/DSSC and (right) AR25/DSSC. Both cells have the same absorption (MLCT λ_{abs} = 0.6). The excitation wavelength was 620 nm. The electrolyte was AF19

The L-TAS study of complete functional devices (Figure 4.18) reveals that, in the presence of I^-/I_3^-, the amplitude of the initial signal is strongly reduced for **AR24** relative to **AR25**. Note that Figure 4.16 indicates the same degree of luminescence quenching for both dyes. This indicates that either the photoinduced electron injection is strongly reduced when I^-/I_3^- is present in **AR24**/DSSC (the same behaviour is observed for **AR27**/DSSC) or the oxidised dye is removed by a very fast recombination with the injected electron, or both. For efficient devices based on homo- or heteroleptic ruthenium(II) complexes, in the presence of redox-active electrolyte the L-TAS recombination dynamics always appears associated with the appearance of long-lived transient decays assigned previously by Montanari *et al.* to the electrons at TiO_2.[72, 93] In our case, when we measured the dynamics of **AR24**/DSSC (Figure 4.18 left, λ_{probe} = 1000 nm), the amplitude of this slow decay component on the L-TAS recombination kinetics was remarkably low. In fact, the comparison of the yield of photoinduced electrons at TiO_2 between **AR24**/DSSC and **AR25**/DSSC shows that for **AR25**/DSSC the yield of electrons is 8 times higher than for **AR24**/DSSC. It clear that the differences in the molecular structure of both dyes are playing a major role in the interfacial charge transfer reactions at the devices.

Sample	Half-time recombination decay ($\tau_{1/2}$, ms)	α^a	$E_{1/2}$ ($Ru^{II/III}$) (V) in MeCN *vs* SCE electrode at 25 °C^b	$E_{1/2}$ ($Ru^{II/III*}$) (V) in MeCN *vs* SCE electrode at 25 °C
AR20	0.045	0.27	0.73	-1.2
AR24a	0.015	0.16	0.75	-1.14
AR24b	0.015	0.16	0.75	-1.15
AR25	0.026	0.27	0.74	-1.19
AR27a	0.052	0.2	0.72	-0.8
AR27b	0.052	0.2	0.72	-0.81
N719	0.44	0.26	0.73	-1.2

Table 4.3. Charge recombination and electrochemical potentials for the heteroleptic Ru$^{(II)}$ complexes. ^{a} α corresponds to the parameter obtained from the curve fitting of the decay experimental points using the stretched exponential function $I \propto e^{\left(-t/\tau\right)^{\alpha}}$. *^{b} The solutions (3 mM) were purged with argon for 5 min*

Moreover, these differences cannot be explained in terms of different energy levels of the molecular orbitals since the analysis of the cyclic voltammetry reveals that **AR24** and **AR25** show almost identical reduction potentials as confirmed by the theoretical study below.

4.3.4.3. Computational study

We have performed theoretical calculations using the software package Gaussian 03 as described in the Experimental Section. Figure 4.19 illustrates the graphical representation of the HOMO and LUMO orbitals of the heteroleptic Ru$^{(II)}$ complexes. In all cases the electrons on the HOMO are centered on the axial thiocyanate ligands and, within those, on the sulfur atoms. On the other hand, the electrons on the LUMO are localised on the bipyridine ligand for the **AR20**, **AR24**, and **AR25** complexes in good agreement with previous theoretical calculations.[42] In fact, these computational results also support the hypothesis of efficient electron injection in these complexes since the electronic coupling between the 3d Ti orbitals and the LUMO of the Ru$^{(II)}$ complexes must be very strong. However, in the case of the **AR27** complex, the electrons on the LUMO orbital are delocalised on the phenanthroline ligand, and thus, this could be one of the reasons for the low device performance.

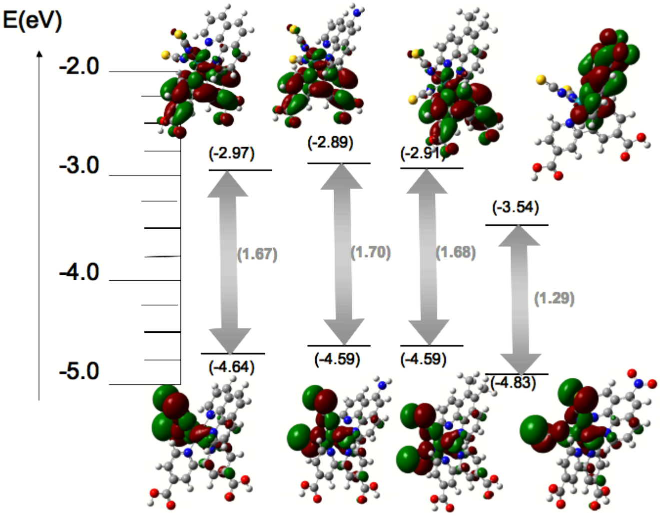

Figure 4.19. Molecular orbitals and energy gaps of AR20, AR24a, AR25 and AR27a (DFT/6-31H(d), isodensitiy value 0.02)

In fact, we point out that although it was impossible to observe the luminescence dynamics in the case of the **AR27**/TiO_2 or the **AR27**/Al_2O_3 sample, due to the time response of our TCSPC measurement system, the signal at the TAS measurements (Figure 4.17) reveals that the injection kinetics are not as efficient as for **AR20** and **AR25** sensitised TiO_2 samples. Thus, we can expect a low photocurrent on devices made using **AR27**. Furthermore, the computational study reveals that the HOMO-LUMO energy gaps for the **AR20**, **AR24**, and **AR25** dyes show little difference. On the other hand, in the case of the **AR27** complex, with the electron-withdrawing nitro group, the HOMO-LUMO energy gap is noticeably smaller. It is worth noting, too, that the theoretical model also predicts small differences between the different **AR24** and **AR27** diastereoisomers as has been observed in the experimental results. Taking into account that in all cases the binding of the $Ru^{(II)}$ complexes onto the nanoparticles occurs through the bipyridine carboxylic groups, we can assume that the distance between the semiconductor nanoparticle surface and the HOMO orbital for all complexes is almost the same. We have estimated that the distance is about 8 Å. It has been previously reported that, for **N719** and other $Ru^{(II)}$ complexes, there is a clear correlation between the HOMO/TiO_2 distance and the e^--TiO_2/dye^+ electron recombination kinetics.[26] In our hands all decay kinetics were faster than those of the standard molecule **N719** under the same experimental conditions.

4.3.4.4. Photovoltaic device characterisation

After the spectroscopic characterisation of all the ruthenium(II) complexes described above, we focused on the measurement and analysis of the photoelectrochemical characteristics of the solar cell devices. The IPCE reveals that in the case of devices made using **AR20** and **AR25** $Ru^{(II)}$ complexes the photon-to-electron conversion efficiency is similar to that reported for **N719**. However, for the **AR24** complex the conversion efficiency is much lower, in good agreement with the low electron injection yield observed in the results above. Nonetheless, the lower photovoltage observed (Table 4.4) for those cells (V_{oc} = 0.48 V) when compared with that of **AR20** (V_{oc} = 0.67 V) or **AR25** (V_{oc} = 0.67 V) cells was also surprising. The origin of such an effect on the photovoltage will be discussed in the next section.

Cell	I_{sc} (mA)	V_{oc} (V)	ff	η (%)
AR20	1.91	0.67	46.93	3.98
AR25	2.05	0.67	50.20	4.56
AR24a	0.22	0.48	31.45	0.22
AR24b	0.15	0.46	30.72	0.14
AR27a	0.8	0.44	34.21	0.8
AR27b	0.12	0.44	35.23	0.13
N719	1.5	0.46	68.32	4.45

Table 4.4. Device parameters when irradiated with stimulated sunlight (100 mW·cm^{-2}, 1.5 AM G). The cell area was 0.152 cm^{2} and the AF4 electrolyte

We focus now on **AR27**/DSSC, as can be seen in Figure 4.20 the IPCE was very low for these devices too. This could be expected from the kinetic measurements and the theoretical calculations that predict a low-lying LUMO level unable to achieve high electron injection yields. On the other hand, the IPCE results for **AR24**/DSSC cannot be explained like those for **AR27**, since for **AR24** the experimental and the theoretical results predict a high LUMO energy level and, therefore, enough driving force for electron injection onto the TiO_2 conduction band. We believe that the results obtained for **AR24**/DSSC can be explained either in terms of inefficient electron regeneration from the liquid electrolyte due to an increase in the electron recombination kinetics between the photoinjected electrons and the electrolyte or the low yield of electron injection due to the quenching of the dye excited state by the redox electrolyte. To seek further information on these two hypotheses, we have also studied the photocurrent *vs* voltage device characteristics of the DSSC under standard illumination conditions (100 mW·cm^{-2}). The results are shown in Table 4.4. We observed that for the solar cells the photocurrent was in good agreement with the measured IPCE.

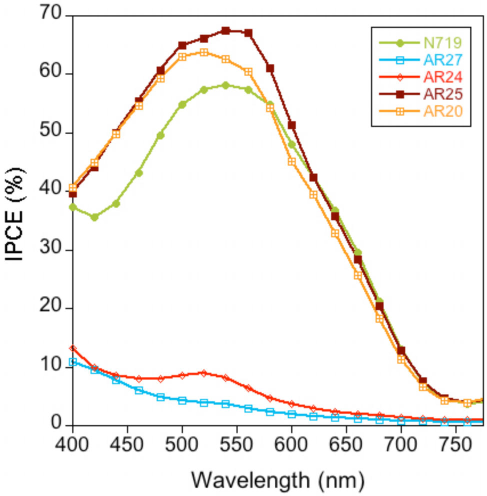

Figure 4.20. Incident photon to current efficiency curves for 12 + 4 µm thick DSSC using the AF4 electrolyte

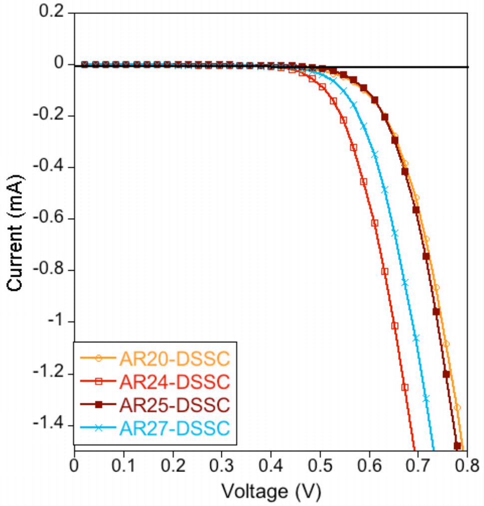

Figure 4.21. I-V curves measured for the indicated devices in the dark. The electrolyte was AF19

Moreover, as we mentioned before, it was very interesting to note that the voltage and hence the dark current curves (Figure 4.21) were much different between the different cells despite the fact that all heteroleptic $Ru^{(II)}$ complexes in this study have almost identical energy gaps (except, of course, **AR27**). Thus, the inefficient performance of these heteroleptic ruthenium dyes must be related to the charge recombination kinetics between the photoinjected electrons and the oxidised redox couple.

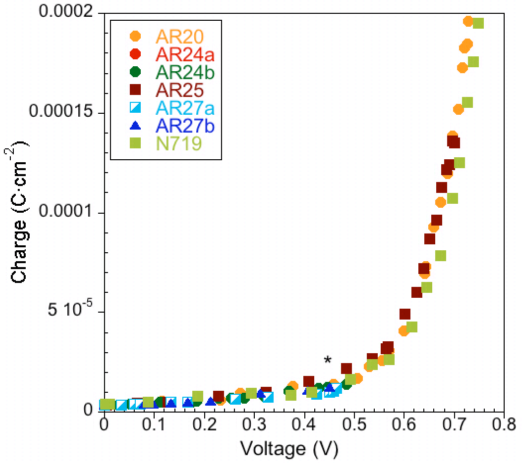

Figure 4.22. Charge extraction measurements for all devices. The DSSC active area is 1 cm^2. The cells were made using a transparent 4 μm thick TiO_2 film sensitised with the $Ru^{(II)}$ complexes and AF19 electrolyte. The asterisk indicates the voltage at which all the devices have the same charge

For a more detailed study on this issue, we carried out photovoltage transient experiments. Recently, we have employed those measurements, also known as V_{oc} decays, to evaluate the electron recombination dynamics between the photoinjected electrons at TiO_2 and the oxidised electrolyte in porphyrin sensitised solar cells.[94] It is worth noting that V_{oc} decays are measurements strongly dependent on the accumulated charge at the semiconductor (charge density), and hence, to obtain a fair comparison of the e^--TiO_2/electrolyte$^+$ recombination dynamics between different devices, the charge densities on both cells must be equal. As illustrated in Figure 4.22, in our case, this condition can be achieved when the cell voltage is 475 mV. As indicated in Table 4.4 the different solar cells have different V_{oc} values when illuminated at 1 sun. The differences in the voltage can be due to (a) a shift of the TiO_2 conduction band with respect to the electrolyte potential or (b) differences in the e^--TiO_2/electrolyte$^+$ recombination reaction. The former hypothesis can be discarded due to the fact that a change in the TiO_2 conduction band position implies also a shift in the cell charge density as demonstrated previously by other authors.[94-97] As can be seen in Figure 4.22 for all DSSCs the experimental points emerge along the same curve. Thus, in our case, the differences in voltage must be due to an increase in the e^--TiO_2/electrolyte$^+$ recombination reaction in devices made using **AR24**.

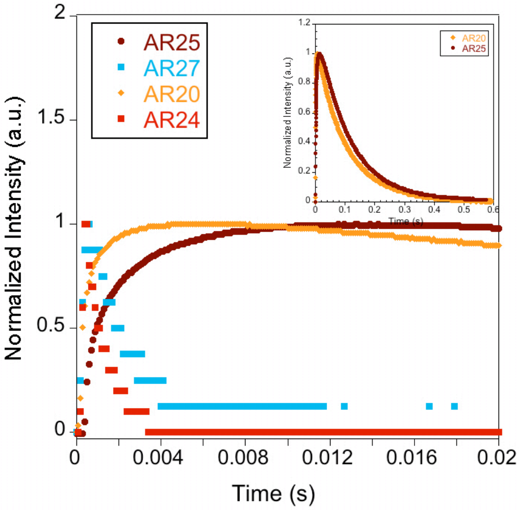

Figure 4.23. Photovoltage transient decays of the DSSC. The inset shows the decay recombination dynamics for AR20/DSSC and AR25/DSSC at longer time scales. The electrolyte was AF19

The electron recombination dynamics between the photoinjected electrons at TiO_2 and the oxidised electrolyte are illustrated in Figure 4.23. As can be seen the kinetics are 2 orders of magnitude faster for devices made using either **AR24** and **AR27**.

It is obvious that the presence of the electron donor group at the phenanthroline is responsible for the extraordinarily fast electron recombination kinetics between the electrons injected at the semiconductor upon light excitation of the **AR24** molecules and the oxidised electrolyte. The origin of such an effect remains unclear, but interestingly, on this series of $Ru^{(II)}$ complexes the presence of a nitrogen-containing group (either the amino or the nitro) affected not only the photoinduced electron injection from the dye excited state into the TiO_2 conduction band, but also the charge transfer reaction between the electrons at the semiconductor film and the iodine/iodide electrolyte.

4.3.5. Conclusions

We have demonstrated that for the design and synthesis of heteroleptic $Ru^{(II)}$ complexes the presence of substituents on one of the aromatic ligands coordinated to the ruthenium atom has a strong influence not only on the molecule spectroscopic and electrochemical properties but also on the device performance. In fact, we have demonstrated that in the case of the ruthenium complex bearing an amino moiety or a nitro group the molecule affects dramatically the open circuit voltage of the cell. Although a more detailed study is probably needed to find the mechanisms that are deactivating the electron injection on these devices too, we have shown that the low device performance is influenced by the acceleration of the electron transfer dynamics between the photoinjected electrons and the oxidised electrolyte. For devices made using the phenanthroline substituted heteroleptic Ru$^{(II)}$ complexes the reaction is 2 orders of magnitude faster when compared to that of **N719** (data not shown) and **AR20** or **AR25**.

We believe that the results presented in this paper have important implications for the future design of new ruthenium heteroleptic complexes that attempt to achieve higher open circuit voltages in the DSSC without reducing the photocurrent, using electron-donating or -withdrawing groups to control the photophysical properties of the molecules. However, those modifications, as in our case, could lead instead to a poor device performance by the enhancement of undesirable interfacial transfer reactions.

4.3.6. Acknowledgements

Financial support from the Spanish MEC is gratefully acknowledged (CONSOLIDER-HOPE 0007-2007 project). E.M.F. thanks the MEC for a Juan de la Cierva fellowship. B.O. and E.P. thank the EU-FP6 OrgaPVNet project for funding. E.P. and A.R. are also grateful to the ICIQ Foundation for financial support.

4.4. Article C. Dye structure-charge transfer process relationship in efficient ruthenium-dye based dye sensitised solar cell

Energy Env. Sci., 2010, 3(6), 805

Anna Reynal,[a] Amparo Forneli,[a] Emilio Palomares*[a,b]

[a] Institute of Chemical Research of Catalonia (ICIQ), Avda. Països Catalans, 16, 43007, Tarragona. E-mail address: epalomares@iciq.es, fax:+34 977 920 241, tel: +34 977 920 200, [b] Institució Catalana de Recerca i Estudia Avançats (ICREA), Avda. Lluís Companys, 25, 08040, Barcelona, Spain.

4.4.1. Abstract

The characterisation of the interfacial charge transfer processes taking place in dye solar cells made using the most efficient ruthenium complexes, namely *cis*-bis(isothiocyanato)bis(2,2'-bipyridyl-4,4'-dicarboxylato)-ruthenium(II)bis-tetrabutylammonium (**N719**), tris(isothiocyanato)-ruthenium(II)-2,2':6',2"-terpyridine-4,4',4"-tricarboxylic acid tris-tertrabutylammonium salt (**Black Dye**) and *cis*-bis(isothiocanate)(4,4'-bis(5-hexylthiophene-2-yl)-2,2'-bipyridine)(4-carboxylic acid-4'-carboxylate-2,2'-bipyridine)ruthenium(II) sodium (**C101**), has been carried out. The comparison between these devices shows that devices made using **N719** have the slowest recombination dynamics between the photo-injected electrons and the oxidised electrolyte. Moreover, for devices made using **Black Dye**, the dye ground state regeneration dynamics are faster than for **C101** and **N719**. The implications for future ruthenium dyes are discussed.

4.4.2. Introduction

In the last five years rapid progress towards stable and efficient dye sensitised solar cells (DSSC) have been possible thanks to the development of new ruthenium polypyridyl dyes.[23, 42, 98-104] Such dyes, when covalently attached to nanocrystalline TiO_2 nanoparticles and irradiated with light, are capable of generating large photocurrents, which are nowadays in the order of twenty milliamps per square centimetre. A wide range of ruthenium dyes have been designed, but only a few have been able to reach solar-to-energy conversion efficiencies as high as 10–11 %[46, 105] due to different reasons ranging from inappropriate dye oxidation potential,[106] low energy level of the dye excited state[80] and secondary reactions still not well defined between the dye and the red/ox electrolyte.[107-110] Certainly, of all the organic ligands used to coordinate the ruthenium centre, the use of 2,2'-

thiocyanate ligands, giving hexa-coordinated ruthenium(II) complexes absorbing almost in the near IR region of the solar spectrum (λ = 700 nm).[112] Nowadays, a new ruthenium polypyridyl complex named **C101**[10] that contains the above mentioned features has been used to achieve efficiencies above 11 % in a reproducible manner under standard conditions (100 mW·cm^{-2}, 1.5 AM G solar spectrum). Indeed, the study of the relationship between the dye structure and their light-to-electrical current conversion performance is of utmost interest, since it will help to understand the parameters to design efficient and robust sensitisers for DSSC, as well as to determine the reactions occurring at the molecular level between the different cell components that limit the device performance.

In this paper, we aim to study in detail the three most efficient dyes reported so far in the DSSC literature (Figure 4.24) using liquid electrolyte composed by the red/ox pair I_2/I^- and TiO_2 as electron transport mesoporous material. Moreover, we will monitor the interfacial charge transfer reactions taking place at the interface of these devices and observe the differences between electron injection, back electron transfer from the photo-injected electrons at the TiO_2 and the oxidised species at the device (either dye or electrolyte) and the regeneration process between the electrolyte and the oxidised dye. Although for **N719** there is a wide range of studies available[30, 40, 113-115] and, surely, this is also the case for the complex named **Black Dye** (**BD**),[49, 116-119] neither the former nor the latter have been previously measured and compared under the same conditions, which is, in our opinion, an important factor to take into account when the researchers look for clear dye structure–device function correlation. In addition to these two widely known sensitisers, we have included in our study the new paradigm, the ruthenium complex **C101**, and analysed its performance too.

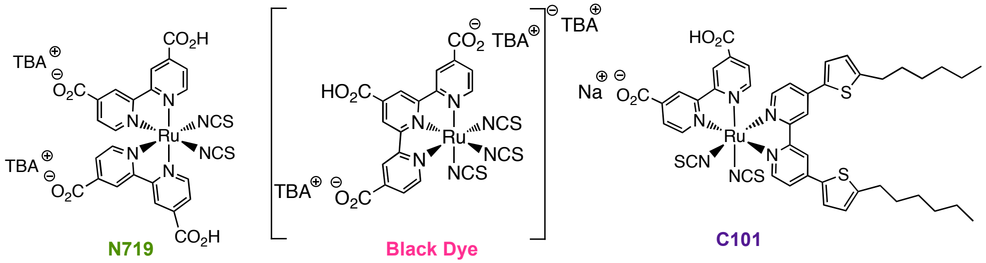

Figure 4.24. Chemical structure of the molecules N719, Black Dye and C101. TBA stands for tetrabutylammonium cation

4.4.3. Experimental section

4.4.3.1. Materials

The solvents, and other reagents or products used were purchased from Sigma-Aldrich and used without further purification. The **N719** and **Black Dye** were purchased from Solaronix. The **C101** complex was received as a courtesy from the group of Professor Grätzel at EPFL (Lausanne, Switzerland).

4.4.3.2. Optical, electrochemical and spectroscopic measurements

The UV-visible and emission spectra were recorded using a 1 cm path length quartz cell on a Shimadzu UV spectrophotometer 1700 and an Aminco-Bowman series 2 luminescence spectrometer with a temperature controller, respectively. The electrochemical data was obtained employing a conventional three-electrode cell connected to a CH Instruments 660c potentiostat-galvanostat. For cyclic voltammetry, we used a platinum foil as working electrode, a calomel reference electrode and a platinum wire as the auxiliary electrode. The picoseconds to microsecond emission lifetime measurements were carried out with a Lifespec picosecond fluorescence lifetime spectrometer from Edinburgh Instruments. As excitation source, a fast diode laser, with 405 nm nominal wavelength, was used. The instrument response measured at the full-width at half maximum was shorter than 360 ps. Laser transient absorption spectroscopy measurements were carried out with a home-built system as reported before.[43] Charge extraction and photovoltage measurements were carried out using a home-built system. In brief, the charge extraction data were acquired using a pulse generated by an array of white LEDs. The decay was monitored using a Tektronics oscilloscope TDS 2022 and recorded using the Tektronics data acquisition software. We applied different light intensities to achieve different open circuit voltages of the cell, and straight after the light pulse the device was short-circuited to extract the charge. All electronic processes to short-circuit the photovoltaic cell were controlled with a home-made electronic switch. For the photovoltage transients, the pulse was generated with red-emitting diodes while the cell was illuminated with the same array of white light diodes.

4.4.3.3. Nanoparticle synthesis and film preparation

The nanocrystalline TiO_2 particles were synthesised as reported before.[44] In brief: titanium isopropoxide (40 mL, 0.13 mol) was added to glacial acetic acid (9.12 g) under argon atmosphere while stirring. The reaction mixture was cooled into an ice bath and 0.1 M nitric acid (240 mL) was added while vigourously stirring. The mixture was heated in an oil bath at 80 °C for 8 h and, after cooling, was filtered through a 0.45 µm syringe filter. The resulting product was diluted to 5 % in weight of TiO_2 by adding water and was then was autoclaved at 220 °C for 12 h. The aqueous phase was removed by centrifugation and the solid nanoparticles were isolated and rinsed twice with ethanol. An ultrasonic horn was used to break the aggregates and the solvent was removed under vacuum. The solid nanoparticles were diluted to 15 % in TiO_2 weight using ethyl cellulose and terpineol and the paste was homogenised by ball milling.

The Al_2O_3 mesoporous films were synthesised using commercially available Al_2O_3 nanoparticles.

4.4.3.4. Device preparation and characterisation

In the present work, we have utilised and characterised two different types of device. Highly transparent thin film devices were utilised for time-correlated single photon counting and L-TAS experiments. These devices were made using 4 µm thick films and sensitised with the ruthenium complexes until the absorbance at the metal-to-ligand charge transfer band of the sensitised film was 0.6 absorption units. On the other hand, for optimised efficiencies, all the devices studied during this work were made using 16 µm thick films consisting of a layer of between 8–12 µm of 20 nm TiO_2 nanoparticles and a layer of 4 µm of 400 nm TiO_2 nanoparticles (scatter layer). In both cases, the films were deposited onto a conducting glass substrate (Nippon Sheet Glass Co. with 10 $\Omega\cdot cm^{-2}$ resistance) using the manual doctor blade technique. For the thin film devices, the area was 1 cm^2 while in the case of the thick film DSSC, the active area was between 0.14 and 0.15 cm^2. The counter electrodes were made by spreading a $5 \cdot 10^{-3}$ M solution of H_2PtCl_6 in ethanol onto a conducting glass substrate with a small drilled hole to allow the introduction of the liquid electrolyte using low vacuum pressure. Two liquid electrolytes were used depending on the measurements; electrolyte A, which does not contain *tert*-butylpyridine, is composed of 1 M BMII (1-butyl-3-methylimidazolium iodide), 0.03 M I_2, 0.05 M LiI and 0.1 M GuNCS (guanidinium thiocyanate) in acetonitrile/valeronitrile 85:15, and electrolyte B, which contains *tert*-butylpyridine, was made using 1 M BMII, 0.03 M I_2, 0.05 M LiI, 0.1 M GuSCN and 0.5 M *tert*-butylpyridine in acetonitrile/valeronitrile (85:15). The photovoltaic measurements were carried out with a 150 W xenon lamp from ABET Instruments with the appropriate filter for the correct simulation of the 1.5 AM G solar spectrum. The incident light power was calibrated using a silicon photodiode previously calibrated at 1000 $W\cdot m^{-2}$ at 1.5 AM G.

4.4.4. Results and discussion

4.4.4.1. Spectroscopic properties: UV-visible absorption spectra and photoluminescence measurements

The absorbance spectra of the three different dyes anchored onto 4 µm thick Al_2O_3 and TiO_2 mesoporous films were measured.

The films were immersed into a 10^{-3} M solution of each dye using as solvent a mixture of acetonitrile: *tert*-butanol (1:1) for **N719** and **C101**, while in the case of the **Black Dye**, we used ethanol. The lowest absorption energy band was centered at λ = 523 nm for **N719** and λ = 533 nm for **C101**. The absorption bands were assigned to the metal to ligand charge transfer process between the ruthenium atom and the polypyridyl ligands. In the case of the **Black Dye**, two MLCT transition bands were observed centered at λ = 414 nm, assigned to a spin-allowed Ru → terpyridine ligand charge transfer transition and at λ = 617 nm, assigned to a medium intensity singlet-singlet spin-allowed MLCT transition.[117] The absorption bands at λ = 388 nm (**N719**), λ = 396 nm (**C101**) and λ = 335 nm (**Black Dye**) were assigned to the π–π* electronic transitions.

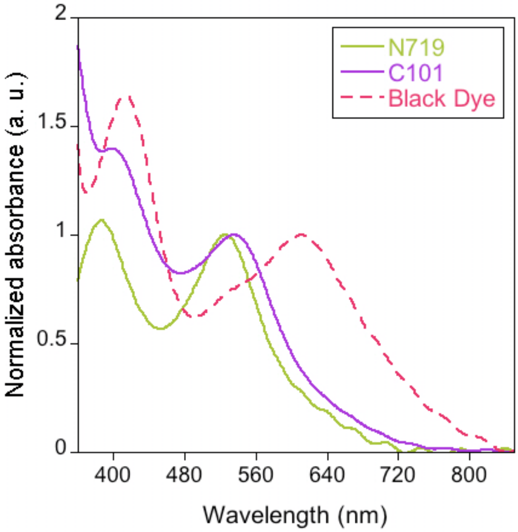

Figure 4.25. UV-Visible absorption spectra of N719, C101 and Black Dye when anchored onto a 4 ηm thick Al_2O_3 film

As can be seen in Figure 4.25, the **Black Dye** is red shifted compared to the **N719** or **C101** dyes. This bathochromic shift is due to the favoured stabilisation of the excited state by the electro action of the thiocyanato anionic ligands as well as the conjugated terpyridine ligand anchored to the ruthenium.[116]

The absorbance spectra of **C101** and the **Black Dye** were also measured when chenodeoxycholic acid was present in the film, as a co-adsorbent to prevent possible dye aggregation processes, as reported in the literature for efficient device performance.[62] Either the Al_2O_3 or the TiO_2 films were immersed into a 300 M chenodeoxycholic acid acetonitrile: *tert*-butanol (1:1) solution and into a 200 M **Black Dye** and 20 mM chenodeoxycholic acid ethanol solution.

The use of the chenodeoxycholic acid as co-adsorbent may also shift the semiconductor conduction band and, in the case of the **Black Dye**, it may act as a buffer by changing the dye protonation degree onto the surface of the nanoparticles and, thus, changing the maximum of the dye absorbance towards the blue.[120] However, in our case, the absorbance spectra of the **Black Dye** and the **C101** in cheno/TiO_2 films present a smaller amount of adsorbed dye than expected, but no shift at the absorbance maximum was observed.

Using the same Al_2O_3 sensitised films, the luminescence spectra of the different dyes were measured (figure not shown). The maximum luminescence wavelength was found to be λ_{em} = 731 nm for **N719** and λ_{em} = 759 nm for **C101**. In the case of the **Black Dye** we were unable to measure the complete emission spectrum due to the limits of our system but it is worthwhile to notice that the emission peak was estimated to be near 900 nm. For the samples with the cheno co-adsorbed molecule, no shift was observed for **C101** or the **Black Dye** emission spectrum.

The emission decay kinetics of the excited state were measured for the three dyes too, either in Al_2O_3 or in TiO_2 films. As illustrated in Figure 4.26, the amplitude of the different emission decays for the TiO_2 sensitised samples is quenched when compared with the Al_2O_3 sensitised films under the same conditions. The quenching is assigned to the efficient photo-induced electron injection process from the dye-excited state into the semiconductor conduction band. In the case of the Al_2O_3 films, the dye excited state is below the conduction band of the metal oxide, which prevents the electron injection reaction. From Figure 4.26, we can already estimated that the **C101** dye has the highest photo-induced electron injection yield.

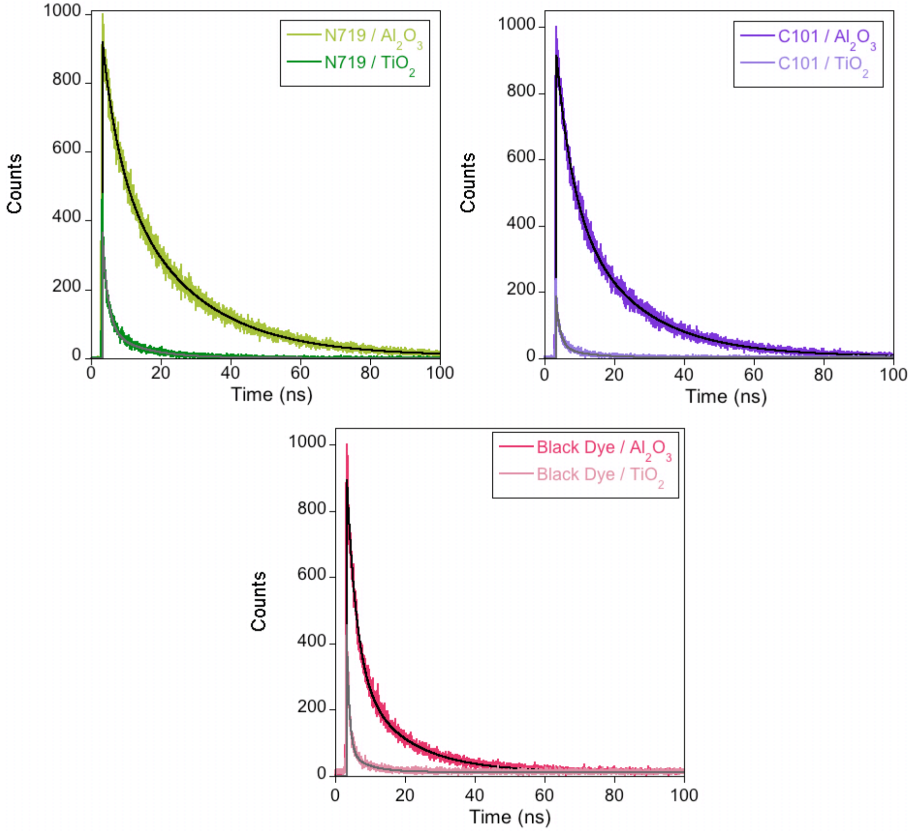

Figure 4.26. Emission decays for N719, C101 and Black Dye when anchored onto Al_2O_3 and TiO_2 4 μm thick films without electrolyte, under air conditions

In previous work, we have shown that the presence of active red/ox electrolyte induced changes on the emission decay dynamics of polypyridyl ruthenium complexes.[107] The reasons for those changes are still under active debate, but several authors have already proved the interaction between the dye and the red/ox active species at the iodine/iodide liquid electrolyte.[108-110] In order to shed some light onto this topic, we have prepared non-functional devices using, as mesoporous material, Al_2O_3 sensitised films with liquid red/ox active iodine/iodide electrolyte. The results of our TCSPC measurements for the different set of dyes anchored onto Al_2O_3 and TiO_2 films measured under air conditions and in complete devices are listed in Table 4.5.

Dye	Surface	Electrolyte	l_{em} (nm)	Lifetime (ns)
Black Dye	Al_2O_3	No electrolyte	805	20.5
C101	Al_2O_3	No electrolyte	760	19.9
N719	Al_2O_3	No electrolyte	730	19.7
Black Dye	Al_2O_3	A	805	14.6
C101	Al_2O_3	A	760	12.2
N719	Al_2O_3	A	730	21.8
Black Dye	TiO_2	No electrolyte	805	5.5
C101	TiO_2	No electrolyte	760	8.5
N719	TiO_2	No electrolyte	730	10.2

Table 4.5. TC-SPC parameters of C101, N719 and the Black Dye measured in Al_2O_3 and TiO_2 4 μm thick films under air conditions and in complete non-functional Al_2O_3 cells using electrolyte A

The measured lifetime of all the dyes is around 20 ns when anchored onto mesoporous Al_2O_3 films. Chenodeoxycholic acid was used as coadsorbent for the **C101** and **Black Dye** cells. Afterwards, complete devices were prepared using these films and the lifetime of the cells were measured at equal acquisition time and experimental parameters. In all the cases, the luminescence amplitude is not quenched in the presence of electrolyte. However, the emission decay kinetics in the case of **C101** and **Black Dye** devices are faster, in clear contrast with the non-functional cells sensitised with **N719**.

On the other hand, the luminescence decays of **C101** and **Black Dye** non-functional devices were also measured without the cheno molecule as co-adsorbent. The presence of the cheno molecule does not affect the signal amplitude, however, the emission decay dynamics of the **Black Dye** sample are slower (Figure 4.27). This behaviour is probably due to the fact that chenodeoxycholic acid avoids some dye-dye interactions which occur in the absence of it.[121]

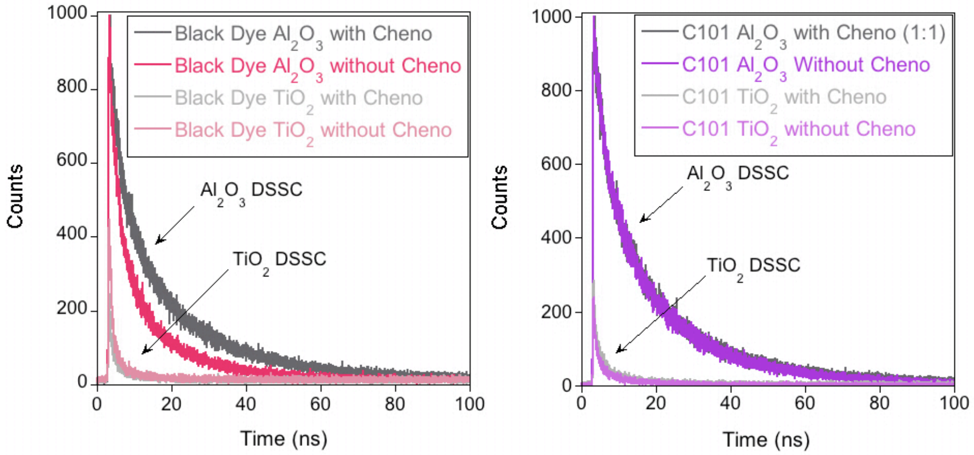

Figure 4.27. Emission luminescence decays for the C101 and the Black Dye samples in Al_2O_3 and TiO_2 4 µm films measured under air conditions with and without chenodeoxycholic acid as coadsorbent

4.4.5.2. Electron recombination measurements. L-TAS experiments

Laser transient absorption spectroscopy measurements were carried on dye-sensitised 4 µm thick TiO_2 mesoporous nanocrystalline films and in complete devices too. For the complete cells, we used different electrolytes as mentioned in the experimental section: electrolyte A and electrolyte B. Since each sample has a different absorption maximum, we used the appropriate excitation wavelength to keep the laser pulse energy invariable. The most relevant data for the electron recombination process between the photo-injected electrons at the TiO_2 and the oxidised dye (dye^+/e^--TiO_2) are listed in Table 4.6.

Dye	$\tau_{1/2}(s)$	$\tau(s)$	α
Black Dye	0.0011	0.0012	0.34
C101	0.00027	0.00064	0.28
N719	0.0016	0.0027	0.28

Table 4.6. Dye^+/e^--TiO_2 electron recombination decay lifetimes for the N719, C101 and Black Dye

As can be seen in Figure 4.28, the presence of the electrolyte induces a decrease in the signal amplitude and faster decay dynamics, which we assign to the efficient regeneration of the dye cations by the electrolyte which occurs much faster (on a nanosecond time scale) than the back electron transfer from the TiO_2 to the oxidised dyes. Furthermore, the transient decay shows a slow phase that we have previously assigned to electrons at the TiO_2 or new species formed due to the presence of the iodine/iodide liquid electrolyte. On the other hand, it seems important to notice that in the case of the devices made using the **Black Dye**, the yield (amplitude of the transient signal at λ_{probe} = 1000 nm) is much less, suggesting that either the species are not formed or the regeneration process occurs much more efficiently and the dye cation species disappear faster than the time scale used in our experiments.

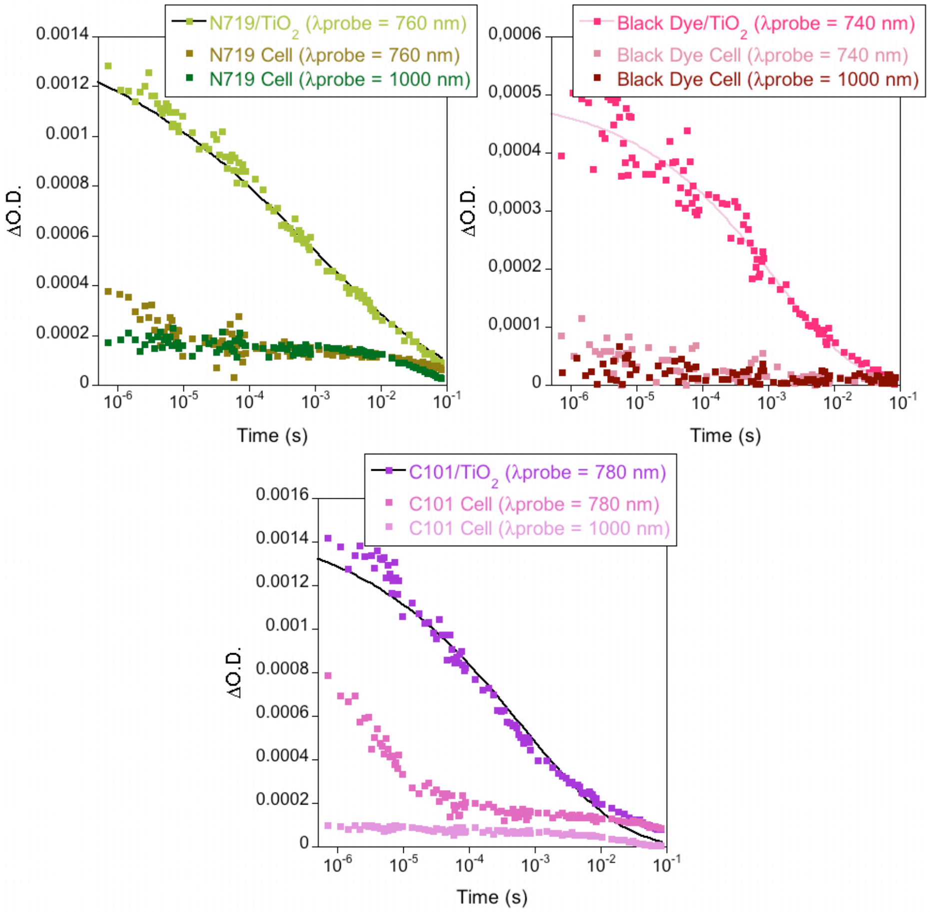

Figure 4.28. L-TAS decay of N719, C101 and Black Dye anchored onto a 4 μm thick TiO_2 film and in complete device using electrolyte A. The laser excitation wavelength was 353 nm for N719 and C101 and 640 nm for Black Dye sensitised films

4.4.5.3. Electrochemistry

The electrochemical properties of the ruthenium complexes were analysed by cyclic voltammetry in acetonitrile (**N719** and **C101**) and in ethanol (**Black Dye**) using a 10^{-3} M solution of each dye with 0.1 M of tetrabutylammonium hexafluorophosphate ($TBAPF_6$).

The LUMO energy levels can be obtained using Equation 4.1, where q is the elementary charge and $E_{0,0}$ is the excited-state zero-zero energy, measured from the intersection between the absorption and emission spectra of the dyes.

$$E_{1/2}(Ru_{ox}) = E_{1/2}(Ru_{red}) + E_{0,0}/q \qquad \text{(Equation 4.1)}$$

Dye	E_{ox} (V) *vs* SCE	$E_{0,0}$ (V)^a	E_{red} (V)
N719	0.73	1.64	-1.39
C101	0.71	1.85	-1.14
Black Dye	0.79	---^{b}	-1.09^c

Table 4.7. Electrochemical properties of N719, C101 and Black Dye sensitizers in solution. ^{a} $E_{0,0}$ was measured from the intersection between the absorption and emission spectra. ^{b} Due to the experimental characteristics of our luminescence spectrophotometer, we could not measure the entire luminescence emission of the Black Dye sensitiser. ^{c} Experimental result taken from a previous article published in the literature[48]

As listed in Table 4.7, we observed for the **N719** dye an oxidation potential of 0.73 V *vs* SCE. The electrochemical wave was irreversible, in good agreement with previous results published in the scientific literature.[105] In the case of the **C101** dye, we obtained a quasi-reversible wave at 0.71 V *vs* SCE. That was also the case for the **Black Dye**. All the waves were assigned to the formation of the $Ru^{II/III}$ redox couple.

4.4.5.4. Light-to-energy conversion measurements

Once we analysed all the photo-physical and electrochemical properties of the ruthenium dyes, we carried out our measurements and analysis of the photo-electrochemical properties of the complete solar cells. Complete devices were prepared as described below, co-sensitising the films with the cheno molecules in the case of **C101** and **Black Dye** and using Electrolyte B in all cases.

The incident photon to current efficiencies for all the DSSC were higher than 70 %, with **C101** being the most efficient dye, with a maximum conversion efficiency of 96 % at λ = 530 nm (Figure 4.29), which is in good agreement with the electron injection data measured using TCSPC. In the case of the **Black Dye**, we obtained proficient photon-to-current conversions near to the IR region. For example, the conversion efficiency at λ = 755 nm was 35 %, while for **C101** and **N719** it was only 7 % and 3 %, respectively.

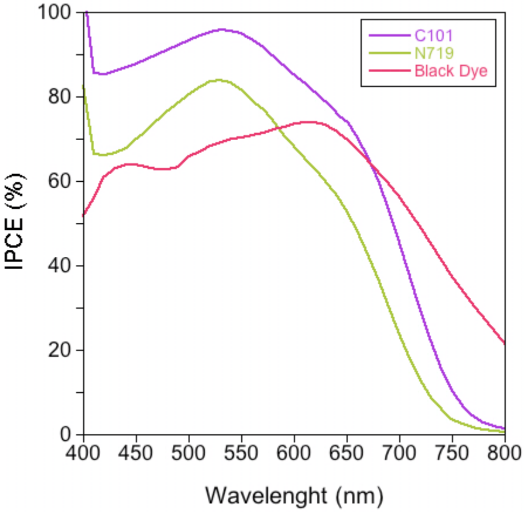

Figure 4.29. IPCE of DSSC using N719, C101 and the Black Dye. The electrolyte used was the electrolyte B

As can be seen in Table 4.8, the photo-current obtained for the DSC under standard conditions of simulated sun light (100 mW·cm^{-2}, 1.5 AM G) are in good agreement with the IPCE values. The devices made using the **C101** dye have not only the highest current, but also the highest light-to-energy conversion efficiency.

Cell	I_{sc} (mA)	V_{oc} (mV)	ff	η (%)
N719	16.91	700	70.83	8.26
C101	19.95	670	68.96	9.21
Black Dye	18.25	680	68.01	8.51

Table 4.8. DSSC measured using a mask (0.2 cm^2) under standard conditions

The I–V curves for **N719**, **C101** and **Black Dye** measured at different light intensities are depicted in Figure 4.30. As can be seen, the highest efficiency in all cases were recorded when they were irradiated using sun simulated light with an intensity of 50 mW·cm^{-2}. For the devices made using **N719**, we have always obtained higher photo-voltages than for the devices made using **C101** or the **Black Dye**. These results confirm published work on the difference between homoleptic and heteroleptic ruthenium dyes.[33]

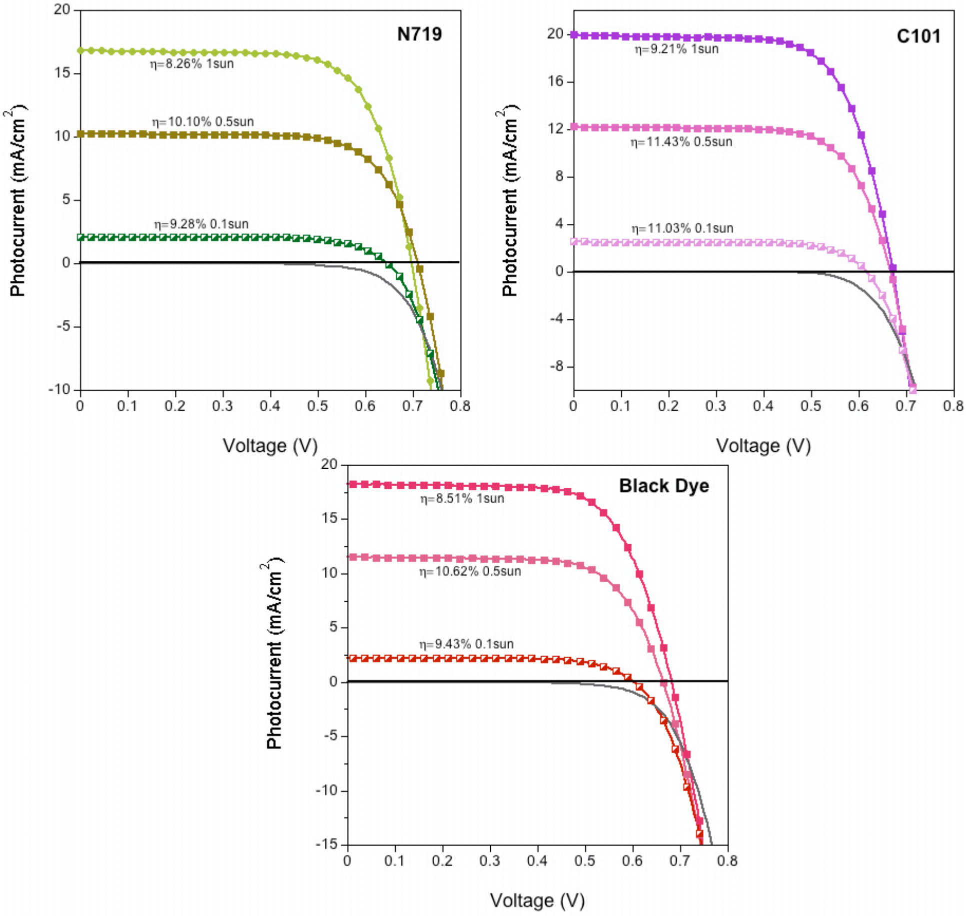

Figure 4.30. Photocurrent vs voltage plot for N719, C101 and Black Dye cells measured at different light intensities

This observation is rather interesting since the oxidation potentials between **C101** and **N719** are not much different. On the other hand, **C101** and the **Black Dye** have different organic ligands coordinated to the ruthenium center than **N719**. In the former case, the heteroleptic complex has a moiety that contains sulfur atoms in its structure, while in the later case the ligand is more conjugated than the bipyridine ligands present in either **N719** or **C101**. Recently, it has been described that the presence of a high degree of conjugation on the organic ligand can induce faster recombination dynamics between the photo-injected electrons at the semiconductor and the oxidised electrolyte.[122]

The use of light-induced photovoltage and charge extraction techniques has been very useful to elucidate the nature of such loss in voltage and the catalytic process involved in the electron/electrolyte recombination reaction.

Figure 4.31 illustrates the charge density *vs* voltage plot for the different DSSC. All the measured experimental points for the charge extraction experiment lie more or less under the same exponential curve and can be fitted to Equation 4.2.

$$e^{-}_{density}\left(e^{-}/cm^{3}\right) = A_0 - A_1 \cdot e^{k \cdot V} \qquad \text{(Equation 4.2)}$$

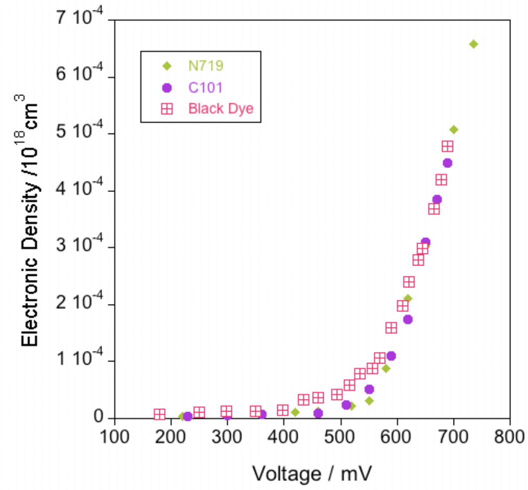

Figure 4.31. Electron density vs voltage plots for the different DSSC

These results indicate that none of the dyes shifts the TiO_2 conduction band energy level with respect to the electrolyte to such a degree that could justify the differences in voltage. Notice that the dyes have a different number of protons (2 in the case of **N719**, 1 for **C101** and **Black Dye**), and the absorption mode of **N719** can cause an up-shift of the conduction band. However, this behaviour is masked by the effect of the counteracting proton-induced down shift of the conduction band energy. Thus, we measured the electron lifetimes for the different DSSC plotted *vs* the electron density (Figure 4.32) and we observed that at higher electron density, corresponding to the maximum V_{oc} on the DSSC, the recombination lifetime for **N719** is slower when compared with the **C101** or the **Black Dye**. The increase of recombination dynamics can explain the lower V_{oc} observed for devices using **C101** and the **Black Dye**, which has also been observed in other ruthenium dyes bearing more conjugated ligands, such as phenanthroline.[42, 123] etc.

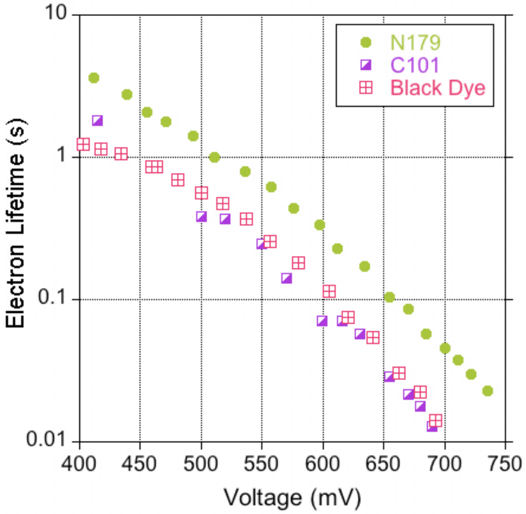

Figure 4.32. Recombination lifetimes for N719, C101 and Black Dye devices vs electron density. All cells were made using Electrolyte B

4.4.6. Conclusions

We have evaluated, using identical conditions, the different charge transfer reactions that limit the light-to-energy conversion performance on the most efficient sensitisers known nowadays in dye sensitised solar cells. We demonstrated that the dye **C101** has the highest electron injection yield, which is in good agreement with the IPCE and the photocurrent measured in complete devices. Interestingly, the presence of typical iodine/iodide redox electrolyte (Electrolyte A) induces faster emission kinetics for **C101** and **Black Dye** DSSC while in the case of **N719** the luminescence decay process is almost unaffected. We assigned the emission quenching dynamics to the interaction of the electrolyte with the dyes bearing more conjugated organic ligands coordinating the ruthenium metal centre. In addition, in the case of the **Black Dye**, using the cheno molecules, to avoid the formation of molecular aggregates on the TiO_2 surface, we also observed faster emission decay dynamics. On the other hand, the photo-induced electron recombination dynamics for all dyes showed typical stretched exponential decays. However, the analysis of the results obtained in complete devices shows that **Black Dye** DSSC have very efficient regeneration dynamics since no signal was detected for dye cations in the presence of iodine/iodide electrolyte.

Finally, light-induced photovoltage transient spectroscopy was employed to investigate the origin of the lower voltages on **C101** and **Black Dye** DSSC when compared to **N719** cells. The results show that, for the above mentioned dyes, at the same charge density they do have higher recombination dynamics than the **N719** DSSC. This observation implies that for the design of new and efficient ruthenium complexes, we ought to block the interactions between the organic ligands, used in the complex to increase the dye absorbance in the red region of the solar spectrum, and the red/ox active species at the iodine/iodide electrolyte.

4.4.7. Acknowledgments

Financial support from the Spanish MICINN (CONSOLIDER-HOPE 0007-2007 and CTQ-2007-60746-BQU projects), ICREA and EU-FP7-ROBUST project is gratefully acknowledged. A.R. would like to thank the MICINN for her PhD grant. The authors also would like to thank Dr Brian C. O'Regan for his useful comments and suggestions.

4.5. References

1. Nazeeruddin, M. K.; Gratzel, M., *Struct. Bonding* **2007,** *123* (Photofunctional Transition Metal Complexes), 113-175.
2. O'Regan, B.; Graetzel, M., *Nature* **1991,** *353* (6346), 737-740.
3. Amadelli, R.; Argazzi, R.; Bignozzi, C. A.; Scandola, F., *J. Am. Chem. Soc.* **1990,** *112* (20), 7099-7103.
4. Robertson, N., *Angew. Chem., Int. Ed.* **2006,** *45* (15), 2338-2345.
5. Ito, S.; Zakeeruddin, S. M.; Humphry-Baker, R.; Liska, P.; Charvet, R.; Comte, P.; Nazeeruddin, M. K.; Péchy, P.; Takata, M.; Miura, H.; Uchida, S.; Grätzel, M., *Adv. Mater.* **2006,** *18* (9), 1202-1205.
6. Wang, Z.-S.; Kawauchi, H.; Kashima, T.; Arakawa, H., *Coord. Chem. Rev.* **2004,** *248* (13-14), 1381-1389.
7. Wang, P.; Zakeeruddin, S. M.; Moser, J. E.; Humphry-Baker, R.; Comte, P.; Aranyos, V.; Hagfeldt, A.; Nazeeruddin, M. K.; Grätzel, M., *Adv. Mater.* **2004,** *16* (20), 1806-1811.
8. Jang, S.-R.; Lee, C.; Choi, H.; Ko, J. J.; Lee, J.; Vittal, R.; Kim, K.-J., *Chem. Mater.* **2006,** *18* (23), 5604-5608.
9. Chen, C.-Y.; Wu, S.-J.; Li, J.-Y.; Wu, C.-G.; Chen, J.-G.; Ho, K.-C., *Adv. Mater.* **2007,** *19* (22), 3888-3891.
10. Gao, F.; Wang, Y.; Shi, D.; Zhang, J.; Wang, M.; Jing, X.; Humphry-Baker, R.; Wang, P.; Zakeeruddin, S. M.; Gratzel, M., *J. Am. Chem. Soc.* **2008,** *130* (32), 10720-10728.
11. Lee, C.; Yum, J.-H.; Choi, H.; Ook Kang, S.; Ko, J.; Humphry-Baker, R.; Grätzel, M.; Nazeeruddin, M. K., *Inorg. Chem.* **2008,** *47* (7), 2267-2273.
12. Kim, J.-J.; Choi, H.; Kim, C.; Kang, M.-S.; Kang, H. S.; Ko, J., *Chem. Mater.* **2009,** *21* (24), 5719-5726.
13. Nazeeruddin, M. K.; Klein, C.; Liska, P.; Graetzel, M., *Coord. Chem. Rev.* **2005,** *249* (13-14), 1460-1467.
14. Kalyanasundaram, K.; Nazeeruddin, M. K., *Chem. Phys. Lett.* **1992,** *193* (4), 292-297.
15. Nazeeruddin, M. K.; Kay, A.; Rodicio, I.; Humphry-Baker, R.; Mueller, E.; Liska, P.; Vlachopoulos, N.; Grätzel, M., *J. Am. Chem. Soc.* **1993,** *115* (14), 6382-6390.
16. Wadman, S. H.; Kroon, J. M.; Bakker, K.; Lutz, M.; Spek, A. L.; van Klink, G. P. M.; van Koten, G., *Chem. Commun.* **2007,** (19), 1907-1909.
17. Bessho, T.; Yoneda, E.; Yum, J.-H.; Guglielmi, M.; Tavernelli, I.; Imai, H.; Rothlisberger, U.; Nazeeruddin, M. K.; Grätzel, M., *J. Am. Chem. Soc.* **2009,** *131* (16), 5930-5934.
18. Wadman, S. H.; Kroon, J. M.; Bakker, K.; Havenith, R. W. A.; van Klink, G. P. M.; van Koten, G., *Organometallics* **2010,** *29* (7), 1569-1579.
19. Islam, A.; Sugihara, H.; Singh, L. P.; Hara, K.; Katoh, R.; Nagawa, Y.; Yanagida, M.; Takahashi, Y.; Murata, S.; Arakawa, H., *Inorg. Chim. Acta* **2001,** *322* (1-2), 7-16.
20. Galoppini, E., *Coord. Chem. Rev.* **2004,** *248* (13-14), 1283-1297.
21. Gillaizeau-Gauthier, I.; Odobel, F.; Alebbi, M.; Argazzi, R.; Costa, E.; Bignozzi, C. A.; Qu, P.; Meyer, G. J., *Inorg. Chem.* **2001,** *40* (23), 6073-6079.

22. Wang, P.; Klein, C.; Moser, J.-E.; Humphry-Baker, R.; Cevey-Ha, N.-L.; Charvet, R.; Comte, P.; Zakeeruddin, S. M.; Gratzel, M., *J. Phys. Chem. B* **2004,** *108* (45), 17553-17559.
23. Nazeeruddin, M. K.; Zakeeruddin, S. M.; Lagref, J. J.; Liska, P.; Comte, P.; Barolo, C.; Viscardi, G.; Schenk, K.; Grätzel, M., *Coord. Chem. Rev.* **2004,** *248* (13-14), 1317-1328.
24. Zakeeruddin, S. M.; Nazeeruddin, M. K.; Humphry-Baker, R.; Péchy, P.; Quagliotto, P.; Barolo, C.; Viscardi, G.; Grätzel, M., *Langmuir* **2002,** *18* (3), 952-954.
25. Klein, C.; Nazeeruddin, M. K.; Di Censo, D.; Liska, P.; Grätzel, M., *Inorg. Chem.* **2004,** *43* (14), 4216-4226.
26. Clifford, J. N.; Palomares, E.; Nazeeruddin, M. K.; Grätzel, M.; Nelson, J.; Li, X.; Long, N. J.; Durrant, J. R., *J. Am. Chem. Soc.* **2004,** *126* (16), 5225-5233.
27. Argazzi, R.; Bignozzi, C. A.; Heimer, T. A.; Castellano, F. N.; Meyer, G. J., *J. Am. Chem. Soc.* **1995,** *117* (47), 11815-11816.
28. Hirata, N.; Lagref, J.-J.; Palomares, E. J.; Durrant, J. R.; Nazeeruddin, M. K.; Gratzel, M.; Di Censo, D., *Chem. Eur. J.* **2004,** *10* (3), 595-602.
29. Abrahamsson, M.; Johansson, P. G.; Ardo, S.; Kopecky, A.; Galoppini, E.; Meyer, G. J., *J. Phys. Chem. Lett.* **2010**, 1725-1728.
30. Nazeeruddin, M. K.; Zakeeruddin, S. M.; Humphry-Baker, R.; Jirousek, M.; Liska, P.; Vlachopoulos, N.; Shklover, V.; Fischer, C.-H.; Grätzel, M., *Inorg. Chem.* **1999,** *38* (26), 6298-6305.
31. Yanagida, M.; Singh, L. P.; Sayama, K.; Hara, K.; Katoh, R.; Islam, A.; Sugihara, H.; Arakawa, H.; Nazeeruddin, M. K.; Gratzel, M., *J. Chem. Soc. Dalton Trans.* **2000,** (16), 2817-2822.
32. O'Regan, B. C.; Walley, K.; Juozapavicius, M.; Anderson, A.; Matar, F.; Ghaddar, T.; Zakeeruddin Shaik, M.; Klein, C.; Durrant, J. R., *J. Am. Chem. Soc.* **2009,** *131* (10), 3541-3548.
33. De Angelis, F.; Fantacci, S.; Selloni, A.; Grätzel, M.; Nazeeruddin, M. K., *Nano Lett.* **2007,** *7* (10), 3189-3195.
34. Grätzel, M., *Prog. Photovolt.* **2006,** *14* (5), 429-442.
35. Durrant, J. R.; Haque, S. A.; Palomares, E., *Coord. Chem. Rev.* **2004,** *248* (13-14), 1247-1257.
36. Kuang, D.; Klein, C.; Ito, S.; Moser, J.-E.; Humphry-Baker, R.; Evans, N.; Duriaux, F.; Grätzel, C.; Zakeeruddin, S. M.; Grätzel, M., *Adv. Mater.* **2007,** *19* (8), 1133-1137.
37. Karthikeyan, C. S.; Wietasch, H.; Thelakkat, M., *Adv. Mater.* **2007,** *19* (8), 1091-1095.
38. Lakowicz, J. R., *Principles of Fluorescence Spectroscopy* **1999**, Kluwer Academic/Plenum Publishers:New York.
39. Tatay, S.; Haque, S. A.; O'Regan, B.; Durrant, J. R.; Verhees, W. J. H.; Kroon, J. M.; Vidal-Ferran, A.; Gavina, P.; Palomares, E., *J. Mater. Chem.* **2007,** *17* (29), 3037-3044.
40. Haque, S. A.; Palomares, E.; Cho, B. M.; Green, A. N. M.; Hirata, N.; Klug, D. R.; Durrant, J. R., *J. Am. Chem. Soc.* **2005,** *127* (10), 3456-3462.
41. Stufkens, D. J.; Vlcek, A., Jr., *Coord. Chem. Rev.* **1998,** *177*, 127-179.
42. Onozawa-Komatsuzaki, N.; Kitao, O.; Yanagida, M.; Himeda, Y.; Sugihara, H.; Kasuga, K., *New J. Chem.* **2006,** *30* (5), 689-697.
43. Tachibana, Y.; Moser, J. E.; Gratzel, M.; Klug, D. R.; Durrant, J. R., *J. Phys. Chem.* **1996,** *100* (51), 20056-20062.

45. Kong, F. T.; Dai, S. Y.; Wang, K. J., *Adv. OptoElec.* **2007,** *2007*.

46. Chiba, Y.; Islam, A.; Watanabe, Y.; Komiya, R.; Koide, N.; Han, L., *Jpn. J. Appl. Phys., Part 2* **2006,** *45* (24-28), L638-L640.

47. Kuang, D.; Klein, C.; Ito, S.; Moser, J.-E.; Humphry-Baker, R.; Zakeeruddin, S. M.; Grätzel, M., *Adv. Funct. Mater.* **2007,** *17* (1), 154-160.

48. Nazeeruddin, M. K.; Pechy, P.; Renouard, T.; Zakeeruddin, S. M.; Humphry-Baker, R.; Comte, P.; Liska, P.; Cevey, L.; Costa, E.; Shklover, V.; Spiccia, L.; Deacon, G. B.; Bignozzi, C. A.; Grätzel, M., *J. Am. Chem. Soc.* **2001,** *123* (8), 1613-1624.

49. Wang, Z.-S.; Yamaguchi, T.; Sugihara, H.; Arakawa, H., *Langmuir* **2005,** *21* (10), 4272-4276.

50. Barolo, C.; Nazeeruddin, M. K.; Fantacci, S.; Di Censo, D.; Comte, P.; Liska, P.; Viscardi, G.; Quagliotto, P.; De Angelis, F.; Ito, S.; Grätzel, M., *Inorg. Chem.* **2006,** *45* (12), 4642-4653.

51. Anderson, N. A.; Lian, T., *Coord. Chem. Rev.* **2004,** *248* (13-14), 1231-1246.

52. Ghosh, H. N.; Asbury, J. B.; Weng, Y.; Lian, T., *J. Phys. Chem. B* **1998,** *102* (50), 10208-10215.

53. Weng, Y.-X.; Wang, Y.-Q.; Asbury, J. B.; Ghosh, H. N.; Lian, T., *J. Phys. Chem. B* **1999,** *104* (1), 93-104.

54. Zhang, Z.; Zakeeruddin, S. M.; O'Regan, B. C.; Humphry-Baker, R.; Grätzel, M., *J. Phys. Chem. B* **2005,** *109* (46), 21818-21824.

55. Kusama, H.; Kurashige, M.; Arakawa, H., *J. Photochem. Photobiol., A Chem.* **2005,** *169* (2), 169-176.

56. Zhang, Z.; Evans, N.; Zakeeruddin, S. M.; Humphry-Baker, R.; Grätzel, M., *J. Phys. Chem. C* **2007,** *111* (1), 398-403.

57. Kopidakis, N.; Neale, N. R.; Frank, A. J., *J. Phys. Chem. B* **2006,** *110* (25), 12485-12489.

58. Kusama, H.; Arakawa, H., *J. Photochem. Photobiol., A Chem.* **2003,** *160* (3), 171-179.

59. Kusama, H.; Arakawa, H., *J. Photochem. Photobiol., A Chem.* **2004,** *165* (1-3), 157-163.

60. Kusama, H.; Arakawa, H., *J. Photochem. Photobiol., A Chem.* **2004,** *164* (1-3), 103-110.

61. Kusama, H.; Arakawa, H., *J. Photochem. Photobiol., A Chem.* **2004,** *162* (2-3), 441-448.

62. Neale, N. R.; Kopidakis, N.; van de Lagemaat, J.; Grätzel, M.; Frank, A. J., *J. Phys. Chem. B* **2005,** *109* (49), 23183-23189.

63. Huang, S. Y.; Schlichthorl, G.; Nozik, A. J.; Gratzel, M.; Frank, A. J., *J. Phys. Chem. B* **1997,** *101* (14), 2576-2582.

64. Nozik, A. J., *Annu. Rev. Phys. Chem.* **2003,** *29* (1), 189-222.

65. Yan, S. G.; Hupp, J. T., *J. Phys. Chem.* **1996,** *100* (17), 6867-6870.

66. Watanabe, T., Fujishima, A., Tatsuoki. O., Honda, K., , *Bull. Chem. Soc. Jpn.* **1976,** *49*, 8-11.

67. Gerischer, H., *Electrochim. Acta* **1989,** *34* (8), 1005-1009.

68. Hara, K.; Dan-oh, Y.; Kasada, C.; Ohga, Y.; Shinpo, A.; Suga, S.; Sayama, K.; Arakawa, H., *Langmuir* **2004,** *20* (10), 4205-4210.

69. Yin, X.; Zhao, H.; Chen, L.; Tan, W.; Zhang, J.; Weng, Y.; Shuai, Z.; Xiao, X.; Zhou, X.; Li, X.; Lin, Y., *Surf. Interface Anal.* **2007,** *39* (10), 809-816.

70. Bandaranayake, K. M. P.; Indika Senevirathna, M. K.; Prasad Weligamuwa, P. M. G. M.; Tennakone, K., *Coord. Chem. Rev.* **2004,** *248* (13-14), 1277-1281.

71. Diamant, Y.; Chappel, S.; Chen, S. G.; Melamed, O.; Zaban, A., *Coord. Chem. Rev.* **2004,** *248* (13-14), 1271-1276.

72. O'Regan, B. C.; López-Duarte, I.; Martínez-Díaz, M. V.; Forneli, A.; Albero, J.; Morandeira, A.; Palomares, E.; Torres, T.; Durrant, J. R., *J. Am. Chem. Soc.* **2008,** *130* (10), 2906-2907.
73. Palomares, E.; Martinez-Diaz, M. V.; Haque, S. A.; Torres, T.; Durrant, J. R., *Chem. Commun* **2004,** (18), 2112-2113.
74. Islam, A.; Sugihara, H.; Arakawa, H., *J. Photochem. Photobiol., A Chem.* **2003,** *158* (2-3), 131-138.
75. Hara, K.; Horiuchi, H.; Katoh, R.; Singh, L. P.; Sugihara, H.; Sayama, K.; Murata, S.; Tachiya, M.; Arakawa, H., *J. Phys. Chem. B* **2001,** *106* (2), 374-379.
76. Hara, K.; Sugihara, H.; Singh, L. P.; Islam, A.; Katoh, R.; Yanagida, M.; Sayama, K.; Murata, S.; Arakawa, H., *J. Photochem. Photobiol., A Chem.* **2001,** *145* (1-2), 117-122.
77. Hara, K.; Sugihara, H.; Tachibana, Y.; Islam, A.; Yanagida, M.; Sayama, K.; Arakawa, H.; Fujihashi, G.; Horiguchi, T.; Kinoshita, T., *Langmuir* **2001,** *17* (19), 5992-5999.
78. Schwarz, O.; van Loyen, D.; Jockusch, S.; J. Turro, N.; Dürr, H., *J. Photochem. Photobiol., A Chem.* **2000,** *132* (1-2), 91-98.
79. Kukrek, A.; Wang, D.; Hou, Y.; Zong, R.; Thummel, R., *Inorg. Chem.* **2006,** *45* (25), 10131-10137.
80. Yanagida, M.; Yamaguchi, T.; Kurashige, M.; Hara, K.; Katoh, R.; Sugihara, H.; Arakawa, H., *Inorg. Chem.* **2003,** *42* (24), 7921-7931.
81. Bessho, T.; Constable, E. C.; Grätzel, M.; Redondo, A. H.; Housecroft, C. E.; Kylberg, W.; Nazeeruddin, M. K.; Neuburger, M.; Schaffner, S., *Chem. Commun.* **2008,** (32), 3717-3719.
82. Hara, K.; Miyamoto, K.; Abe, Y.; Yanagida, M., *J. Phys. Chem. B* **2005,** *109* (50), 23776-23778.
83. Hara, K.; Sato, T.; Katoh, R.; Furube, A.; Ohga, Y.; Shinpo, A.; Suga, S.; Sayama, K.; Sugihara, H.; Arakawa, H., *J. Phys. Chem. B* **2002,** *107* (2), 597-606.
84. Frisch, M. J., et al., *Gaussian 03, Revision C.02* **2004**, Gaussian, Inc.: Wallingford, CT.
85. Andrae, D.; Häussermann, U.; Dolg, M.; Stoll, H.; Preuss, H., *Theor. Chim. Acta* **1990,** *77* (2), 123-141.
86. Koops, S. E.; Durrant, J. R., *Inorg. Chim. Acta* **2008,** *361* (3), 663-670.
87. Tachibana, Y.; Rubtsov, I. V.; Montanari, I.; Yoshihara, K.; Klug, D. R.; Durrant, J. R., *J. Photochem. Photobiol., A Chem.* **2001,** *142* (2-3), 215-220.
88. Balzani, V.; Scandola, F., *Supramolecular photochemistry*. Chinchester, U. K., 1991.
89. Myahkostupov, M.; Piotrowiak, P.; Wang, D.; Galoppini, E., *J. Phys. Chem. C* **2007,** *111* (7), 2827-2829.
90. Myllyperkioe, P.; Benko, G.; Korppi-Tommola, J.; Yartsev, A. P.; Sundstroem, V., *Phys. Chem. Chem. Phys.* **2008,** *10* (7), 996-1002.
91. Hao, E.; Anderson, N. A.; Asbury, J. B.; Lian, T., *J. Phys. Chem. B* **2002,** *106* (39), 10191-10198.
92. Palomares, E.; Clifford, J. N.; Haque, S. A.; Lutz, T.; Durrant, J. R., *J. Am. Chem. Soc.* **2003,** *125* (2), 475-482.
93. Montanari, I.; Nelson, J.; Durrant, J. R., *J. Phys. Chem. B* **2002,** *106* (47), 12203-12210.
94. Bisquert, J.; Zaban, A.; Greenshtein, M.; Mora-Seró, I., *J. Am. Chem. Soc.* **2004,** *126* (41), 13550-13559.
95. O'Regan, B. C.; Durrant, J. R., *J. Phys. Chem. B* **2006,** *110* (17), 8544-8547.

97. Zaban, A.; Greenshtein, M.; Bisquert, J., *ChemPhysChem* **2003,** *4* (8), 859-864.

98. Reynal, A.; Forneli, A.; Martinez-Ferrero, E.; Sanchez-Diaz, A.; Vidal-Ferran, A.; Palomares, E., *Eur. J. Inorg. Chem.* **2008,** (12), 1955-1958.

99. Abbotto, A.; Barolo, C.; Bellotto, L.; De Angelis, F.; Grätzel, M.; Manfredi, N.; Marinzi, C.; Fantacci, S.; Yum, J.-H.; Nazeeruddin, M. K., *Chem. Commun* **2008,** (42), 5318-5320.

100. Nazeeruddin, M. K.; Bessho, T.; Cevey, L.; Ito, S.; Klein, C.; De Angelis, F.; Fantacci, S.; Comte, P.; Liska, P.; Imai, H.; Grätzel, M., *J. Photochem. Photobiol., A Chem.* **2007,** *185* (2-3), 331-337.

101. Matar, F.; Ghaddar, T. H.; Walley, K.; DosSantos, T.; Durrant, J. R.; O'Regan, B., *J. Mater. Chem.* **2008,** *18* (36), 4246-4253.

102. Martineau, D.; Beley, M.; Gros, P. C.; Cazzanti, S.; Caramori, S.; Bignozzi, C. A., *Inorg. Chem.* **2007,** *46* (6), 2272-2277.

103. Kuang, D.; Klein, C.; Snaith Henry, J.; Moser Jacques, E.; Humphry-Baker, R.; Comte, P.; Zakeeruddin Shaik, M.; Gratzel, M., *Nano Lett.* **2006,** *6* (4), 769-773.

104. Chen, C.-Y.; Wu, S.-J.; Wu, C.-G.; Chen, J.-G.; Ho, K.-C., *Angew. Chem., Int. Ed.* **2006,** *45* (35), 5822-5825.

105. Nazeeruddin, M. K.; De Angelis, F.; Fantacci, S.; Selloni, A.; Viscardi, G.; Liska, P.; Ito, S.; Takeru, B.; Grätzel, M., *J. Am. Chem. Soc.* **2005,** *127* (48), 16835-16847.

106. Islam, A.; Sugihara, H.; Hara, K.; Singh, L. P.; Katoh, R.; Yanagida, M.; Takahashi, Y.; Murata, S.; Arakawa, H., *J. Photochem. Photobiol., A Chem.* **2001,** *145* (1-2), 135-141.

107. Reynal, A.; Forneli, A.; Martinez-Ferrero, E.; Sanchez-Diaz, A.; Vidal-Ferran, A.; O'Regan Brian, C.; Palomares, E., *J. Am. Chem. Soc.* **2008,** *130* (41), 13558-13567.

108. Clifford, J. N.; Palomares, E.; Nazeeruddin, M. K.; Graetzel, M.; Durrant, J. R., *J. Phys. Chem. C* **2007,** *111* (17), 6561-6567.

109. Gardner, J. M.; Giaimuccio, J. M.; Meyer, G. J., *J. Am. Chem. Soc.* **2008,** *130* (51), 17252-17253.

110. Privalov, T.; Boschloo, G.; Hagfeldt, A.; Svensson, P. H.; Kloo, L., *J. Phys. Chem. C* **2009,** *113* (2), 783-790.

111. Polo, A. S.; Itokazu, M. K.; Murakami Iha, N. Y., *Coord. Chem. Rev.* **2004,** *248* (13-14), 1343-1361.

112. Nazeeruddin, M. K.; Zakeeruddin, S. M.; Humphry-Baker, R.; Gorelsky, S. I.; Lever, A. B. P.; Gratzel, M., *Coord. Chem. Rev.* **2000,** *208*, 213-225.

113. Wolfbauer, G.; Bond, A. M.; Deacon, G. B.; MacFarlane, D. R.; Spiccia, L., *J. Am. Chem. Soc.* **2000,** *122* (1), 130-142.

114. Kusama, H.; Arakawa, H., *Sol. Energy Mater. Sol. Cells* **2004,** *82* (3), 457-465.

115. Argazzi, R.; Bignozzi, C. A.; Heimer, T. A.; Castellano, F. N.; Meyer, G. J., *Inorg. Chem.* **1994,** *33* (25), 5741-5749.

116. Nazeeruddin, M. K.; Pechy, P.; Grätzel, M., *Chem. Commun.* **1997,** (18), 1705-1706.

117. Aiga, F.; Tada, T., *J. Mol. Struct.* **2003,** *658* (1-2), 25-32.

118. Katoh, R.; Furube, A.; Kasuya, M.; Fuke, N.; Koide, N.; Han, L., *J. Mater. Chem.* **2007,** *17* (30), 3190-3196.

119. Ikeda, M.; Koide, N.; Han, L.; Sasahara, A.; Onishi, H., *Langmuir* **2008,** *24* (15), 8056-8060.

120. Bauer, C.; Boschloo, G.; Mukhtar, E.; Hagfeldt, A., *J. Phys. Chem. B* **2002,** *106* (49), 12693-12704.

122. Clifford, J. N.; Forneli, A.; Lopez-Arroyo, L.; Caballero, R.; Cruz, P. d. l.; Langa, F.; Palomares, E., *ChemSusChem* **2009,** *2* (4), 344-349.

123. Chen, C.-Y.; Lu, H.-C.; Wu, C.-G.; Chen, J.-G.; Ho, K.-C., *Adv. Funct. Mater.* **2007,** *17* (1), 29-36.

Chapter 5. Effect of coadsorbents on solar cell performance

This Chapter is based on the study of the influence of coadsorbents on photosensitiser function in DSSC and ultimately on solar cell efficiency. In this work, coadsorbents are used to reduce the electron recombination between photoinjected electrons in the conduction band of the semiconductor and the oxidised species present in the electrolyte.

This chapter is based on the following publication:
Reynal, A., Palomares, E., Energy Env. Sci., 2009, 2, 1078-1081

TABLE OF CONTENTS

5.1. Introduction

In DSSCs there are two possible recombination reactions which can take place at the TiO_2/dye/redox couple interface: recombination between photoinjected electrons in the TiO_2 conduction band with either the dye$^+$ or the electrolyte$^+$.

For efficient DSSCs, the recombination reaction of the electrons injected into the conduction band of the semiconductor with the oxidised dye does not influence significantly the device performance, mainly because this reaction is inherently slow resulting in efficient regeneration by the I^-/I_3^- redox couple present in the electrolyte.[1] Although this is still under debate, the slow recombination rates are thought to be due to the large distance between the photoinjected electrons in the TiO_2 and the dye cation on the TiO_2 surface which results in weak electronic coupling between these two species.

Therefore the most important recombination reaction in DSSCs is the recombination of photoinjected electrons in the TiO_2 with the electrolyte. This recombination reaction is also known as the “dark current”. The control of this back electron transfer reaction is key to the development of efficient DSSC devices, since it strongly influences cell V_{oc}.

Several strategies have been employed in order to reduce the e^--TiO_2/electrolyte$^+$ recombination reaction, such as the use of dyes with long alkyl chains or bulky groups,[2] or the introduction of an insulating Al_2O_3 blocking layer between the TiO_2 surface and the dye sensitiser.[3] However, one of the most efficient ways to decrease the dark current is through the attachment of coadsorbent molecules to the TiO_2 semiconductor nanoparticles.[4] Coadsorbents are small molecules consisting of an anchoring group and a carbon skeleton. The function of this class of additives in DSSCs is to act as a barrier to prevent the approach of the electrolyte to the TiO_2 surface, especially towards areas not covered by the photosensitiser.

Different types of coadsorbents have been used in molecular photovoltaic devices, such as chenodeoxycholic acid,[5] 1-decylphosphonic acid,[6] 4-guanidinobutyric acid[7] or hexadecylmalonic acid[8] (Figure 5.1).

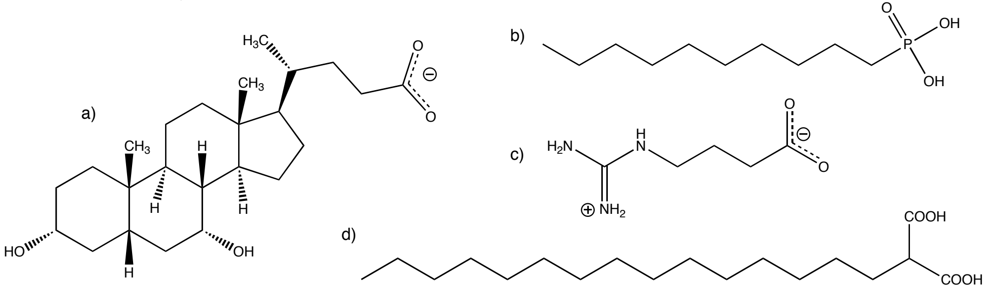

Figure 5.1. Molecular structures of chenodeoxycholic acid (a), 1-decylphosphonic acid (b), 4-guanidinobutyric acid (c) and hexadecylmalonic acid (d)

The blocking effect achieved by a packed monolayer of dye and coadsorbent molecules decreases the e^--TiO_2/electrolyte$^+$ recombination rate. For this reason, the photovoltage of devices usually increases by using coadsorbents. On the other hand, the use of coadsorbents can reduce the number of adsorbed dye molecules on the semiconductor film, which obviously reduces the number of electrons injected into the conduction band of the semiconductor. However, studies indicate that this does not affect significantly the photocurrent generated by the cell.[5]

The presence of dye aggregates is a very important issue in DSSCs, especially for devices made using organic photosensitisers, as they strongly reduce electron injection into the conduction band of the semiconductor. However, the intercalation of coadsorbents between the dye molecules prevents their aggregation. This behaviour usually results in an increase of the photocurrent.

The effects of coadsorbents on the I_{sc} and V_{oc} values of DSSCs can vary with the nature of the dye and the coadsorbent, as well as with other external conditions, such as the composition of the electrolyte. In this Chapter, the behaviour of the DSSCs sensitised with two different ruthenium dyes was studied when citric acid was used as the coadsorbent (Article D).

5.2. Article D. Increasing the performance of *cis*-dithiocyanato(4,4'-dicarboxy-2,2'-bipyridine)(1,10-phenanthroline)ruthenium(II) based DSC using citric acid as co-adsorbent

Energy Env. Sci., 2009, 2, 1078

Anna Reynal, Emilio Palomares*

We describe the use of citric acid as co-adsorbent in dye solar cells. As we demonstrate herein, it is possible to increase the photocurrent of DSSC without loosing photovoltage when we employed *cis*-dithiocyanato(4,4'-dicarboxy-2,2'-bipyridine)(1,10-phenanthroline)ruthenium(II) (**AR20**). Moreover, we show that the molecular structure of the coadsorbent also plays a major role due to its interaction with the sensitiser.

The basic research to improve DSSC stability power conversion efficiency stems from the need to reach commercial applications in the next five to six years. Although there is not yet a clear niche application for DSSC, it is widely accepted that DSSC represents a low-cost alternative to traditional single gap semiconductor crystalline devices.[1, 9-12]

The research strategies used to increase DSSC efficiency have traditionally focused on the composition,[13, 14] size[15-17] and shape[18-20] of the semiconductor nanoparticles, the adsorption of dyes with broad absorption band and high molar extinction coefficient[21-24] in the visible–near IR of the solar spectrum, the composition of the electrolyte,[25-28] and the use of coadsorbents.[29-31] Regarding the latter strategy, several kinds of additives such as deoxycholic acid,[32] hexadecylmalonic acid,[8] guanidinium thiocyanante,[33] *tert*-butylpyridine[34] have been added to dye sensitised solar cells in order to improve the short circuit photocurrent or the open circuit photovoltage of the solar cells. In this communication we have focused on the study of a new co-adsorbent and its effect on the DSSC using two different ruthenium dyes (*cis*-dithiocyanato(4,4'-dicarboxy-2,2'-bipyridine)(1,10-phenanthroline) ruthenium (II) (**AR20**) and *cis*-bis(isothiocyanato) bis-(4,4'-dicarboxylato-2,2'-bipyridine) bis-(tetrabutylammonium)ruthenium(II), also known as **N719** (Figure 5.2).The **AR20** dye was chosen due to the structural differences from the dye paradigm in DSSC, the **N719** sensitiser. The more conjugated ligand in **AR20**, a phenanthroline, gives **AR20** different molecular electronic properties compared to **N719** and it also interacts with the electrolyte differently, as we have recently demonstrated.[35]

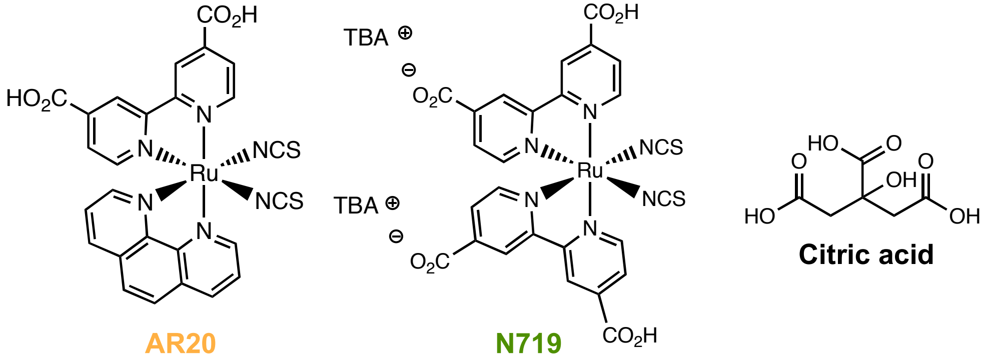

Figure 5.2. Molecular structure of the molecules AR20, N719 and citric acid

Citric acid is a tri-protic weak organic acid with a pK_a of 6.4. The presence of three carboxylate groups on its molecular structure ensures anchoring of this acid onto the TiO_2 surface, and it can act as a buffer on the surface of the semiconductor nanoparticles.

The UV–visible absorption spectra of ruthenium-sensitised 4 μm TiO_2 films were measured (Figure 5.3). The films were immersed into a 300 μM solution of either **AR20** or **N719** sensitisers containing different concentrations of citric acid in acetonitrile/*tert*-butanol (1 : 1) solution. Firstly, it is important to note that a decrease of 20 % and 30 % of the total dye adsorption is observed for **AR20** and of 40 % and 60 % in the case of **N719**, when we use citric acid concentrations of 150 and 300 μM, respectively. Secondly, in the **N719** dye, the maximum absorbance wavelength when adsorbed onto a TiO_2 film was red shifted when citric acid was present.

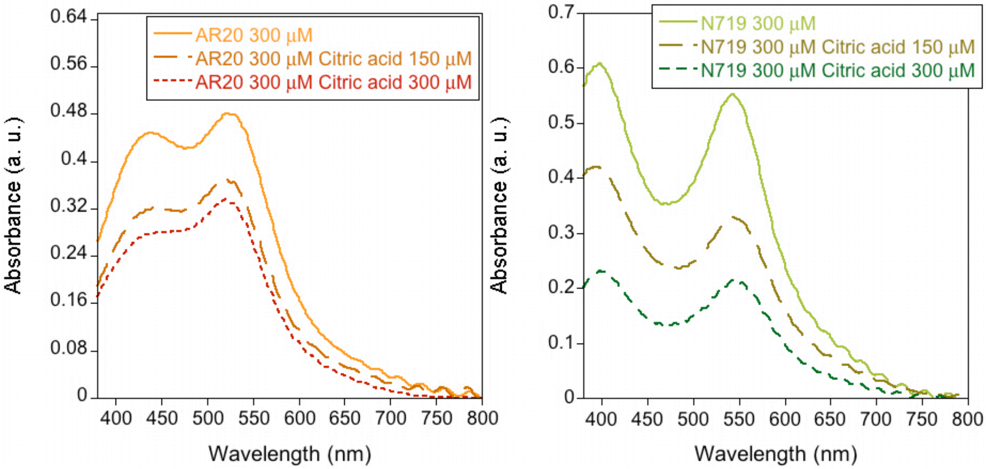

Figure 5.3. The absorption spectra of N719/TiO_2 and AR20/TiO_2 (film thickness 4 μm) at different concentrations of citric acid as co-adsorbent

This batochromic shift of 9 nm may be due to the interaction between the dye and the citric acid due to a change on the TiO_2 surface pH. Interestingly, the absorption spectrum of the **AR20** sensitiser is not shifted. Different groups have already reported that the treatment of the TiO_2 surface with different organic molecules can cause shifts in the conduction band edge, by positively or negatively charging the TiO_2 surface and, thus, it is possible to increase or decrease the device photocurrent, respectively.[4, 36] Hence, to further prove this hypothesis, we carried out photo-induced charge extraction measurements to register the shift of the semiconductor band edge.

The DSSCs were prepared using 8 µm thick TiO_2 films (20 nm particle diameter) plus 4 µm TiO_2 scatter layer (400 nm particle diameter). The electrolyte composition used was, 1 M BMII, 0.03 M I_2, 0.05 M LiI, 0.1 M GuNCS and 0.5 M *tert*-butylpyridine in acetonitrile/valeronitrile 85:15. Figure 5.4 illustrates the measured experimental points at different light bias for the two different devices.

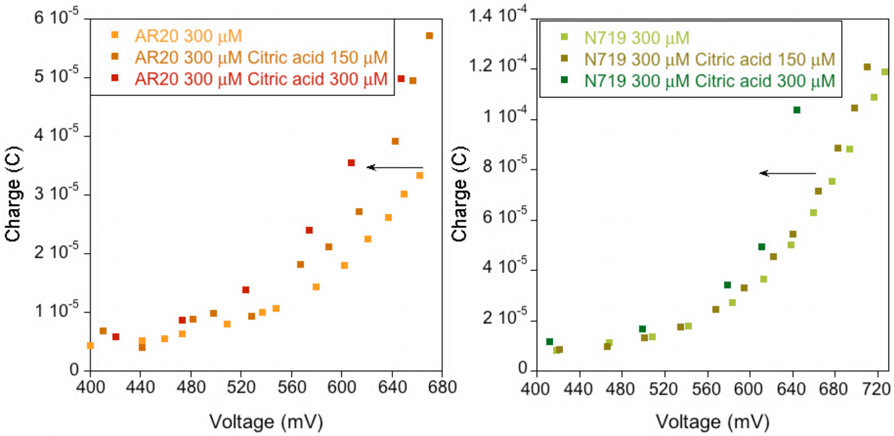

Figure 5.4. Charge extraction measurements for N719 and AR20 dye solar cells at different citric acid concentrations

As we see, at equal photo-induced charge density, the photovoltage of the cell with the dye and the co-adsorbed citric acid (300 µM) is about 60 mV and 70 mV lower for **AR20** and **N719**, respectively. These results indicate that the addition of citric acid (300 µM) shifts the conduction band edge downwards in both cases. Thus, an increase in short circuit photocurrent or a decrease in open circuit voltage must be observed.

As listed in Table 5.1, DSSC based on the sensitisation of TiO_2 using **AR20** shows a high increase in power conversion efficiency but, this is not only due to the increase in photocurrent but also in photovoltage and fill factor. This was unexpected since as mentioned above, and based on Figure

5.4, we expected an increase only in photocurrent. Moreover, taking the **N719** as a blank (standard DSSC using **N719** gave us above 7.7 % power conversion efficiencies under standard measurement conditions) we observed an important decrease in device efficiency due to the decrease in photocurrent, photovoltage and fill factor. Therefore, the presence of citric acid not only affects/ interacts with the TiO_2 and shifts the conduction band edge position but also interacts with the anchored dye.

Dye	Citric acid concentration (10^{-6} M)	I_{sc} (mA)	V_{oc} (V)	ff	η^a (%)
AR20	0	1.83	0.61	48.5	2.8
AR20	150	2.88	0.65	63.4	6.1
AR20	300	2.36	0.64	63.2	4.8
N719	0	3.65	0.72	57.6	7.7
N719	150	3.27	0.69	49.8	5.8
N719	300	2.54	0.64	30.3	2.5

Table 5.1. Photovoltaic characteristics of DSSC (cell area 0.196 cm^2) sensitised with N719 and AR20 with different amounts of citric acid. ^{a} Power conversion efficiency at 1 sun (100 $mW \cdot cm^{-2}$)

To shed some light on these results we carried out light-induced photovoltage transient spectroscopy, a technique that is used to measure the recombination rate between the photo-injected electrons and the oxidised electrolyte.[37-39] Figure 5.5 shows the measured electron lifetimes at each light bias. As can be seen, for **AR20** DSSC the presence of citric acid induces slow recombination dynamics at each bias, including light bias equal to V_{oc}. On the contrary for **N719** DSSC, although at low light intensities (low induced V_{oc}) it shows similar recombination lifetimes, at light bias equal to V_{oc} the recombination is much faster when in the presence of citric acid.

The results in Figure 5.5 clearly show that one of the major reasons for the increase in power conversion efficiency for **AR20** based DSSC is the slower recombination dynamics due to the presence of citric acid as an additive in combination with the **AR20** sensitiser.

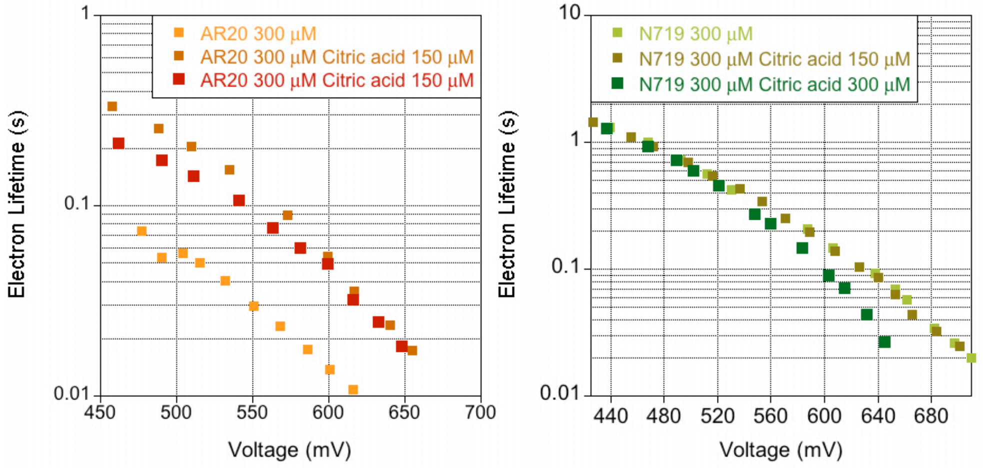

Figure 5.5. Recombination lifetime vs cell V_{oc} for AR20 and N719 DSSC with different concentrations of citric acid

In conclusion, the results confirm that the use of citric acid in DSSC sensitised with **AR20** results in slower recombination dynamics and an important increase in power conversion efficiency from 2.76 % to 6.08 %. However, while in the case of **AR20**, with phenanthroline, citric acid slows the interfacial charge transfer recombination dynamics; for **N719**, with bipyridine bearing carboxylic acids as the ligand, it accelerates the process. Further experiments to uncover the molecular mechanism of this unprecedented interaction between citric acid and the dye are being carried out to increase the device efficiency further.

5.2.1. Acknowledgments

AR and EP would like to acknowledge the MICIIN for financial suport. Project CONSOLIDER-HOPE CSD-0007-2007 and CTQ- 2007-60746-BQU and to the ICIQ Foundation.

5.3. References

1. Ardo, S.; Meyer, G. J., *Chem. Soc. Rev.* **2009,** *38* (1), 115-164.
2. Kroeze, J. E.; Hirata, N.; Koops, S.; Nazeeruddin, M. K.; Schmidt-Mende, L.; Grätzel, M.; Durrant, J. R., *J. Am. Chem. Soc.* **2006,** *128* (50), 16376-16383.
3. Palomares, E.; Clifford, J. N.; Haque, S. A.; Lutz, T.; Durrant, J. R., *J. Am. Chem. Soc.* **2003,** *125* (2), 475-482.
4. Neale, N. R.; Kopidakis, N.; van de Lagemaat, J.; Grätzel, M.; Frank, A. J., *J. Phys. Chem. B* **2005,** *109* (49), 23183-23189.
5. Lee, K.-M.; Suryanarayanan, V.; Ho, K.-C.; Justin Thomas, K. R.; Lin, J. T., *Sol. Energy Mater. Sol. Cells* **2007,** *91* (15+16), 1426-1431.
6. Wang, P.; Zakeeruddin, S. M.; Humphry-Baker, R.; Moser, J. E.; Grätzel, M., *Adv. Mater.* **2003,** *15* (24), 2101-2104.
7. Zhang, Z.; Zakeeruddin, S. M.; O'Regan, B. C.; Humphry-Baker, R.; Grätzel, M., *J. Phys. Chem. B* **2005,** *109* (46), 21818-21824.
8. Wang, P.; Zakeeruddin, S. M.; Comte, P.; Charvet, R.; Humphry-Baker, R.; Grätzel, M., *J. Phys. Chem. B* **2003,** *107* (51), 14336-14341.
9. O'Regan, B.; Graetzel, M., *Nature* **1991,** *353* (6346), 737-740.
10. Gratzel, M., *J. Photochem. Photobiol., C.* **2003,** *4* (2), 145-153.
11. Islam, A.; Sugihara, H.; Arakawa, H., *J. Photochem. Photobiol., A Chem.* **2003,** *158* (2-3), 131-138.
12. Robertson, N., *Angew. Chem., Int. Ed.* **2008,** *47* (6), 1012-1014.
13. O'Regan, B. C.; Scully, S.; Mayer, A. C.; Palomares, E.; Durrant, J., *J. Phys. Chem. B* **2005,** *109* (10), 4616-4623.
14. Palomares, E.; Clifford, J. N.; Haque, S. A.; Lutz, T.; Durrant, J. R., *Chem. Commun* **2002,** (14), 1464-1465.
15. Chou, T. P.; Zhang, Q.; Russo, B.; Fryxell, G. E.; Cao, G., *J. Phys. Chem. C* **2007,** *111* (17), 6296-6302.
16. Dor, S.; Grinis, L.; Ruhle, S.; Zaban, A., *J. Phys. Chem. C* **2009,** *113* (5), 2022-2027.
17. Ofir, A.; Dor, S.; Grinis, L.; Zaban, A.; Dittrich, T.; Bisquert, J., *J. Chem. Phys.* **2008,** *128* (6), 064701-064709.
18. Liu, J.; Cao, G.; Yang, Z.; Wang, D.; Dubois, D.; Zhou, X.; Graff, G. L.; Pederson, L. R.; Zhang, J.-G., *ChemSusChem* **2008,** *1* (8-9), 676-697.
19. Jennings, J. R.; Ghicov, A.; Peter, L. M.; Schmuki, P.; Walker, A. B., *J. Am. Chem. Soc.* **2008,** *130* (40), 13364-13372.
20. Cass, M. J.; Walker, A. B.; Martinez, D.; Peter, L. M., *J. Phys. Chem. B* **2005,** *109* (11), 5100-5107.
21. Nazeeruddin, M. K.; De Angelis, F.; Fantacci, S.; Selloni, A.; Viscardi, G.; Liska, P.; Ito, S.; Takeru, B.; Grätzel, M., *J. Am. Chem. Soc.* **2005,** *127* (48), 16835-16847.
22. Gao, F.; Wang, Y.; Shi, D.; Zhang, J.; Wang, M.; Jing, X.; Humphry-Baker, R.; Wang, P.; Zakeeruddin, S. M.; Gratzel, M., *J. Am. Chem. Soc.* **2008,** *130* (32), 10720-10728.
23. Gao, F.; Cheng, Y.; Yu, Q.; Liu, S.; Shi, D.; Li, Y.; Wang, P., *Inorg. Chem.* **2009,** *48* (6), 2664-2669.

24. Reynal, A.; Forneli, A.; Martinez-Ferrero, E.; Sanchez-Diaz, A.; Vidal-Ferran, A.; Palomares, E., *Eur. J. Inorg. Chem.* **2008,** (12), 1955-1958.
25. Hara, K.; Nishikawa, T.; Kurashige, M.; Kawauchi, H.; Kashima, T.; Sayama, K.; Aika, K.; Arakawa, H., *Sol. Energy Mater. Sol. Cells* **2005,** *85* (1), 21-30.
26. Cao, Y.; Zhang, J.; Bai, Y.; Li, R.; Zakeeruddin, S. M.; Gratzel, M.; Wang, P., *J. Phys. Chem. C* **2008,** *112* (35), 13775-13781.
27. Nogueira, A. F.; De Paoli, M.-A.; Montanari, I.; Monkhouse, R.; Nelson, J.; Durrant, J. R., *J. Phys. Chem. B* **2001,** *105* (31), 7517-7524.
28. Sapp, S. A.; Elliott, C. M.; Contado, C.; Caramori, S.; Bignozzi, C. A., *J. Am. Chem. Soc.* **2002,** *124* (37), 11215-11222.
29. Boschloo, G.; Haeggman, L.; Hagfeldt, A., *J. Phys. Chem. B* **2006,** *110* (26), 13144-13150.
30. Ikeda, M.; Koide, N.; Han, L.; Sasahara, A.; Onishi, H., *Langmuir* **2008,** *24* (15), 8056-8060.
31. Kusama, H.; Konishi, Y.; Sugihara, H.; Arakawa, H., *Sol. Energy Mater. Sol. Cells* **2003,** *80* (2), 167-179.
32. Yum, J.-H.; Jang, S.-r.; Humphry-Baker, R.; Grätzel, M.; Cid, J.-J.; Torres, T.; Nazeeruddin, M. K., *Langmuir* **2008,** *24* (10), 5636-5640.
33. Kopidakis, N.; Neale, N. R.; Frank, A. J., *J. Phys. Chem. B* **2006,** *110* (25), 12485-12489.
34. Durr, M.; Yasuda, A.; Nelles, G., *Appl. Phys. Lett.* **2006,** *89* (6), 061110.
35. Reynal, A.; Forneli, A.; Martinez-Ferrero, E.; Sanchez-Diaz, A.; Vidal-Ferran, A.; O'Regan Brian, C.; Palomares, E., *J. Am. Chem. Soc.* **2008,** *130* (41), 13558-13567.
36. Schlichthoerl, G.; Huang, S. Y.; Sprague, J.; Frank, A. J., *J. Phys. Chem. B* **1997,** *101* (41), 8141-8155.
37. Mori, S. N.; Kubo, W.; Kanzaki, T.; Masaki, N.; Wada, Y.; Yanagida, S., *J. Phys. Chem. C* **2007,** *111* (8), 3522-3527.
38. Planells, M.; Forneli, A.; Martinez-Ferrero, E.; Sanchez-Diaz, A.; Sarmentero, M. A.; Ballester, P.; Palomares, E.; O'Regan, B. C., *Appl. Phys. Lett.* **2008,** *92* (15), 153506.
39. Green, A. N. M.; Chandler, R. E.; Haque, S. A.; Nelson, J.; Durrant, J. R., *J. Phys. Chem. B* **2005,** *109* (1), 142-150.

Chapter 6. General conclusions and future work

This thesis has focused mainly on how dye sensitiser structure influences cell performance in TiO_2 dye sensitised solar cells. Different ruthenium photosensitisers were employed, containing different electron donor or electron acceptor groups, which modulate redox, absorption and luminescence properties, while also strongly affecting the DSSC electron transfer processes. In addition, the influence of the coadsorbent citric acid on cell performance was investigated.

In this work, special attention was paid to the properties and synthesis of heteroleptic ruthenium polypyridyl complexes containing bidentate and tridentate chelating ligands. More precisely, the ligands 2,2'-bipyridine, 2,2':6',2"-terpyridine and 1,10-phenanthroline ligands were chosen due to their high stability under light, humidity and oxygen conditions, allowing ease of preparation and storage. Furthermore, functionalisation at the different positions of the pyridine ring was studied in depth.

In the articles A and B, a series of ruthenium complexes were studied containing a bipyridine, two thiocyanates and a phenanthroline moiety. Electron donor and electron withdrawing groups were used in the functionalisation of polypyridyl ligands in order to tune their electrochemical, photophysical and photochemical properties. These ruthenium complexes were then used as photosensitisers in dye sensitised solar cells and compared to devices made using the well-known commercial dye **N719**. Their cell performances as well as the kinetics of the reactions occurring in these photovoltaic devices were correlated to the molecular structure of the photosensitisers.

Indeed, it was observed that the introduction of substituents on the polypyridyl ligands coordinated to the ruthenium metal center strongly influences the spectroscopical and electrochemical properties of the complexes. Furthermore, these modifications in the structure of the ruthenium complexes strongly affect the performance of the solar cells. Such direct structure-device function relationship is crucial in the preparation of highly efficient devices.

The key results in this study can be summarised as follows:

- Despite the presence of a π^* low-lying molecular orbital localised on the phenanthroline moiety of the ruthenium(II) heteroleptic complex, efficient light induced electron injection into the TiO_2 conduction band (> 70 %) is estimated from TC-SPC measurements for **AR20**, **AR25** and **AR24**. Although the luminescence decay of **AR27** could not be measured because it was faster than the instrument response, the theoretical calculations of the molecular orbitals of this ruthenium complex predict a low-lying LUMO energy level, resulting in minimal electron injection into the semiconductor conduction band.

- Theoretical calculations show that HOMO is centered on the thiocyanate ligands for all of the ruthenium complexes. On the other hand, the LUMO is localised on the bipyridines for **AR20**, **AR24** and **AR25**. However, the presence of the strong electron acceptor ($-NO_2$) present in the **AR27** molecular structure, localises the LUMO on the phenanthroline moiety.

- The L-TAS decays of sensitised TiO_2 films can be fitted to a classic stretched exponential. However, the measurement of complete devices, in the presence of the I^-/I_3^- redox couple exhibits a strongly reduced signal for **AR24** and **AR27** compared to **AR20** or **AR25**. The behavior of **AR27** can be explained in terms of inefficient electron injection due to the presence of a low-lying molecular orbital, as well as an inadequate localisation of the LUMO far away from the TiO_2 surface. The reduced signal in the case of cells containing **AR24** is discussed below.

- The V_{oc} decay measurements of the DSSCs reveal a much faster e^--TiO_2/electrolyte$^+$ recombination reaction when the **AR24** and **AR27** ruthenium complexes are employed as photosensitisers. This back electron transfer strongly reduces the open circuit voltage of the cell, and thus the overall performance of the solar cell.

- As expected, the IPCE and overall efficiency values for **AR20** and **AR25** are similar to that reported for **N719**. On the other hand, the efficiency parameters for **AR27** and **AR24** are much lower. As explained above, the poor results were expected for devices prepared with **AR27**, whereas those prepared with **AR24**, which show efficient electron injection into TiO_2, are more difficult to explain (see below).

- The low efficiencies of the **AR24** solar cell can be explained due to inefficient electron injection in the presence of I^-/I_3^-, or to a fast disappearance of the oxidised dye by a very fast recombination with the injected electrons, or both. Although the former hypothesis is still under debate, several authors have shown evidence of the interaction between the dye and the I^-/I_3^- redox pair present in the electrolyte. Further experiments to study the interaction between the dye and the redox couple should be carried out in the future in order to understand the interaction between both components and to increase the efficiency of the devices.

The introduction of electron donating and electron withdrawing groups to the molecular structure of the ruthenium complexes is a strategy often used to tune their photophysical and electrochemical properties. However, as shown above, the presence of these substituents can also strongly influence photoinduced electron injection from the dye excited state into the conduction band of the TiO_2 and the recombination reaction between the photoinjected electrons and the redox couple present in the electrolyte. Both of these electron transfer reactions have a direct effect on the overall device performance.

The ruthenium polypyridyl complexes **N719**, **Black Dye** and **C101** have shown the highest efficiencies reported to date when used as photosensitisers in dye sensitised solar cells. In particular, **N719** and **Black Dye** have been utilised in DSSC for a long time and their measurements have been used as control samples in many papers and reports.

However, to the best of our knowledge, comparison of the device parameters of these three dyes under the same conditions had not been reported before. The overall efficiency of the DSSCs prepared with these ruthenium polypyridyl complexes was measured and correlated to their molecular structure.

The key results in this study can be summarised as follows:

- The photophysical and redox properties of the ruthenium photosensitisers is strongly dependent on the nature of their ligands, therefore the absorption spectrum of **Black Dye** is red-shifted compared to that for **N719** and **C101** due to the electron-donating effect of the three thiocyanate ligands and the terpyridine ligand coordinated to the ruthenium metal ion.

- Although the light induced electron injection yield estimated from the TC-SPC measurements is higher than 70 % for all dyes, **C101** shows the highest yield. The luminescence decay kinetics of an Al_2O_3 film sensitised with **Black Dye** and Cheno is slower than without Cheno. This behavior is attributed to the obstruction of the formation of **Black Dye** aggregates.

- L-TAS measurements carried out on sensitised TiO_2 films exhibit a decay of the order of microseconds which fits to a classic stretched exponential decay for the three dyes. On the other hand, the measurement of complete devices shows a decrease in the signal amplitude associated with the efficient regeneration of the dye by the redox couple. Of special emphasis is the strongly reduced signal of **Black Dye** when measured in complete devices, suggesting a extremely fast dye regeneration.

- The IPCE spectra of all the dyes in DSSC devices have a maximum value higher than 70 %. Nevertheless, **C101** shows the maximum conversion efficiency reported for these three dyes (96 % at λ=530 nm). On the other hand, the IPCE spectrum of **Black Dye** is broader than the spectra of their analogues, in good agreement with its absorption spectra.

- The devices prepared with **C101** as the photosensitiser exhibit the highest photocurrent, as well as the highest overall efficiency. These results are in good agreement with the high electron injection yield reported from the luminescence decay measurements.

- Although charge extraction experiments do not show a shift in the TiO_2 conduction band for any of the three dyes, **N719** DSSC shows the highest open circuit photovoltage. The V_{oc} value is related to the e^--TiO_2/electrolyte$^+$ back electron transfer, which is much slower for **N719** than for **C101** and **Black Dye** devices as transient photovoltage measurements indicate. Moreover, in good agreement with other dyes incorporating conjugated units into their structure, the more conjugated structure of the ligands coordinated to the ruthenium metal ion in **C101** and **Black Dye** induce faster recombination dynamics between the photoinjected electrons and the oxidised electrolyte, decreasing the open circuit voltage of the cell, and thus, the device efficiency.

- Highly conjugated ligands are introduced into dye structure in order to increase he molar extinction coefficient and shift the absorption spectra to the near-IR. However, it is important to minimise the interaction between these organic ligands and the oxidised species present in the electrolyte which can severely limit device V_{oc}.

The sensitisation of nanocrystalline TiO_2 with ruthenium polypyridyl complexes using different coadsorbents can increase the photocurrent and photovoltage of DSSC devices. However, the overall device efficiency strongly depends on the molecular structure of both the photosensitiser and the coadsorbent, as well as on the interaction of the coadsorbent with the surface of the semiconductor.

The key results in this study can be summarised as follows:

- The amount of photosensitiser anchored onto a TiO_2 film is reduced when citric acid is used as coadsorbent. A decrease of 20 % and 30 % for **AR20**, and of 40 % and 60 % for **N719** is observed when the ruthenium complexes are co-sensitised with a concentration of citric acid of 150 µM and a 300 µM, respectively. Furthermore, the absorption spectra of TiO_2 film sensitised with **N719** is red shifted when citric acid is coadsorbed. This shift is attributed to the interaction of citric acid with **N719** due to a change in the pH. On the other hand, however, no shift is observed in the absorption spectra of **AR20**.

- Charge extraction measurements reveal a downward shift in the semiconductor conduction band for both dyes as a result of the TiO_2 surface protonation.

- The use of citric acid as coadsorbent in DSSC devices sensitised with **AR20** increases both photocurrent and photovoltage. The high photocurrent is attributed to the shift in the TiO_2 conduction band. On the other hand, the increase in photovoltage was found to be due to a reduction in the e^--TiO_2/electrolyte$^+$ recombination reaction as indicated by transient photovoltage measurements.

- The co-sensitisation of **N719** and citric acid results in a decrease in both photocurrent and photovoltage for these devices. The transient photovoltage decay measurements exhibit a faster recombination reaction between the photoinjected electrons and the oxidised species present in the electrolyte. This phenomena explains the low efficiency yields obtained by **N719** DSSCs co-sensitised with citric acid.

- The use of citric acid with **AR20** results in an increase in overall device efficiency, from 2.76 % to 6.08 %. On the other hand, the use of citric acid with **N719** has the reverse effect. These results show that the presence of citric acid not only affects the semiconductor, but also interacts with the anchored dye.

Annex I: Contribution to the scientific community

Journal articles

Reynal, A., Forneli, A., Martínez-Ferrero, E., Sánchez-Díaz, A., Vidal-Ferran, A., Palomares, E., A phenanthroline heteroleptic ruthenium complex and its application to dye-sensitized solar cells, *Eur. J. Inorg. Chem.*, **2008**, 1955-1958.

Reynal, A., Forneli, A., Martínez-Ferrero, E., Sánchez-Díaz, A., Vidal Ferran, A., O'Regan B., Palomares, E., Interfacial charge recombination between the e^--TiO_2 and the I^-/I_3^- electrolyte in ruthenium heteroleptic complexes: dye molecular structure-open circuit voltage relationship, *J. Am. Chem. Soc.*, **2008**, 130, 13558-13567.

Reynal, A., Forneli, A., Palomares, E., Dye structure - charge transfer processes relationship in the most efficient ruthenium complexes used in dye solar cells, *Energy Environm. Sci.*, **2010**, 3, 805-812.

Reynal, A., Palomares, E., Increasing the performance of cis-dithiocyanato(4,4'-dicarboxy-2,2'-bipyridine)(1,10-phenanthroline)ruthenium(II) based DSC using citric acid as coadsorbent, *Energy Environm. Sci.*, **2009**, 2, 1078-1081.

Reynal, A., Albero, J., Vidal-Ferran, A., Palomares, E., diastereoselectivity and molecular recognition of mercury(II) ions, *Inorg. Chem. Commun.*, **2009**, 12 (2), 131-134.

Reynal, A., Etxebarria, J., Nieto, N., Serres, S., Palomares, E., Vidal-Ferran, A., A bipyridine based Cu^{2+} optical chemosensor, *Eur. J. Inorg. Chem.*, **2010**, 1360-1365.

Conferences

Reynal, A., Forneli, A., Martínez-Ferrero, E., Sánchez-Díaz, A., Vidal-Ferran, A., Palomares, E.
Heteroleptic ruthenium(II) polypyridyl complexes as new efficient sensitizers for molecular photovoltaic devices
Poster presentation
Materials for renewable energies: organic and hybrid solar cells, Madrid, Spain, **2007**

Reynal, A., Forneli, A., Martínez-Ferrero, E., Sánchez-Díaz, A., Vidal-Ferran, A., O'Regan, B. Palomares, E.
Understanding the relationship between dye structure and device efficiency
Poster presentation
2nd Meeting on organic photovoltaics and optoelectronic devices, Madrid, Spain, **2008**

Annex II: Glossary of terms and abbreviations

(NN)	Bidentate chelate nitrogen containing ligand
(NNN)	Tridentate chelate nitrogen containing ligand
a. u.	Arbitrary units
AFM	Atomic force microscopy
BMII	1-butyl-3-methylimidazolium iodide
bpy	2,2-bipyridine
CB	Conduction band
Cheno	Chenodeoxycholic acid
COD	1,5-cyclooctadiene
CTTS	Charge transfer to solvent
CV	Cyclic voltammetry
DMF	Dimethylformamide
DMPII	1-propyl-2,3-dimethylimidazolium iodide
DMSO	Dimethylsulfoxide
DSPEC	Dye sensitised photoelectrochemical cell
DSSC	Dye sensitised solar cell
$E_{0,0}$	Excited state 0,0 energy
EtOH	Ethanol
fac	Facial
ff	Fill factor
FT-IR	Fourier transform-infrared spectroscopy
FTO	Fluorine doped tin oxide
GuNCS	Guanidinium thiocyanate
HOMO	Highest occupied molecular orbital
HTM	Hole transporting material
IPCE	Incident photon to current conversion efficiency
IR	Infrared
I_{sc}	Short circuit current

ITO	Tin-doped indium oxide
J (in NMR)	Coupling constant
J_{sc}	Short circuit density of current
L	Ligand
L-TAS	Laser-transient absorbance spectroscopy
LC	Ligand centered transition
LMCT	Ligand to metal charge transfer
LUMO	Lowest unoccupied molecular orbital
M	Metal
m/z	Mass-to-charge ratio
MeCN	Acetonitrile
mer	Meridional
MLCT	Metal to ligand charge transfer
NMR	Nuclear magnetic resonance
Oh	Octahedral geometry
OLED	Organic light emitting diode
phen	1,10-phenanthroline
P_{lamp}	Power of the incident light
SEM	Scanning electron microscopy
TBA^+	Tetrabutylammonium
$TBAPF_6$	Tetrabutylammonium hexafluorophosphate
TBP	*Tert*-butylpyridine
^tBuOH	*Tert*-butanol
TC-SPC	Time correlated-single photon counting
Td	Tetrahedral geometry
TEM	Transmission electron microscopy
TFA	Trifluoroacetic acid
TPV	Transient photovoltage measurements
tpy	2,2':6',2"-terpyridine
t_R	Retention time
UV	Ultraviolet
VB	Valence band
V_{oc}	Open circuit voltage
δ (in NMR)	Chemical shift (in ppm)
η_{eff}	Overall efficiency

RUTHENIUM POLYPYRIDYL COMPLEXES AS PHOTOSENSITIZERS FOR MOLECULAR PHOTOVOLTAICDEVICES:
INFLUENCE OF THE DYE STRUCTURE AND THE PRESENCE OF ADDITIVES TO THE DEVICE
PERFORMANCE
Anna Reynal Verdú
ISBN:978-84-693-8863-1/DL:T.1944-2010